High Schmidt-number turbulent advection and giant concentration fluctuations

Gregory Eyink [1,2,*] and Amir Jafari [1,†]

[1]*Department of Applied Mathematics and Statistics, The Johns Hopkins University, Baltimore, Maryland 21218, USA*
[2]*Department of Physics & Astronomy, The Johns Hopkins University, Baltimore, Maryland 21210, USA*

We consider the effects of thermal noise on the Batchelor-Kraichnan theory of high Schmidt-number mixing in the viscous dissipation range of turbulent flows at sub-Kolmogorov scales. Starting with the nonlinear Landau-Lifshitz fluctuating hydrodynamic equations for a binary fluid mixture at low Mach numbers, we justify linearization around the deterministic Navier-Stokes solution in the dissipation range. For the latter solution we adopt the standard Kraichnan model, a Gaussian random velocity with spatially constant strain but white noise in time. Then, following prior work of Donev, Fai, and Vanden-Eijnden [J. Stat. Mech.: Theory Exp. (2014) P04004], we derive asymptotic high Schmidt limiting equations for the concentration field, in which the thermal velocity fluctuations are exactly represented by a Gaussian random velocity that is likewise white in time. We obtain the exact solution for concentration spectrum in this high Schmidt limiting model, showing that the Batchelor prediction in the viscous-convective range is unaltered. Thermal noise dramatically renormalizes the bare diffusivity in this range, but the effect is the same as in laminar flow and thus hidden phenomenologically. However, in the viscous-diffusive range at scales below the Batchelor length (typically micron scales) the predictions based on deterministic Navier-Stokes equations are drastically altered by thermal noise. Whereas the classical theories predict rapidly decaying spectra in the viscous-diffusive range, either Gaussian or exponential, we obtain a k^{-2} power-law spectrum over a couple of decades starting just below the Batchelor length. This spectrum corresponds to nonequilibrium giant concentration fluctuations, which are due to the imposed concentration variations being advected by thermal velocity fluctuations and which are experimentally well observed in quiescent fluids. At higher wave numbers, the concentration spectrum instead goes to a k^2 equipartition spectrum due to equilibrium molecular fluctuations. We work out detailed predictions for water-glycerol and water-fluorescein mixtures. Finally, we discuss broad implications for turbulent flows and applications of our methods to experimentally accessible laminar flows.

I. INTRODUCTION

Recent work [1–4] has sparked renewed interest in the effects of thermal noise on turbulent flow, a problem much neglected since the pioneering work of Betchov more than 60 years ago [5–7]. These new studies have confirmed Betchov's insight that the dissipation range of turbulent flows must be strongly affected by thermal noise. In particular, the energy spectrum below the Kolmogorov dissipation scale [8], which has long been expected to exhibit an exponential decay [9–16], instead demonstrates an equilibrium equipartition energy spectrum in numerical simulations which incorporate molecular noise [1–3]. The question remains which turbulent processes at sub-Kolmogorov length scales can be essentially altered by such noise. Prominent among the candidates

for essential modifications is the turbulent mixing of a high Schmidt-number passive concentration field. On the one hand, the viscous-convective and viscous-diffusive ranges in the Batchelor theory [17] of turbulent mixing occur entirely at scales below the Kolmogorov scale. On the other hand, thermal fluctuations have long been known to produce striking effects in the diffusion of scalar concentration in laminar flows, including a renormalization of the diffusion constant [18–20] and large, long-range nonequilibrium correlations of concentration fluctuations [21–23]. We shall therefore focus in this work on the effects of thermal noise in the turbulent mixing of a binary fluid mixture at high Schmidt numbers.

Past research on turbulent scalar mixing has rested upon the assumption that the relevant advecting velocity field must solve the deterministic Navier-Stokes equation below the Kolmogorov scale $\ell_K = \nu^{3/4}\varepsilon^{-1/4}$ (with ν the kinematic viscosity and ε the energy dissipation rate per mass) and down to nearly the mean-free path of the fluid. Assuming that the smoothing effects of viscosity would produce a velocity field with nearly constant gradient at lengths well below the Kolmogorov scale, Batchelor in [17] constructed a model of distortion of small blobs of scalar field by straining motions which were assumed to be statistically sharp and time independent in a coordinate system fixed in the blobs. The chief prediction of Batchelor's

model with velocity gradient frozen in time was a cascade of scalar fluctuations c' at wave numbers $k\ell_K \gtrsim 1$ with Fourier spectrum

$$E_c(k) \sim C_B(\chi/\gamma)k^{-1}\exp[-C_B(k\ell_B)^2/2], \qquad (1)$$

where $\int_0^\infty E_c(k)dk = (\frac{1}{2})\langle|c'|^2\rangle$ and χ is the rate of injection of scalar fluctuations (or, in a statistical steady-state, the rate of dissipation $\chi = D\langle|\nabla c|^2\rangle$ for diffusivity D), $\gamma = (\varepsilon/\nu)^{1/2}$ is the strain rate at the Kolmogorov scale, and $\ell_B = (D/\gamma)^{1/2}$ is the scalar dissipation length scale, now termed the "Batchelor length." Note that $\ell_K/\ell_B = Sc^{1/2}$ where $Sc = \nu/D$ is the Schmidt number. The constant prefactor C_B in the power-law spectrum $E_c(k) \sim C_B(\chi/\gamma)k^{-1}$ in the viscous-convection range for $1/\ell_K \lesssim k \lesssim 1/\ell_B$ is often presumed universal and called the "Batchelor constant." In his subsequent works, Kraichnan [24,25] argued that the turbulent velocity gradient in the sub-Kolmogorov scales, while constant in space, was rapidly varying in time and he proposed another soluble model in which the advecting random velocity field was taken to be Gaussian, white noise in time. Kraichnan's model predicts a spectrum at wave numbers $k\ell_K \gtrsim 1$ of the form

$$E_c(k) \sim C_B(\chi/\gamma k)(1+\sqrt{6C_B}k\ell_B)\exp(-\sqrt{6C_B}k\ell_B), \quad (2)$$

reproducing Batchelor's $1/k$ spectrum in the viscous-convective range but exhibiting exponential decay in the viscous-diffusive range for $k\ell_B \gtrsim 1$. Such spectra have been widely expected in the turbulence community to hold down to nearly molecular scales.

Later studies have largely verified these predictions of Batchelor and Kraichnan. A recent paper of Sreenivasan succinctly reviews observations both by experiment and by simulation [26]. Experiments have been performed in laboratory flows or by field measurements in the ocean, both for concentration fields and for temperature fields. Note that it has largely been assumed in the turbulence literature that, when buoyancy effects are negligible, advection of concentration at high Schmidt numbers and of temperature at high Prandtl number will be equivalent. Experiments supporting the Batchelor k^{-1} spectrum have been performed for concentration [27–29], for temperature [30,31], and for both simultaneously [32]. These studies either did not measure spectra in the viscous-diffusive range or did not resolve with enough accuracy to discriminate between the distinct predictions of Batchelor and Kraichnan. The experimental picture is a bit unclear, furthermore, as some other laboratory experiments with high Schmidt dye as solute have reported spectra different than the predicted k^{-1} [33,34]. Most recent studies have resorted instead to numerical simulations of incompressible Navier-Stokes turbulence [35–38], obtaining thereby increasingly long intervals of k^{-1} spectra in the viscous-convective range and furthermore strong evidence in favor of Kraichnan's exponential decay spectrum (2) over Batchelor's prediction (1) in the viscous-diffusion range. The Batchelor regime of high Schmidt scalar advection has achieved an iconic status as "a rare thing in turbulence theory" [25] where exact results are possible. The theory has since been extended in various ways, e.g., to allow for finite correlation time of the advecting velocity (see [39] and further references in [40]), and recently a rigorous mathematical proof has even been given of the

Batchelor k^{-1} spectrum in a forced two-dimensional (2D) Navier-Stokes flow [41].

There is reason to believe, however, that thermal fluctuations at sub-Kolmogorov scales will fundamentally change the picture of high Schmidt-number turbulent advection. Indeed, thermal fluctuations have long been known to have profound effects on high Schmidt mixing, prominently diffusion in liquids. One of the oldest pieces of evidence is the Stokes-Einstein relation

$$D = k_B T/6\pi\eta\sigma, \qquad (3)$$

which connects the diffusivity D to fluid temperature T, shear viscosity η, and the radius σ of a spherical particle in solution. Significantly, this relation has long been known to be empirically valid quite generally for solutes in liquids, with σ close to the particle radius. We quote from a seminal 1945 paper of Onsager on liquid diffusion:

> "the ratio $l = kT/D\eta$ is a length of the order of magnitude of molecular dimensions, normally smaller than the value $6\pi a$...
>
> From the point of view of molecular theory, viscous flow and diffusion present parallel problems. It would seem that for an exact theory of either, we should have to analyze the cooperative character of the molecular motion involved; but this difficult analysis has not yet been developed further than the hydrodynamic approximation." [42]

The appearance of shear viscosity in the empirical Stokes-Einstein relation thus hints that mass diffusion and momentum diffusion are strongly coupled processes. Indeed, the observed diffusivity D in liquids generally differs considerably from the "bare" collisional diffusivity D_0 predicted by Enskog kinetic theory [20].

A second striking piece of evidence for the importance of thermal noise is the "giant concentration fluctuations" (GCF's) observed both in free diffusive mixing [43,44] and in nonequilibrium steady states with an imposed concentration gradient [45,46]. These effects were predicted using linearized fluctuating hydrodynamics [21–23] and are a particular instance of the spatial long-range correlations of fluctuations which are generic for systems away from global thermodynamic equilibrium [47–50]. The basic prediction involves the static structure function $S_{cc}(k)$ defined in terms of the Fourier transform of concentration fluctuations $\widehat{c}'(\mathbf{k})$ by

$$\langle\widehat{c}'(\mathbf{k})\widehat{c}'(\mathbf{k}')\rangle = (2\pi)^3\delta^3(\mathbf{k}+\mathbf{k}')S_{cc}(k). \qquad (4)$$

It should be noted here that this structure function is related to the scalar spectrum commonly considered in turbulence theory by the relation $E_c(k) = \frac{1}{(2\pi)^2}k^2 S_{cc}(k)$. The result which has been confirmed by experiment is a power-law scaling

$$S_{cc}(k) \sim \frac{k_B T}{D\eta}|\nabla c|^2 k^{-4} \qquad (5)$$

down to very low wave numbers, limited only by the fluid domain size or by buoyancy effects [51,52]. In low-gravity environments these fluctuations are truly "giant," growing to macroscopic scales and with amplitudes orders of magnitude larger than equilibrium concentration fluctuations [43,46]. The scale invariance corresponds to fractality of the concentration isosurfaces, which are being advected by thermal

velocity fluctuations with long-range correlations induced by pressure forces. These striking nonequilibrium fluctuation effects have been the subject of many experimental investigations, including the up-coming NEUF-DIX microgravity experiment of the European Space Agency [53,54]. It is worth remarking that these long-range fluctuation correlations and the Stokes-Einstein relation for diffusivity are not necessarily independent manifestations of thermal noise, but may be connected by heuristic arguments [55].

A remarkable link of such thermal effects with turbulence theory has been discovered in the work of Donev, Fai, and Vanden-Eijnden [56] (hereafter, DFV). In most liquids, a large separation of timescales exists between the fast viscous dynamics of the thermal velocity fluctuations and the slow diffusive dynamics of solute molecules, i.e., momentum diffusion proceeds much faster than mass diffusion. DFV exploited this fact to develop an exact high Sc asymptotic reduction of the equations of fluctuating hydrodynamics for a binary fluid mixture under the condition of incompressible, isothermal flow. Importantly, the DFV theory does not linearize the equation for the concentration field and treats nonlinear advection exactly. The conclusion of the DFV analysis is a reduced stochastic equation for individual realizations of the concentration field on long, diffusive timescales in which the scalar is advected by a modified thermal velocity field which is Gaussian, white noise in time. Thus, the long-time, high Sc limiting equation for the concentration field is a version of the exactly soluble Kraichnan model [24,25,40] which has been widely used to study turbulent scalar advection.

As a result, the DFV theory yields exact closed equations for the correlation functions of all orders in the scalar concentration field. In particular, DFV showed that the equation for the ensemble-average concentration field exhibits a renormalization of the bare molecular diffusivity D_0 and yields naturally the Stokes-Einstein diffusivity D as a renormalized "eddy diffusivity" due to advection by thermal velocity fluctuations. As discussed in [56], the effective stochastic equations for individual realizations of the concentration field are furthermore more efficient to solve numerically than the original fluctuating hydrodynamics equations, by a factor of Sc, since the fast viscous dynamics of the thermal velocity fluctuations has been eliminated. DFV demonstrated in numerical simulations of free diffusive mixing that these model equations produce the fractal scalar interfaces which are observed experimentally and also power-law GCF's of the concentration. They did not, however, observe clearly the k^{-4} scaling (5) of the concentration structure function, as predicted by linearized theory, but instead observed a scaling closer to k^{-3} in the quasisteady regime of decay. It has therefore been unclear how to reconcile the DFV asymptotic theory with the experimental observations verifying the prediction (5).

In this paper we shall illuminate the latter issue and, furthermore, we generalize the DFV theory to include turbulent advection by combining it with the original approach of Kraichnan [24,25]. In this manner, we can study analytically the effects of thermal noise in the sub-Kolmogorov scales on high Schmidt turbulent advection. We choose to consider here a statistically stationary turbulent cascade with injection of concentration fluctuations at a constant rate χ at a length scale

$L \gtrsim \ell_K$ by a stochastic source field. We find that the Batchelor k^{-1} scalar spectrum in the viscous-convective interval is unaffected by thermal noise, despite the rapid decay of kinetic energy spectrum in sub-Kolmogorov scales being replaced by a k^2 equipartition spectrum. Working in physical space, we find more precisely that the steady-state concentration correlation function $C(r) = \langle c'(\mathbf{r})c'(\mathbf{0})\rangle$, with $r = |\mathbf{r}|$, exhibits the logarithmic scaling

$$C(r) \sim C(\ell_K) + C_B \frac{\chi}{\gamma} \ln(\ell_K/r), \quad \ell_B \lesssim r \lesssim \ell_K \quad (6)$$

whose Fourier transform yields exactly the Batchelor-Kraichnan k^{-1} spectrum. Our key finding, however, is that giant concentration fluctuations with a k^{-2} power-law scalar spectrum occur in the viscous-diffusive range, replacing the rapidly decaying spectra predicted by Batchelor and Kraichnan. In physical space we get

$$C(r) \sim C(0) - \frac{\chi}{2D}(r^2 + 3\sigma r + \cdots), \quad \sigma \lesssim r \lesssim \ell_B \quad (7)$$

where σ is a length of order of the radius of the solute particle. The first term in (7) is the one $\propto \langle|\nabla c|^2\rangle r^2$ which is expected for a smooth concentration field and which would arise from the rapidly decaying spectra of Batchelor and Kraichnan. The second term appears to be subleading and negligible until $r \simeq \sigma$. However, this term is *nonanalytic* in r and on Fourier transforming produces a k^{-2} power law which dominates the spectrum for $k\ell_B \gtrsim 1$. We obtain an exact solution for the scalar spectrum $E_c(k)$ of our model in terms of known special functions, which exemplifies this behavior. Note using the Stokes-Einstein relation (3) and $\chi = D\langle|\nabla c|^2\rangle$ that the Fourier transform of the term $\propto r$ in (7) yields the concentration spectrum

$$E_c(k) \sim \frac{\chi\sigma}{\pi D}k^{-2} \sim \frac{1}{6\pi^2}\frac{k_B T}{D\eta}\langle|\nabla c|^2\rangle k^{-2}, \quad k\ell_B \gtrsim 1 \quad (8)$$

which, except for being smaller by a factor of $\frac{2}{3}$, corresponds exactly to the structure function scaling in (5) associated to the giant concentration fluctuations observed experimentally in laminar flows. Eventually, at higher wave numbers, thermal equilibrium fluctuations of the concentration field must begin to dominate and an equipartition spectrum $E_c(k) \propto k^2$ should appear; for a detailed discussion of the equilibrium spectrum see Sec. IV and Appendix A. Because of this effect of molecular fluctuations, the concentration gradients ∇c become dependent upon a high-wave-number cutoff Λ in the model and the estimates by the relation $\langle|\nabla c|^2\rangle = \chi/D$ must be interpreted as "effective gradients" holding over a certain range of scales. This somewhat subtle issue will be discussed at length in the following.

The theoretical predictions of our analysis for the concentration spectrum are illustrated in Fig. 1 for the specific case of a water-glycerol mixture. The Kolmogorov turnover rate $\gamma = 10^2$ s^{-1} is chosen very close to that in recent fluid turbulence experiments with water-glycerol solutions in a von Kármán flow [57]. No experiments have been performed on turbulent high Schmidt mixing with water-glycerol mixtures, as far as we are aware, so that we have chosen $\chi = 10^2$ s^{-1} from one of the more recent laboratory experiments with a water solution of disodium fluorescein [28]. In this hypothetical
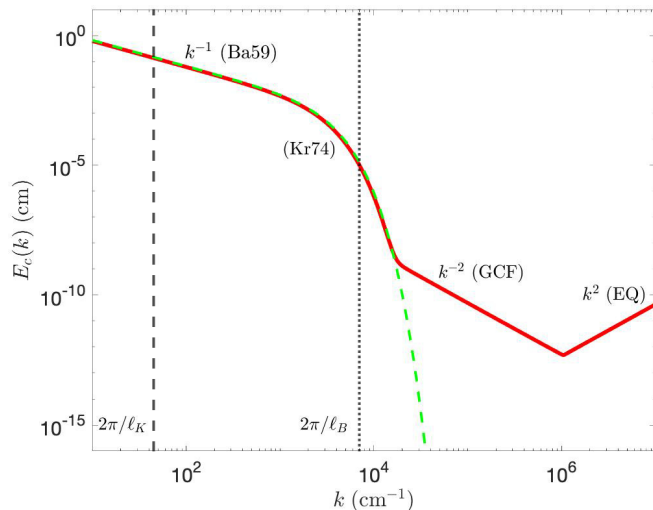
FIG. 1. Our predicted scalar concentration spectrum (red solid line, —) and the prediction of Kraichnan [25] (Kr74; green dashed line, - - -), for a water-glycerol solution at temperature $T = 25\,^{\circ}$C, pressure $p = 1$ bar, and mean concentration of glycerol $\bar{c} = 0.5$, with $\gamma = 10^2$ s^{-1} and $\chi = 10^2$ s^{-1}. Distinct ranges of the concentration spectrum are labeled as follows: Batchelor's k^{-1} spectrum (Ba59); k^{-2} power law associated to giant concentration fluctuations (GCF); k^2 equipartition spectrum (EQ). The vertical dashed (- - -) and dotted lines (·····) indicate, respectively, the Kolmogorov wave number $2\pi/\ell_K = 44.7$ cm^{-1} and Batchelor wave number $2\pi/\ell_B = 7034.5$ cm^{-1}.

experiment, we predict more than two decades of power-law spectrum $E_c(k) \propto k^{-2}$ associated to giant concentration fluctuations appearing at scales just below the Batchelor length, which is here $\ell_B = 1.98\ \mu$m.

It is important to emphasize that, even if there is no turbulent velocity field and the scalar is advected by thermal velocity fluctuations only, then the power law (8) still holds, extending down now to wave numbers $k \simeq 1/L$ in our steady-state model with a random, spatially distributed source of concentration fluctuations. Including turbulent shear, these GCF's of thermal origin are supplanted by the Batchelor-Kraichnan k^{-1} spectrum of concentration fluctuations at the wave numbers $k\ell_B \lesssim 1$ in the viscous-convective range. This effect is similar to the "shear quenching" of GCF's predicted for small departures from global equilibrium (weak shear) using linearized fluctuating hydrodynamics [58], although the turbulent k^{-1} spectrum differs substantially from the $k^{2/3}$ spectrum predicted for the weakly sheared case. There has been some question whether such shear quenching will hold in experimentally realizable flows, with gravity and finite-size effects argued instead to limit the GCF's at low wave numbers [59]. We have not included buoyancy in our analysis, but this was done in the work of DFV and gravity effects can thus be considered, in principle, within our framework. Unfortunately, including gravity in the asymptotic mode reduction of DFV for Sc $\gg 1$ produces an effective equation for concentration with a term *quadratic* in c, due to advection of concentration by self-induced velocity fluctuations arising from buoyancy. [See Eq. (102) later in the text.] Because of this quadratic nonlinearity, closed equations are no longer obtained for the correlation functions of the concentration,

fundamentally complicating mathematical analysis. We shall comment more on this issue below.

The main message of our work for turbulence theory is that thermal noise completely alters the character of the viscous-diffusive range of high Schmidt-number turbulent advection, leading to fundamentally different predictions than those based on deterministic Navier-Stokes dynamics. This is likely to be true also for other physical processes in turbulent flows that involve essentially the sub-Kolmogorov scale motions, such as combustion [60–62], condensation [63–65], and locomotion of micro-organisms [66–68], not to speak of the intrinsic nonlinear turbulent dynamics itself. The presence of giant concentration fluctuations in turbulent flows should not have been unexpected because they are a generic feature of diffusive mixing far from global equilibrium. We quote from the paper of Vailati and Giglio:

"So the orders-of-magnitude increase of the fluctuations above the equilibrium value (the most prominent feature that can be captured experimentally) is to be expected for any nonequilibrium fluid that has macroscopic concentration variations comparable to those in this experiment" [43].

It will, unfortunately, be probably very difficult in the near future to observe these effects in laboratory or field experiments on high Schmidt turbulent advection because the Batchelor length ℓ_B is generally near micron scales and no current experimental techniques can probe such small scales in a turbulent flow with the required accuracy. The most recent experiment on turbulent high Schmidt mixing of which we are aware [29] measures concentration fluctuations via laser-induced fluorescence with an optical fiber probe having a spatial resolution of 2.8 μm, which is close to the Batchelor scale. However, instrumental noise dominates the measurements before even getting to this scale (see [29], Fig. 3). It should be quite possible, on the other hand, to test our predictions by means of numerical simulations of high Schmidt-number turbulent mixing with existing codes for low Mach-number fluctuating Navier-Stokes equations of multicomponent [69] and binary [70] mixtures.

The main message of our work for statistical physics is that methods from turbulence theory provide effective tools to study nonequilibrium thermal fluctuations more generally, as originally suggested by DFV [56]. The DFV theory applies not only to turbulent flows, but also to laminar flows, such as the free diffusive mixing of an initial blob of concentration in a quiescent (zero Reynolds-number) fluid. The DFV theory treats nonlinear advection of scalar concentration exactly without need for linearization, and, as seen from our result (8), it is able to recover GCF's with the scaling $S_{cc}(k) \sim k^{-4}$ which is observed experimentally. This approach is thus able to deal with large-amplitude fluctuations driven by strong gradients, high concentrations, and nonsteady transient diffusion processes, which are difficult theoretical problems driving current empirical investigations such as NEUF-DIX. We therefore expect that the first experimental tests of validity of these methods will come from novel applications to diffusive mixing in laminar flows.

Because our paper is somewhat lengthy, it is useful to briefly outline its contents. Section II discusses the DFV asymptotic theory of the high Schmidt-number limit, first

reviewing the original work for zero mean flow (Sec. II A) and then extending that analysis to turbulent flows, assuming Kraichnan's standard model for the dissipation-range velocity field (Sec. II B). In the main mathematical Sec. III we exactly solve the limiting model for the concentration spectrum in a statistical steady state with constant injection of scalar fluctuations. We first review necessary background on the Kraichnan white-noise advection model and mathematical methods employed in its solution (Sec. III A). We apply these methods to solve for the static two-point correlation function of concentration fluctuations (Sec. III B) and then compute analytically its Fourier transform to obtain the concentration spectrum (Sec. III C). In Sec. IV we develop concrete predictions of our theory for turbulent mixing of water glycerol and water fluorescein, and in the final Sec. V we discuss implications and possible extensions of our work. Several Appendixes (A–H) provide technical details of the derivations, background material for easy reference, and numerical methods for plotting our analytical results.

II. DFV THEORY AND HIGH Sc LIMIT

In this section, we shall first concisely review the work of DFV [56] on diffusion of scalar concentration in the asymptotic limit of large Schmidt numbers. DFV considered the problem where the fluid is at rest, in global equilibrium, and performed a formal adiabatic mode-elimination procedure for the fast thermal velocity degrees of freedom. In the limit they obtained reduced model equations for the scalar concentration field in which the effective advecting velocity is Gaussian and white noise in time (Kraichnan velocity), so that closed equations follow for all scalar correlation functions. We shall here extend the asymptotic analysis of DFV to a turbulent fluid in the Kolmogorov dissipation range, adopting further Kraichnan's white-noise velocity approximation for the turbulent velocity field. The result of the adiabatic elimination is another Kraichnan model for the scalar concentration field, in which the Gaussian, white-in-time velocity field has two independent contributions representing advection by turbulent fluctuations and by thermal fluctuations. The resulting closed equations for the scalar two-point correlations in this reduced model will be solved exactly in Sec. III.

A. Fluid at rest

In a fluid at rest, i.e., with no large-scale motion, thermal fluctuations produce the entire velocity field $\mathbf{v} = \mathbf{v}_\theta$. For low Mach-number isothermal fluids, DFV adopted a standard model of linearized incompressible fluctuating Navier-Stokes equation for the velocity field $\mathbf{v}$:

$$\rho \partial_t \mathbf{v} = -\nabla p + \eta \triangle \mathbf{v} + \nabla \cdot (\sqrt{2\eta k_B T} \, \boldsymbol{\eta}(\mathbf{x}, t))$$
$$= \mathcal{P}[\eta \triangle \mathbf{v} + \nabla \cdot (\sqrt{2\eta k_B T} \, \boldsymbol{\eta}(\mathbf{x}, t))], \quad (9)$$

where ρ, η, and T, represent, respectively, the mass density, shear viscosity, and temperature, all assumed to be constant, and k_B is Boltzmann's constant. Also, p is the kinematic pressure, which may be replaced by the tensor operator $\mathcal{P}_{ij} = \delta_{ij} - \partial_i \partial_j \triangle^{-1}$, the Leray-Hodge projection onto the space of divergence-free velocity fields, so that the incompressibility

constraint

$$\nabla \cdot \mathbf{v} = 0 \quad (10)$$

is maintained. The white-noise symmetric, traceless tensor field $\boldsymbol{\eta}(\mathbf{x}, t)$ represents a thermal fluctuating stress, with mean zero and covariance

$$\langle \eta_{ij}(\mathbf{x}, t) \eta_{kl}(\mathbf{x}', t') \rangle = \left(\delta_{ik}\delta_{jl} + \delta_{il}\delta_{jk} - \frac{2}{3}\delta_{ij}\delta_{kl} \right)$$
$$\times \delta^3(\mathbf{x} - \mathbf{x}')\delta(t - t'). \quad (11)$$

The prefactor $\sqrt{2\eta k_B T}$ is chosen according to the standard fluctuation-dissipation relation so that the correct Gibbs equilibrium distribution is obtained for the equal-time velocity statistics, with energy equipartition among wave-number modes. For example, see [2], Appendix A, for a careful discussion.

For the scalar concentration field $c(\mathbf{x}, t)$ in a binary mixture of two identical fluids of molecular mass m, DFV adopted the fluctuating advection-diffusion equation

$$\partial_t c = -\mathbf{u} \cdot \nabla c + \nabla \cdot (D_0 \nabla c + \sqrt{2m D_0 \rho^{-1} c(1-c)} \, \boldsymbol{\eta}_c(\mathbf{x}, t)), \quad (12)$$

where $\mathbf{u}$ is a smoothed advection velocity (see below), D_0 is the bare molecular diffusivity, and $\boldsymbol{\eta}_c(\mathbf{x}, t)$ is a white-noise vector field representing a thermal fluctuating mass flux, with zero mean and covariance

$$\langle \eta_{ci}(\mathbf{x}, t) \eta_{cj}(\mathbf{x}', t') \rangle = \delta_{ij}\delta(t - t')\delta^3(\mathbf{x} - \mathbf{x}') \quad (13)$$

(see also [71]). Here again the factor $\sqrt{2m D_0 \rho^{-1} c(1-c)}$ in the noise term is dictated by the fluctuation-dissipation relation, so that the concentration fluctuations have their equilibrium equal-time statistics given by the Boltzmann-Einstein formula determined from the entropy of mixing. See Appendix A for this standard argument in statistical thermodynamics. Note that DFV considered only the limit of low concentrations $c \ll 1$ in their work, so that they took $c(1-c) \doteq c$, but in our analysis we allow arbitrarily high concentrations. Finally, a key step in the theory of DFV was to assume that the concentration field of tracer particles (tagged particles of the fluid, solute molecules, colloidal particles, etc.) is advected by a coarse-grained velocity $\mathbf{u}$ obtained by convolving $\mathbf{v}$ with a smoothing kernel $\boldsymbol{\sigma}$,

$$\mathbf{u}(\mathbf{x}, t) \equiv \boldsymbol{\sigma} \star \mathbf{v} = \int \boldsymbol{\sigma}(\mathbf{x}, \mathbf{x}') \mathbf{v}(\mathbf{x}', t) \, d^3 x'. \quad (14)$$

This convolution filters out features at scales below a cutoff scale σ, taken to be of order of the typical linear size of a tracer particle.

The theoretical justification for the starting equations (9) and (12) of the DFV theory must be discussed briefly. The fluctuating hydrodynamic equations of a general binary mixture with nonconstant density and temperature fields have been derived in [72] by the phenomenological arguments of statistical thermodynamics, based upon the corresponding hydrodynamic equations (see [73], Sec. 22.7). In principle, these stochastic equations should be derivable by the Zwanzig-Mori projection methods which have been applied to obtain fluctuating hydrodynamics for simple, single-component fluids [74,75]. An important point which becomes clear from these derivations is that the equations of fluctuating hydrodynamics such as (9) and (12) should not be considered as continuum

stochastic partial differential equations. Instead, they are low-wave-number effective theories which describe the physics only of modes at wave numbers less than some cutoff Λ, generally taken to be of order the inverse of the mean-free-path length. Thus, the spatial delta functions which appear in the covariances (11) and (13) should in fact be interpreted as "cutoff delta functions" $\delta_\Lambda(\mathbf{x} - \mathbf{x}')$ [see (A6) in Appendix A and [74]].

To obtain the final form of the fluctuating hydrodynamic equations (9) and (12), the low Mach-number, isothermal limit must be taken. This has been carefully considered for a binary or a general multicomponent fluid in [69,70]. This analysis leads to equations close to (9) and (12), except that the incompressibility constraint differs from (10) and the momentum equation (9) contains the nonlinear advection term $(\mathbf{u} \cdot \nabla)\mathbf{u}$. As to the first, the constraint on the velocity derived in [70] for the binary fluid mixture in the low Mach limit is

$$\nabla \cdot \mathbf{v} = -\nabla \cdot (\beta \mathbf{F}),$$

where $\mathbf{F} = D_0 \nabla c + \sqrt{2mD_0\rho^{-1}c(1-c)}\,\boldsymbol{\eta}_c$ and where $\beta(c) = (1/\rho)(\partial\rho/\partial c)_{P_0,T_0}$ is the solutal expansion coefficient at background pressure P_0 and temperature T_0. The above constraint thus reduces to (10) if either volume changes little with concentration (β near zero) or if the bare diffusivity D_0 is negligible, as DFV explicitly assume. The second difference, the neglect of the nonlinear advection term, is justified by the renormalization group analysis of [76,77], which implies that in thermal equilibrium the nonlinearity becomes negligible at sufficiently low wave numbers and frequencies. A quantitative estimate provided in [2] implies that the nonlinear coupling should be weak except for length scales of order the radius of the fluid molecules, where no hydrodynamic description is valid in any case. Finally, the key assumption of DFV that tracer particles are advected by the smoothed velocity field (14) is intuitively plausible since such particles can feel only a resultant velocity averaged over fluctuations at a scale smaller than their size σ. This hypothesis is further motivated in [56], with reference to earlier works such as [20] on the modeling of fluid-tracer interactions in diffusive mixing.

The essential result of DFV is an exact analysis of the high Schmidt-number limit $\mathrm{Sc}_0 \equiv \frac{\eta}{D_0\rho} \gg 1$ for the model equations (9) and (12). Motivated by the empirical success of the Stokes-Einstein relation $D \sim k_B T / \eta\sigma$, DFV introduced a small parameter $\epsilon \ll 1$ to order quantities for formal asymptotics and adopted a scaling

$$\eta \mapsto \epsilon^{-1}\eta, \quad D_0 \mapsto \epsilon D_0 \qquad (15)$$

so that $D_0\eta \simeq (\text{const})$ and $\mathrm{Sc}_0 \sim \epsilon^{-2}$. In the limit $\epsilon \ll 1$ there is a separation of timescales between the fast viscous dynamics, governing the thermal velocity fluctuations $\mathbf{v}$, and the slow diffusive evolution of the concentration field c. DFV formalized this separation by introducing a "macroscopic" diffusive time τ which is related to the "microscopic" viscous time t of Eqs. (9) and (12) by $t = \epsilon^{-1}\tau$ or, equivalently, by the scaling

$$t \mapsto \epsilon^{-1}t \qquad (16)$$

with τ renamed t. These scalings can be used in a formal adiabatic mode elimination of the fast velocity degrees of freedom, which will be discussed in detail in Sec. II B for the

more general case of a turbulent flow. The result is a limiting stochastic advection-diffusion equation for the concentration field in the "macroscopic" time:

$$\partial_t c = -\mathbf{w} \odot \nabla c + D_0 \triangle c + \nabla \cdot (\sqrt{2mD_0\rho^{-1}c(1-c)}\,\boldsymbol{\eta}_c). \qquad (17)$$

Here $\odot$ represents a Stratonovich dot product and $\mathbf{w}(\mathbf{x}, t)$ is an incompressible, advecting random velocity field which is white noise in time, with zero mean and covariance

$$\langle \mathbf{w}(\mathbf{x}, t) \otimes \mathbf{w}(\mathbf{x}', t') \rangle = \mathbf{R}(\mathbf{x}, \mathbf{x}')\delta(t - t'),$$

$$\mathbf{R}(\mathbf{x}, \mathbf{x}') := 2 \int_0^\infty \langle \mathbf{u}(\mathbf{x}, t) \otimes \mathbf{u}(\mathbf{x}', t + t') \rangle dt' \qquad (18)$$

and which can thus be shown to be given by

$$\mathbf{R}(\mathbf{x}, \mathbf{x}') = \frac{2k_B T}{\eta}(\boldsymbol{\sigma} \star \mathbf{G} \star \boldsymbol{\sigma}^\top)(\mathbf{x}, \mathbf{x}'), \qquad (19)$$

where $\mathbf{G}$ is the Green's function of the linear Stokes operator $\mathcal{A} = -\mathcal{P}\triangle$, or the so-called *Oseen tensor*. For example, in unbounded three-dimensional (3D) space

$$G^{ij}(\mathbf{x}, \mathbf{x}') = G^{ij}(\mathbf{x} - \mathbf{x}') = \frac{1}{8\pi r}\left(\delta^{ij} + \frac{r^i r^j}{r^2}\right) \qquad (20)$$

with $\mathbf{r} = \mathbf{x} - \mathbf{x}'$. Note that $\mathbf{G}$ is singular for $\mathbf{x} = \mathbf{x}'$, but the smoothed tensor $\mathbf{R}$ is regular at coinciding points. The spatial realizations of $\mathbf{w}$ are obtained from the stationary Stokes equation with smoothed thermal forcing

$$\mathcal{P}\left[\nu\triangle\mathbf{w} + \nabla \cdot \left(\sqrt{\frac{2\nu k_B T}{\rho}}\boldsymbol{\eta}_\sigma\right)\right]$$

$$= -\nabla q + \nu\triangle\mathbf{w} + \nabla \cdot \left(\sqrt{\frac{2\nu k_B T}{\rho}}\boldsymbol{\eta}_\sigma\right) = \mathbf{0} \qquad (21)$$

with $\boldsymbol{\eta}_\sigma = \boldsymbol{\sigma} \star \boldsymbol{\eta}$ and q determined by $\nabla \cdot \mathbf{w} = 0$. This equation expresses the physics that viscous diffusion and smoothed thermal fluctuations are in instantaneous balance for the effective velocity $\mathbf{w}$, with long-range spatial correlations induced by the incompressibility constraint.

Although the change from Eq. (12) to (17) in the limit $\epsilon \to 0$ for the concentration field may seem minor, a crucial physical contribution is obscured in (17) by the stochastic calculus. Converting instead to the equivalent Itō form, which is most appropriate to calculate ensemble averages, produces

$$\partial_t c = -\mathbf{w} \cdot \nabla c + D_0 \triangle c + \nabla \cdot [\mathbf{D}(\mathbf{x})\nabla c]$$

$$+ \nabla \cdot (\sqrt{2mD_0\rho^{-1}c(1-c)}\,\boldsymbol{\eta}_c), \qquad (22)$$

with an additional drift term $\nabla \cdot [\mathbf{D}(\mathbf{x})\nabla c]$ which contains a *renormalized diffusivity*

$$\mathbf{D}(\mathbf{x}) = \tfrac{1}{2}\mathbf{R}(\mathbf{x}, \mathbf{x}). \qquad (23)$$

The physical origin of this addition to diffusivity is advection by the eliminated thermal velocity fluctuations, similar to an "eddy diffusivity" due to eliminated turbulent eddies. Under further assumptions of homogeneity and isotropy, $\mathbf{D}$ becomes independent of $\mathbf{x}$ and $D_{ij} = D\delta_{ij}$, with the enhanced scalar diffusivity D calculated in [56] for a particular choice of filter

kernel $\boldsymbol{\sigma}$ as

$$D = \frac{k_B T}{6\pi \eta \sigma}\left(1 - \frac{\sqrt{2}}{2}\frac{\sigma}{L}\right), \qquad (24)$$

where L is the linear dimension of the flow domain and $\sigma \ll L$ is the size of the tracer particle and where space dimension is 3. The size-dependent correction of order $O(\sigma/L)$ is tiny for macroscopic systems but is a well-known effect in molecular dynamics (MD) studies of diffusion coefficients [78,79].

Importantly, (24) corresponds exactly to the Stokes-Einstein formula for the renormalized diffusivity D which, since $D_0 \ll D$, dominates in the total effective diffusivity $D_{\mathrm{eff}} = D_0 + D \doteq D$. Although the filter kernel $\boldsymbol{\sigma}$ was specially selected in [56] to produce the precise numerical prefactor in the original Stokes-Einstein relation for hard spheres, an arbitrary kernel yields (24) with 6π replaced by some other numerical constant of order unity. Thus, the DFV theory explains the empirical success of the Stokes-Einstein formula as the effect of strong renormalization of a small bare diffusivity due to advection of tracer particles by thermal velocity fluctuations. This is one of the significant results of the DFV theory. Note that similar augmented diffusivities have been obtained in renormalization group studies of a passive scalar advected by thermal velocity fluctuations, without the assumption of high Schmidt numbers [76,77]. However, those studies did not incorporate the fluctuation-dissipation relation for the scalar and thus have uncertain relevance to physical diffusion processes.

A further important consequence of the DFV theory, which, however, was not fully utilized in [56], is the existence of closed equations for the scalar correlation functions of any order. This result shall be exploited in Sec. III where it will be shown that the DFV theory predicts the well-known giant concentration fluctuations, but without the usual approximation of linearizing the advection term in the concentration equation. It is this capability to deal with nonlinear advection which makes the DFV approach particularly useful to study the scalar concentration field in a turbulent flow.

B. Turbulent flow

For turbulent flow, the full nonlinear form of the fluctuating hydrodynamics equation [3,69,70,76,77] must be used

$$\partial_t \mathbf{v} = \mathcal{P}[-(\mathbf{v}\cdot\nabla)\mathbf{v} + \nu\triangle\mathbf{v} + \nabla\cdot(\sqrt{2\nu k_B T/\rho}\,\boldsymbol{\eta}(\mathbf{x},t))], \qquad (25)$$

where $\nu = \eta/\rho$ is kinematic viscosity and where the white-noise term $\boldsymbol{\eta}$ has covariance (11), just as before (see [2], Appendix A). We can, however, decompose the velocity into a "turbulent part" and a "thermal part" as

$$\mathbf{v} = \mathbf{v}_T + \mathbf{v}_\theta,$$

where the turbulent velocity $\mathbf{v}_T$ satisfies the deterministic Navier-Stokes equation and $\mathbf{v}_\theta$ represents the small thermal fluctuation around that solution. An equation for $\mathbf{v}_\theta$ follows by the standard approach of linearization:

$$\partial_t \mathbf{v}_\theta = \mathcal{P}[-\mathbf{v}_T\cdot\nabla\mathbf{v}_\theta - \mathbf{v}_\theta\cdot\nabla\mathbf{v}_T + \nu\triangle\mathbf{v}_\theta \\ + \nabla\cdot(\sqrt{2\nu k_B T/\rho}\,\boldsymbol{\eta}(\mathbf{x},t))]. \qquad (26)$$

The neglect of the nonlinear term $\mathbf{v}_\theta\cdot\nabla\mathbf{v}_\theta$ assumed in this approximation is valid because it is small compared with the

viscous term $\nu\triangle\mathbf{v}_\theta$ in the turbulent dissipation range below the Kolmogorov scale ℓ_K, which is our focus of interest here. The matter was discussed in [2], Sec. II B, where it was noted that the ratio of this nonlinear term to the viscous term (which is a kind of scale-dependent "thermal Reynolds number" Re_ℓ^θ) is of order $\theta_K^{1/2}$ at the Kolmogorov scale $\ell = \ell_K$, where $\theta_K = k_B T/\rho v_K^2 \ell_K^3$ is the ratio of fluid thermal energy to the kinetic energy of a Kolmgorov-scale eddy. Since $\theta_K \sim 10^{-6}$–10^{-9} in realistic flows, the neglect of the nonlinear term is justified throughout the turbulent dissipation range and down to nearly molecular scales.

We shall take for the scalar concentration field the same equation as did DFV:

$$\partial_t c = -\mathbf{u}\cdot\nabla c + \nabla\cdot(D_0\nabla c + \sqrt{2mD_0\rho^{-1}c(1-c)}\,\boldsymbol{\eta}_c(\mathbf{x},t)), \qquad (27)$$

but with the crucial difference that now

$$\mathbf{u} = \mathbf{u}_T + \mathbf{u}_\theta, \qquad (28)$$

where $\mathbf{u}_T = \boldsymbol{\sigma}\star\mathbf{v}_T$ and $\mathbf{u}_\theta = \boldsymbol{\sigma}\star\mathbf{v}_\theta$. We emphasize that Eq. (27) is fundamentally different from Eq. (12) since it includes the effects of turbulent advection as well as advection by thermal velocity fluctuations. Because we consider here the turbulent dissipation range at scales below the Kolmogorov length ℓ_K, where the velocity $\mathbf{v}_T$ is smooth, and because $\ell_K \gg \sigma$, we should expect that $\boldsymbol{\sigma}\star\mathbf{v}_T \simeq \mathbf{v}_T$. However, the coarse graining at scale σ remains crucial for the much rougher thermal component.

Equations (26)–(28) are the basis of all of our subsequent analysis. To make the problem mathematically tractable, however, we shall follow Kraichnan [24,25] in further modeling the Navier-Stokes solution $\mathbf{v}_T$ in the turbulent dissipation range as a Gaussian random velocity field, white noise in time, with zero mean and covariance

$$\langle\mathbf{v}_T(\mathbf{x},t)\otimes\mathbf{v}_T(\mathbf{x}',t')\rangle = \boldsymbol{\mathcal{V}}_T(\mathbf{x}-\mathbf{x}')\delta(t-t'), \qquad (29)$$

where

$$\mathcal{V}_{T,ij}(\mathbf{r}) = 2\mathcal{V}_{T0}\delta_{ij} - 2\Gamma(2r^2\delta_{ij} - r_ir_j) \qquad (30)$$

and $2\mathcal{V}_{T0}\delta_{ij} = \mathcal{V}_{T,ij}(0)$. We consider here statistically homogeneous flows (periodic domains or infinite space) so that the covariance depends only upon the difference $\mathbf{r} = \mathbf{x}-\mathbf{x}'$. The constant $\mathcal{V}_{T0}$ with units of $(\text{length})^2/(\text{time})$ represents the sweeping effects of large integral-scale eddies, while the constant Γ has units of $1/(\text{time})$ and its magnitude should be taken to be of order of the inverse Kolmogorov time (the eddy turnover rate at the Kolmogorov scale).[1] Equations (26) and (27) now become

$$\partial_t \mathbf{v}_\theta = \mathcal{P}[-\mathbf{v}_T\odot\nabla\mathbf{v}_\theta - \mathbf{v}_\theta\odot\nabla\mathbf{v}_T + \nu\triangle\mathbf{v}_\theta \\ + \nabla\cdot(\sqrt{2\nu k_B T/\rho}\,\boldsymbol{\eta}(\mathbf{x},t))], \qquad (31)$$

$$\partial_t c = -\mathbf{u}\odot\nabla c + \nabla\cdot(D_0\nabla c \\ + \sqrt{2mD_0\rho^{-1}c(1-c)}\,\boldsymbol{\eta}_c(\mathbf{x},t)). \qquad (32)$$

---

[1]Our constant Γ is chosen to coincide with D_1 in Eq. (48) of [40] for the case $\xi = 2$, $d = 3$ and thus equals $A/30$ in terms of the constant A introduced in the original work of Kraichnan [24,25].

Because of the white-noise character of $\mathbf{u}_T$, we must specify the stochastic calculus and $\odot$ indicates a Stratonovich dot product. This is the standard choice for the Kraichnan model because it is considered as the zero-correlation limit of a model with a stochastic advecting velocity field that has finite-time correlation. By taking space derivatives of (30), one obtains

$$
\begin{aligned}
\langle \partial_k v_{Ti}(\mathbf{x}, t) \partial_\ell v_{Tj}(\mathbf{x}', t') \rangle \\
= 2\Gamma(4\delta_{ij}\delta_{k\ell} - \delta_{ik}\delta_{j\ell} - \delta_{i\ell}\delta_{jk})\delta(t - t'),
\end{aligned}
\tag{33}
$$

which makes clear that Kraichnan's model of the velocity field in the turbulent dissipation range corresponds to a spatially uniform random straining field, rapidly varying in time. As a consequence, the smoothed turbulent velocity field $\mathbf{u}_T = \boldsymbol{\sigma} \star \mathbf{v}_T$ has a spatial covariance $\boldsymbol{\mathcal{U}}_T$ which differs from $\boldsymbol{\mathcal{V}}_T$ in (29) only by the replacement of $\mathcal{V}_{T0}$ with a constant $\mathcal{U}_{T0}$ larger by an amount $\sim \Gamma\sigma^2$. To avoid possible confusion, we note that this constant-strain model introduced by Kraichnan [24,25] was later generalized by him [80] to involve arbitrary spatial covariance and this generalization is now more commonly known as the "Kraichnan model" (see Sec. III A).

The high Schmidt-number limit of our turbulent advection problem can be studied by the same formal asymptotics with the small parameter $\epsilon \ll 1$ used by DFV, with identical rescalings (15) and (16). The key physical issue is the ordering to be adopted for the white-noise turbulent field $\mathbf{v}_T$. The correct ordering can be motivated by the observation that for Navier-Stokes turbulence

$$
\frac{d}{dt} \frac{1}{2} \langle v^2 \rangle = \nu \langle |\boldsymbol{\nabla} \mathbf{v}|^2 \rangle \sim \nu\Gamma^2,
$$

where we used the fact that Γ is of the order of the inverse Kolmogorov time. Now invoking the rescalings $t \mapsto \epsilon^{-1}t$, $\nu \mapsto \epsilon^{-1}\nu$ we see that Γ must be rescaled as $\Gamma \mapsto \epsilon\Gamma$. Stated equivalently, the turbulent velocity gradient must be ordered so that, with large viscosity, a finite total amount of energy is dissipated in a unit "macroscopic" time. Together with the covariance of the white-noise field (29) and (30) and the scaling $t \mapsto \epsilon^{-1}t$, one then obtains

$$
\mathbf{v}_T(\mathbf{x}, t) \mapsto \epsilon \mathbf{v}_T(\mathbf{x}, t).
$$

We shall see below that this ordering leads to turbulent advection making an $O(1)$ contribution in the high Schmidt-number limit.

Before discussing the formal $\epsilon \to 0$ limit, we first consider the inclusion of additional terms into the concentration equation (32) to enable a steady-state scalar cascade. As written, Eq. (32) corresponds to a freely decaying scalar. While this setup permits a Batchelor regime (e.g., see [25,28]), it entails the complication of nontrivial time dependence. It is simpler to analyze instead a steady-state cascade with some external source included to inject concentration fluctuations, so that a time-independent balance can be achieved with diffusive dissipation. That is what we shall do in this work. The simplest source to include for this purpose is a constant mean concentration gradient $\boldsymbol{\gamma} = \langle \boldsymbol{\nabla} c \rangle$, which contributes an additional term $-\boldsymbol{\gamma} \cdot \mathbf{u}$ to (32) that injects scalar fluctuations. Such a constant concentration gradient has been often considered, both in turbulence [36,81] and in statistical physics [23,46,58], having the motivation that it is realizable in laboratory experiments.

An alternative source of scalar fluctuations more amenable to mathematical analysis is a spatially distributed source $s(\mathbf{x}, t)$, which may be either deterministic or random. In the latter case, a Gaussian random source field which is white noise in time is especially convenient because it gives exact control of the rate of injection χ of scalar fluctuations. In particular, with covariance

$$
\langle s(\mathbf{x}, t) s(\mathbf{x}', t') \rangle = \delta(t - t') S\left(\frac{\mathbf{x} - \mathbf{x}'}{L}\right),
\tag{34}
$$

it follows that in the statistically stationary state

$$
\tfrac{1}{2} S(\mathbf{0}) = D_0 \langle |\boldsymbol{\nabla} c|^2 \rangle = \chi
\tag{35}
$$

and rate of input of scalar fluctuations matches the dissipation rate by diffusion [82]. Here S is a smooth, positive-definite function and thus L gives the length scale of injection of the scalar fluctuations. It is such stochastic white-noise forcing which we shall analyze in this work, but for future applications we shall derive the reduced equations for all of the various scalar sources.

What is important to consider in including scalar source terms into Eq. (32) is their ordering in the small parameter $\epsilon \ll 1$. We shall rescale these quantities so that they appear at $O(1)$ in the final equation for the concentration and, thus, a strong scalar cascade is obtained in macroscopic time. The final equations we consider, with all quantities properly ordered but expressed in original microscopic time units, is

$$
\begin{aligned}
\partial_t \mathbf{v}_\theta = \mathcal{P}[-\sqrt{\epsilon} \mathbf{v}_T \odot \boldsymbol{\nabla} \mathbf{v}_\theta - \mathbf{v}_\theta \cdot \sqrt{\epsilon} \boldsymbol{\nabla} \mathbf{v}_T + \nu\epsilon^{-1}\triangle \mathbf{v}_\theta \\
+ \boldsymbol{\nabla} \cdot (\sqrt{2\nu\epsilon^{-1}k_B T/\rho}\ \boldsymbol{\eta}(\mathbf{x}, t))],
\end{aligned}
\tag{36}
$$

$$
\begin{aligned}
\partial_t c' = -\sqrt{\epsilon} \mathbf{u}_T \odot (\boldsymbol{\nabla} c' + \boldsymbol{\gamma}) - \mathbf{u}_\theta \cdot (\boldsymbol{\nabla} c' + \boldsymbol{\gamma}) + \epsilon D_0 \triangle c' \\
+ \epsilon s_0(\mathbf{x}, \epsilon t) + \sqrt{\epsilon} s(\mathbf{x}, t) \\
+ \boldsymbol{\nabla} \cdot (\sqrt{2\epsilon\ m D_0 \rho^{-1} c(1 - c)} \boldsymbol{\eta}_c(\mathbf{x}, t)).
\end{aligned}
\tag{37}
$$

Here c' denotes the *scalar fluctuation*, so that $\langle c' \rangle = 0$, and thus $c = c' + \boldsymbol{\gamma} \cdot \mathbf{x}$. Note that $\sqrt{\epsilon} \mathbf{v}_T(\mathbf{x}, \epsilon^{-1}t) = \epsilon \mathbf{v}_T(\mathbf{x}, t)$ because of the scaling properties of white noise, in agreement with our previous argument. Likewise, the white-noise random scalar source satisfies $\sqrt{\epsilon} s(\mathbf{x}, \epsilon^{-1}t) = \epsilon s(\mathbf{x}, t)$. A deterministic distributed source, denoted here by s_0, is assumed to have zero space average and is scaled as $\epsilon s_0(\mathbf{x}, \epsilon t)$, which amounts to the assumption that it is weak and slowly varying in microscopic time units.

Finally, changing to macroscopic or diffusive time by the substitution $t \mapsto \epsilon^{-1}t$ we get the equations

$$
\begin{aligned}
\partial_t \mathbf{v}_\theta = \mathcal{P}[-\mathbf{v}_T \odot \boldsymbol{\nabla} \mathbf{v}_\theta - \mathbf{v}_\theta \cdot \boldsymbol{\nabla} \mathbf{v}_T + \nu\epsilon^{-2}\triangle \mathbf{v}_\theta \\
+ \boldsymbol{\nabla} \cdot (\sqrt{2\nu\epsilon^{-2}k_B T/\rho}\ \boldsymbol{\eta}(\mathbf{x}, t))],
\end{aligned}
\tag{38}
$$

$$
\begin{aligned}
\partial_t c' = -\mathbf{u}_T(\mathbf{x}, t) \odot (\boldsymbol{\nabla} c' + \boldsymbol{\gamma}) - \epsilon^{-1}\mathbf{u}_\theta(\mathbf{x}, \epsilon^{-1}t) \cdot (\boldsymbol{\nabla} c' + \boldsymbol{\gamma}) \\
+ D_0 \triangle c' + s_0(\mathbf{x}, t) + s(\mathbf{x}, t) \\
+ \boldsymbol{\nabla} \cdot (\sqrt{2m D_0 \rho^{-1} c(1 - c)} \boldsymbol{\eta}_c(\mathbf{x}, t)).
\end{aligned}
\tag{39}
$$

In Appendix B we start with these equations and perform a standard adiabatic mode elimination of the fast velocity degrees of freedom, following closely the argument in [56]. Here, we present the main result of that analysis for the

readers who wish to skip the mathematical details. First, the thermal velocity field $\mathbf{v}_\theta$, to leading order in the asymptotics, is unaffected by the background turbulent velocity $\mathbf{v}_T$ and evidences thermal equilibrium statistics at the temperature T. This result is in agreement with numerical simulations of the full nonlinear fluctuating hydrodynamic equation (25), where the velocity in the far dissipation range of turbulence exhibits Gaussian equipartition statistics [3]. The equation for the concentration fluctuation field on the macroscopic timescale reduces simply to

$$
\begin{aligned}
\partial_t c' = &-(\mathbf{u}_T + \mathbf{w}_\theta) \odot (\nabla c' + \boldsymbol{\gamma}) \\
&+ D_0 \triangle c' + s_0(\mathbf{x}, t) + s(\mathbf{x}, t) \\
&+ \nabla \cdot (\sqrt{2m D_0 \rho^{-1} c(1-c)} \boldsymbol{\eta}_c(\mathbf{x}, t)),
\end{aligned} \tag{40}
$$

where $\mathbf{w}_\theta$ is the Gaussian, white-noise random field $\mathbf{w}$ which appeared in the DFV theory for a fluid at rest, defined by (18) with the space covariance (19). An equivalent Itō form of the equation is

$$
\begin{aligned}
\partial_t c' = &-(\mathbf{u}_T + \mathbf{w}_\theta) \cdot (\nabla c' + \boldsymbol{\gamma}) \\
&+ D_{\text{eff}} \triangle c' + s_0(\mathbf{x}, t) + s(\mathbf{x}, t) \\
&+ \nabla \cdot (\sqrt{2m D_0 \rho^{-1} c(1-c)} \boldsymbol{\eta}_c(\mathbf{x}, t)),
\end{aligned} \tag{41}
$$

where $D_{\text{eff}} = D_0 + D_T + D$ with $D_T = \mathcal{U}_{T0}$ the turbulent eddy diffusivity and with D the diffusivity contribution from thermal fluctuations calculated by DFV. In general, $D_{\text{eff}} \simeq D_T$ because the turbulent diffusivity dominates. The important result, which shall form the basis of all of our conclusions in this paper, is that the equation for the concentration field in the dissipation range reduces to a Kraichnan model with white-noise advecting velocity $\mathbf{v} = \mathbf{u}_T + \mathbf{w}_\theta$ which is an additive sum of contributions from turbulence and from thermal fluctuations.

III. SOLUTION OF THE MODEL

Having developed our reduced model of high Schmidt turbulent mixing by the asymptotic method of DFV, we now solve it exactly for the concentration correlation function $C(r)$ and the corresponding spectrum $E_c(k)$. We consider the simplest situation of a statistically homogeneous and isotropic steady state with concentration fluctuations injected at a constant rate χ at a length scale $L \gtrsim \ell_K$ via a random spatially distributed source $s(\mathbf{x}, t)$, as in (34). In the first subsection below we briefly review the Kraichnan model in general and some of the important mathematical results concerning it. Then, in the following subsections, we employ those standard results as part of the exact solution of our specific problem.

A. Précis of the Kraichnan model

The standard review of the Kraichnan model is the 2001 article of Falkovich *et al.* [40]. Very good discussions for beginners (and even for experts) are contained in published conference lectures by Gawędzki [83–85]. In particular, these reviews discuss the theoretical breakthrough of the exact calculation of anomalous scaling exponents of the passive scalar in the inertial-convective range, which, however, plays no role in our analysis here. For a recent comparison of the Kraichnan

model predictions with experimental data and with simulations of incompressible Navier-Stokes turbulence, see [26]. We draw upon all of these sources for the presentation below.

What is now termed the "Kraichnan model" is described mathematically by an equation for a passive scalar field $c(\mathbf{x}, t)$ which is advected by a Gaussian random velocity field $\mathbf{v}(\mathbf{x}, t)$ which is white noise in time:

$$
\partial_t c = -\mathbf{v} \odot \nabla c + D_0 \triangle c + s, \tag{42}
$$

where the velocity field has zero mean and covariance

$$
\langle v_i(\mathbf{x}, t) v_j(\mathbf{x}', t') \rangle = \mathcal{V}_{ij}(\mathbf{x}, \mathbf{x}') \delta(t - t'). \tag{43}
$$

As in Sec. II, the symbol $\odot$ denotes a Stratonovich dot product and D_0 is the molecular (bare) diffusivity. We have included a random Gaussian source $s(\mathbf{x}, t)$ (independent of velocity) with zero mean and covariance given by Eq. (34). We consider here only a solenoidal (incompressible) velocity field, so that $\nabla_{x^i} \mathcal{V}_{ij}(\mathbf{x}, \mathbf{x}') = 0$, although the compressible case has been studied in the literature [40,85]. In our specific problem, we consider a statistically homogeneous flow, so that $\mathcal{V}_{ij}$ depends only upon the difference $\mathbf{r} = \mathbf{x} - \mathbf{x}'$. However, we present all of the results for general inhomogeneous flows in this summary since many important future applications will involve situations with boundary conditions or initial conditions for velocity and concentration that break homogeneity. Converting to Itō calculus, the Langevin equation (42) gains a noise-induced drift term, hence, in Itō interpretation the equivalent equation is

$$
\partial_t c = -\mathbf{v} \cdot \nabla c + D_0 \triangle c + \nabla \cdot \left(\frac{1}{2} \mathcal{V}(\mathbf{x}, \mathbf{x}) \cdot \nabla c \right) + s. \tag{44}
$$

The additional term has the physical meaning of a turbulent "eddy diffusivity" $\mathbf{D}_{\text{eddy}}(\mathbf{x}) = \frac{1}{2} \mathcal{V}(\mathbf{x}, \mathbf{x})$ which is induced by the random advection.

One of the important features of the Kraichnan model is that there is no closure problem for correlation functions of the advected scalar $c(\mathbf{x}, t)$ and in fact the N-point, equal-time correlation function $C_N(\mathbf{x}_1, \ldots, \mathbf{x}_N; t) := \langle c(\mathbf{x}_1, t) c(\mathbf{x}_2, t) \ldots (\mathbf{x}_N, t) \rangle$ satisfies an exact differential equation [40]:

$$
\begin{aligned}
\partial_t C_N(\mathbf{x}_1, \ldots, \mathbf{x}_N) = &\, \mathcal{M}_N C_N(\mathbf{x}_1, \ldots, \mathbf{x}_N) \\
&+ \sum_{n<m} C_{N-2}(\mathbf{x}_1, \ldots, \underset{n}{\wedge}, \ldots, \underset{m}{\wedge}, \ldots, \mathbf{x}_N) S(\mathbf{x}_n, \mathbf{x}_m),
\end{aligned} \tag{45}
$$

where the notation "$\underset{n}{\wedge}$" indicates that the variable $\mathbf{x}_n$ is omitted, where we have introduced the second-order many-particle diffusion operator

$$
\mathcal{M}_N = \frac{1}{2} \sum_{n,m=1}^{N} \nabla_{x_n^i} [\mathcal{V}_{ij}(\mathbf{x}_n, \mathbf{x}_m) \nabla_{x_m^j}(\cdot)] + D_0 \sum_{n=1}^{N} \triangle_{\mathbf{x}_n}, \tag{46}
$$

and where S is the spatial covariance function of the random source $s(\mathbf{x}, t)$ introduced in Eq. (34) in Sec. II. Note that Eq. (45) is in fact a triangular system of equations with no closure problem since, with lower-point functions at hand, the N-point function is governed by a closed differential equation. While the closed equations (45) can be obtained in many ways (see, e.g., [40,83]), one particularly straightforward approach, which follows directly from our considerations in Sec. II, is

simply to use the backward Kolmogorov operator corresponding to the Itō equation (44):

$$\mathbf{L}_c := \int d^3x \left[D_0 \triangle c + \nabla \cdot \left(\frac{1}{2} \boldsymbol{\mathcal{V}}(\mathbf{x}, \mathbf{x}) \cdot \nabla c \right) \right] \frac{\delta}{\delta c(\mathbf{x})}$$

$$+ \frac{1}{2} \iint d^3x \, d^3x' \, \mathcal{V}_{ij}(\mathbf{x}, \mathbf{x}') \, \partial_i c(\mathbf{x}) \partial'_j c(\mathbf{x}') \frac{\delta^2}{\delta c(\mathbf{x}) \delta c(\mathbf{x}')}$$

$$+ \frac{1}{2} \iint d^3x \, d^3x' \, S(\mathbf{x}, \mathbf{x}') \frac{\delta^2}{\delta c(\mathbf{x}) \delta c(\mathbf{x}')},$$

which appears also in the Markov operator $\mathbf{L}_0$ given by Eq. (B1) of Appendix B, in a slightly different notation. Applying this operator $\mathbf{L}_c$ to the product functional $F[c] = c(\mathbf{x}_1) c(\mathbf{x}_2) \ldots c(\mathbf{x}_N)$ immediately yields (45).

For $N = 1$, the sum on the right-hand side of Eq. (45), which contains lower-order correlations, vanishes and we get $\partial_t C_1(\mathbf{x}) = \mathcal{M}_1 C_1(\mathbf{x})$ with $C_1(\mathbf{x}) := \langle c(\mathbf{x}, t) \rangle$. In fact, the closed equation for C_1 can be simply obtained by taking the average of the Itō equation (44), which yields

$$\partial_t \bar{c} = D_0 \triangle \bar{c} + \nabla \cdot \left(\frac{1}{2} \boldsymbol{\mathcal{V}}(\mathbf{x}, \mathbf{x}) \cdot \nabla \bar{c} \right), \quad (47)$$

where we use the more standard notation $\bar{c}$ for C_1. This equation is trivially solved for the specific problem in this paper, where we consider a statistically homogeneous flow (periodic domain or infinite space) in the long-time steady state, so that $\bar{c}$ is a space-time constant. In more realistic problems concerning GCF's with inhomogeneous statistics and involving transient decay, Eq. (47) must be solved and $\bar{c}$ used as an input to the equation for the concentration cumulant (or connected correlation) function $G_2(\mathbf{x}, \mathbf{x}') = C_2(\mathbf{x}, \mathbf{x}') - C_1(\mathbf{x}) C_1(\mathbf{x}')$. We shall leave such studies, which are directly relevant to experimentally realizable flows in microgravity, to future work.

In this paper, we are concerned with C_N for $N = 2$, although it would be of interest to study also higher-order correlations C_N for $N > 2$ and we shall discuss this matter later in the Conclusions. Equation (45) for $N = 2$ simplifies to $\partial_t C_2 = \mathcal{M}_2 C_2 + S$. We further specialize to the homogeneous case, so that all two-point correlators (C_2, $\boldsymbol{\mathcal{V}}$, etc.) become functions of the difference variable $\mathbf{r} = \mathbf{x} - \mathbf{x}'$ only. The correlation C_2, which shall be hereafter denoted simply as C, then satisfies the equation

$$\partial_t C(\mathbf{r}, t) = [\mathcal{V}_{ij}(\mathbf{0}) - \mathcal{V}_{ij}(\mathbf{r})] \partial_i \partial_j C + 2 D_0 \triangle C + S\left(\frac{\mathbf{r}}{L} \right), \quad (48)$$

where all differential operators are now with respect to the variable $\mathbf{r}$. In the case of interest to us, the velocity statistics (both for turbulent and thermal fluctuations) are in addition isotropic. For such isotropic cases, the spatial velocity covariance can be written in terms of the Leray projection $\mathcal{P}$ as

$$\mathcal{V}_{ij}(\mathbf{r}) = \mathcal{P}_{ij} K(r), \quad (49)$$

where $K(r)$ is a positive-definite function of the radial variable $r = |\mathbf{x} - \mathbf{x}'|$ (see [86]). The general equation for the two-point correlation in the Kraichnan model with isotropic velocity statistics was implicit in the paper [86], but not written explicitly there. We thus derive this equation in our Appendix C, where we show that for any space dimension d the equation for $C(r, t)$ can be expressed in terms of the ball-averaged

function

$$J(r) = -\frac{1}{r^d} \int_0^r K(\rho) \, \rho^{d-1} d\rho \quad (50)$$

as

$$\partial_t C = \frac{1}{r^{d-1}} \frac{\partial}{\partial r} \left([2 D_0 - (d-1)\triangle J(r)] r^{d-1} \frac{\partial C}{\partial r} \right) + S\left(\frac{r}{L} \right), \quad (51)$$

where $\triangle J(r) = J(0) - J(r)$ and we have also assumed that the source covariance function $S(r/L)$ is isotropic. This equation is already indicative of a renormalized diffusivity $-\triangle J(r)$; cf. Eq. (56) in Sec. III B.

In the statistical steady state, which is our focus here, $\partial_t C = 0$ and the solution of (51) is easy to obtain by straightforward integration:

$$C(r) = \int_r^\infty \frac{\int_0^\rho S\left(\frac{\rho'}{L} \right) \rho'^{d-1} d\rho'}{\rho^{d-1} [2 D_0 - (d-1)\triangle J(\rho)]} d\rho, \quad (52)$$

where we have applied boundary conditions $\partial_r C(0) = 0$ and $C(\infty) = 0$ [83]. The above expression represents the final form of the steady-state two-point correlation function for the passive scalar in the Kraichnan model with homogeneous, isotropic statistics.

Before we proceed with evaluating this expression, we first observe that the steady-state balance equation (35) follows directly from (51) by setting $\partial_t C = 0$ and $r = 0$, which yields

$$2 D_0 \langle |\nabla c|^2 \rangle = -2 D_0 \frac{1}{r^{d-1}} \frac{\partial}{\partial r} \left(r^{d-1} \frac{\partial C}{\partial r} \right) \bigg|_{r=0} = S(\mathbf{0}) = 2\chi, \quad (53)$$

and thus $\chi = D_0 \langle |\nabla c|^2 \rangle$. Although this result is an exact consequence of our mathematical model when ignoring thermal fluctuations of the concentration field, the latter invalidates this result physically. We shall see in the following that a physically valid balance equation for the concentration fluctuations involves instead a "renormalized diffusivity" D and "effective gradients" $(\nabla c)_{\text{eff}}$.

B. Concentration correlation function

We now apply these general results on the Kraichnan model to the high Schmidt limit equations (41). Throughout this entire subsection we shall neglect the final term in that equation representing molecular noise in the dynamics of the concentration field because of the presumed smallness of the molecular mass m and the bare diffusivity D_0. This term, however, can become important at sufficiently small scales and we shall evaluate its contribution in Sec. IV. With omission of the molecular noise term, (41) becomes a particular case of the Kraichnan model, with white-noise advecting velocity $\mathbf{u}_T + \mathbf{w}_\theta$, representing statistically independent contributions from turbulent fluctuations and from thermal fluctuations. Therefore, the equation for the steady-state two-point correlation function $C(r)$ in our model is exactly Eq. (51) in $d = 3$ spatial dimensions, with $\triangle J = \triangle J_T + \triangle J_\theta$. Solution of this differential equation requires expressions for the scale-dependent diffusivities.

The turbulent velocity field with space covariance (30) for $r \ll \ell_K$ is easily checked to be given by (49) with $K_T(r) =$

$-5\Gamma r^2$ and thus

$$\triangle J_T(r) := J_T(0) - J_T(r) = -J_T(r) = -\Gamma r^2. \quad (54)$$

To obtain the scale-dependent diffusivity from thermal fluctuations, we need first to determine $K_\theta(r)$ corresponding to the spatial covariance $R_{ij}(\mathbf{r}, \mathbf{r}')$ given by (19) and (20) and then calculate the associated $\triangle J_\theta(r)$. A suitable choice of the filter kernel must be made in (19). DFV employed the isotropic kernel $\sigma = \sigma \mathbf{I}$ with Fourier transform specified as

$$\widehat{\sigma}(k) := \frac{k^2 L^2}{\sqrt{(1 + k^4 L^4)(1 + k^2 \sigma^2)}} \quad (55)$$

which leads to the thermally renormalized diffusivity $D = k_B T / 6\pi\eta\sigma$ given by (24). As noted by DFV, the kernel (55) was chosen for convenience to give the prefactor $(6\pi)^{-1}$ of the conventional Stokes-Einstein relation for hard spheres, but any isotropic kernel will lead to a similar result with a different prefactor of order unity. Employing (55), with $\sigma \ll L$, we find (for details see Appendix D)

$$\triangle J_\theta(r) = \frac{k_B T}{6\pi\eta\sigma}\left[-1 + 3\left(\frac{1}{2}\frac{1}{\frac{r}{\sigma}} + \frac{e^{-r/\sigma}}{\left(\frac{r}{\sigma}\right)^2} - \frac{1 - e^{-r/\sigma}}{\left(\frac{r}{\sigma}\right)^3}\right)\right]. \quad (56)$$

Most important is the asymptotic limit

$$\triangle J_\theta(r) \sim -D\left(1 - \frac{3\sigma}{2r}\right), \quad r \gg \sigma \quad (57)$$

which will be universal for any filter kernel which is rapidly decaying in physical space, up to a different choice of σ rescaled by a factor of order unity. The physical meaning of the result (57) is that diffusivity becomes *scale dependent* due to the renormalization by thermal velocity fluctuations, with effective molecular diffusivity

$$D(r) = D_0 + D\left(1 - \frac{3\sigma}{2r}\right) \quad (58)$$

at length scale r. Thus, $D(r) \simeq D_0$ for $r \simeq \sigma$ but $D(r) \simeq D_0 + D := D_{\text{eff}}$ for $r \gg \sigma$. This scale dependence in the diffusivity $D(r)$ for correlations of concentration fluctuations is closely related to the dependence on system size L in the effective diffusivity (24) for the mean concentration. Note likewise that the turbulent velocity fluctuations according to (54) contribute an effective turbulent eddy diffusivity $D_T(r) = \Gamma r^2$ at length scale r.

We shall be concerned in this paper only with the regime $L > \ell_K \gg r \gg \sigma$ and hence need only the asymptotic expression (57). However, if one considers also $r \simeq \sigma$, then the specific choice of kernel influences the results. Here we note that the Fourier-transformed kernel (55) adopted by DFV decays very slowly $\sim 1/k$ at high wave numbers k and the physical space kernel is thus not differentiable in space. This kernel leads to a renormalized diffusivity $\triangle J_\theta(r)$ which is not smooth in the separation $\mathbf{r}$. Whereas a general filter kernel that is smooth in physical space would produce $\triangle J_\theta(r) \propto r^2$ for $r \ll \sigma$, instead the choice (55) of DFV leads to $\triangle J_\theta(r) \propto r$, as may easily be checked from (56). To avoid this undesirable feature, we can choose instead, for example, an exponentially decaying kernel

$$\widehat{\sigma}(k) \sim e^{-k\sigma/\pi}, \quad kL \gg 1, \quad (59)$$

with π added to reproduce the Stokes-Einstein relation for D. In that case, for $r \ll L$

$$\triangle J_\theta(r) = \frac{k_B T}{6\pi\eta\sigma}\left\{-1 + \frac{3\sigma}{\pi r^3}\left[\left(\frac{4\sigma^2}{\pi^2} + r^2\right)\arctan\left(\frac{\pi r}{2\sigma}\right) - \frac{2}{\pi}\sigma r\right]\right\}, \quad (60)$$

as also shown in Appendix D. Because the physical-space kernel corresponding to (59) is C^∞, then $\triangle J_\theta(r) \propto r^2$ for $r \ll \sigma$ as may be verified from (60). On the other hand, (57) is recovered for $r \gg \sigma$.

We consider only the regime $L > \ell_K \gg r \gg \sigma$ hereafter and we restrict attention also to the steady-state correlation $C(r)$ given by the integral (52). We find it easiest to study the derivative $\partial_r C(r)$ and, because $r \ll L$, we can take $S(r/L) \simeq S(0)$. These approximations together with the asymptotic expression (57) yield

$$\partial_r C(r) \cong -\frac{\chi}{3D}\frac{r}{1 - \frac{3}{2}\frac{\sigma}{r} + \frac{r^2}{\ell_B^2}}, \quad (61)$$

where we used $\chi = S(0)/2$ and neglected the bare diffusivity under the assumption that $D_0 \ll D$. We have also introduced the Batchelor dissipation length with convenient definition $\ell_B^2 := D/\Gamma$, which agrees with the standard definition up to a constant of order unity since Γ is assumed to be of order $\gamma = (\varepsilon/\nu)^{1/2}$. We may now consider separately the two relevant subranges, the viscous-convective range $\ell_K \gg r \gg \ell_B$ and the viscous-diffusive range $\ell_B \gg r \gg \sigma$.

In the viscous-convective range we can keep only the r^2 term in the denominator of (61) obtaining thus by integration over r

$$C(r) \cong \text{const} + \frac{\chi}{3\Gamma}\ln\left(\frac{\ell_K}{r}\right), \quad \ell_K \gg r \gg \ell_B. \quad (62)$$

Taking the Fourier transform with the standard isotropic relation [[87], Eq. (3-229)]

$$E_c(k) = \frac{1}{\pi}\int_0^\infty kr\,\sin(kr)\,C(r)\,dr \quad (63)$$

yields

$$E_c(k) \simeq \frac{\chi}{6\Gamma}\frac{1}{k}, \quad 1/\ell_K \ll k \ll 1/\ell_B \quad (64)$$

in exact agreement with standard theory. Note that our factor 6Γ corresponds to the mean least-rate rate of strain γ of Batchelor [Ref. [17], Eq. (4.9)] and to the corresponding factor $\langle a \rangle = A/5$ of Kraichnan [24,25].

It may at first sight be surprising that we recover this standard theoretical result. As we have noted at the end of Sec. II B and in Appendix B, the thermal velocity fluctuations in our model to leading order in the high Schmidt-number limit exhibit Gaussian thermal equilibrium statistics at temperature T, in agreement with the theoretical arguments and numerical results of [1–3] for the turbulent dissipation range. The velocity field thus has the equilibrium equipartition spectrum $E_v(k) \sim (k_B T/2\pi^2\rho)k^2$, drastically different from the steep exponential-decay-type spectrum assumed by Batchelor and Kraichnan in the dissipation range. One might wonder why this drastically different spectrum for $k\ell_K \gg 1$ appears

to have no observable effect on the behavior of the advected concentration field. In fact, there is a very large effect which is hidden from view. Since the classical theory of the Batchelor range was developed without considering thermal fluctuations, the molecular diffusivity in the works [17,24,25] (which was denoted κ in those papers) in fact corresponds to the *bare diffusivity* D_0 in our work. Because $D \gg D_0$, the Batchelor length ℓ_B is thus greatly increased by thermal velocity fluctuations. Note, however, that this effect is purely theoretical because DFV obtained exactly the same diffusivity renormalization in an equilibrium fluid at rest as we do in a turbulent flow and thus the diffusivity measured in most macroscopic experiments will coincide with the effective diffusivity D_{eff} calculated here. Thus, the effect of thermal velocity fluctuations in renormalizing the bare diffusivity is very large but not apparent from a phenomenological point of view.

In the viscous-diffusive range, on the contrary, the effects of the thermal velocity fluctuations are very large and should be directly observable in future experiments that can probe such small scales. We can Taylor expand the right-hand side of (61) in the small quantities σ/r and r/ℓ_B to obtain

$$\partial_r C \cong -\frac{\chi}{3D}\left(r - \frac{r^3}{\ell_B^2} + \frac{3}{2}\sigma\right), \quad \ell_B \gg r \gg \sigma$$

which upon integration yields

$$C(r) \cong C(0) - \frac{\chi}{6D}\left[r^2 - \frac{1}{2}\frac{r^4}{\ell_B^2} + 3r\sigma\right]. \quad (65)$$

The r^2 term due to asymptotic diffusivity D is the dominant one in physical space, with the r^4/ℓ_B^2 term arising from turbulent diffusivity and the $r\sigma$ term from thermally induced scale dependence of diffusivity both subleading. Note, however, that the first two terms are polynomials in r^2 and under Fourier transform contribute terms formally $\propto \delta^3(\mathbf{k})$, consistent with the rapidly decaying spectra (1) and (2) in the viscous-diffusive range predicted by Batchelor and Kraichnan. In fact, we shall see in the following subsection that setting $\sigma = 0$ in our model yields exactly the scalar spectrum (2) of Kraichnan. However, the σr term, although subdominant in physical space, is nonanalytic in $\mathbf{r}$ and the scalar spectrum calculated from (63) is thus a power law in wave number

$$E_c(k) \simeq \frac{1}{\pi}\frac{\chi\sigma}{D}\frac{1}{k^2}, \quad 1/\ell_B \ll k \ll 1/\sigma. \quad (66)$$

This is exactly the result (8) announced in the Introduction. As pointed out there, this power law and the dimensional coefficients multiplying it correspond exactly to the giant concentration fluctuations ubiquitously observed in diffusive mixing [43–46]. We note again that the numerical prefactor $1/\pi$ is smaller by $\frac{2}{3}$ than that predicted by linearized fluctuating hydrodynamics (5). We would not expect linearized theory to be adequate to treat with perfect fidelity our physical situation, which involves nonlinear advection of concentration and large, fluctuating gradients of the concentration field.

There is a subtlety, in fact, in obtaining this agreement with linearized theory because it depends upon the relation $\chi = D\langle|\nabla c|^2\rangle$. However, we have seen that the "correct" result for the model is instead $\chi = D_0\langle|\nabla c|^2\rangle$ which involves the

bare diffusivity. To explain the discrepancy, we use Eq. (65) to obtain

$$\langle\nabla c(\mathbf{r})\cdot\nabla c(\mathbf{0})\rangle = -\triangle C(r)$$
$$= \frac{\chi}{D}\left\{1 + O\left[\left(\frac{r}{\ell_B}\right)^2\right] + O\left(\frac{\sigma}{r}\right)\right\}, \quad (67)$$

which implies that there is a long range of length scales $\ell_B \gg r \gg \sigma$ over which the "effective gradients" $(\nabla c)_{\text{eff}}$ are independent of r and given by $(\nabla c)_{\text{eff}}^2 \simeq \chi/D$. More precisely, these are the gradient magnitudes that would be observed for a coarse-grained field $\nabla \bar{c}_\ell$ which has been low-pass filtered to contain contributions only from length scales $>\ell$ for some $\ell_B \gg \ell \gg \sigma$. These are the gradients that would be seen experimentally by measurements with a space resolution ℓ. In fact, these are the only physically meaningful gradients because the effects of molecular noise on the concentration field, which we have so far ignored, invalidate the "exact" result $\chi = D_0\langle|\nabla c|^2\rangle$. We shall discuss this latter point in more detail in Sec. IV. Using the notion of "effective gradients," we simply note for now that the result (66) can be rewritten in the form

$$E_c(k) \simeq \frac{k_B T}{6\pi^2 D\eta}(\nabla c)_{\text{eff}}^2 k^{-2}, \quad 1/\ell_B \ll k \ll 1/\sigma \quad (68)$$

in formal agreement with linearized theory.

As we now argue, the power law (66) will dominate in the concentration spectrum for k just slightly greater than $1/\ell_B$ even when $\sigma \ll \ell_B$. We may follow a similar argument as that in [1,2] for the kinetic energy spectrum, by simply equating the Kraichnan exponential decay spectrum (2) and the power-law spectrum (66) to obtain the wave number k_{tr} where transition to power law occurs. Setting to 1 all constants of order unity, this estimation yields the condition

$$(k\ell_B)^2 \exp(-k\ell_B) = \sigma/\ell_B \quad (69)$$

which has an exact solution

$$k_{tr}\ell_B = -2W_{-1}\left[-\frac{1}{2}\left(\frac{\sigma}{\ell_B}\right)^{1/2}\right] \quad (70)$$

in terms of the branch $W_{-1}(z)$ of the Lambert W function [88]. This implies only a very slow logarithmic increase of $k_{tr}\ell_B$ with decreasing σ/ℓ_B, corresponding to the asymptotics $W_{-1}(x) \sim \ln(-x) - \ln[-\ln(-x)]$ for small negative arguments x [88]. As a typical example, in the experiment of [28] observing the turbulent Batchelor range with a solution of fluorescein in water, the Batchelor wave number was estimated to be 2800 cm^{-1} corresponding to $\ell_B \simeq 22.44 \, \mu$m whereas the hydrodynamic radius of fluorescein is $\sigma \simeq 0.50$ nm [89], giving a ratio $\sigma/\ell_B \simeq 2.23 \times 10^{-5}$. Nevertheless, according to (70) one obtains only the modest value $k_{tr}\ell_B \simeq 16.3$. Even if one assumes a very small value such as $\sigma/\ell_B = 10^{-10}$, then $k_{tr}\ell_B$ increases only to 29.8, not quite doubled.

The main prediction of our theory is thus that, whereas Batchelor's $1/k$ spectrum for the viscous-convective range survives, thermal fluctuations in the viscous-diffusive range erase entirely the rapidly decaying scalar spectra of Batchelor and Kraichnan and replace those with a k^{-2} power-law spectrum due to giant concentration fluctuations. This occurs at a wave number which is just slightly larger than $1/\ell_B$,

with ℓ_B the Batchelor dissipation length for the concentration field.

The previous simple arguments are rigorous regarding the asymptotic wave-number ranges $1/\ell_K \ll k \ll 1/\ell_B$ and $1/\ell_B \ll k \ll 1/\sigma$, but only crudely treat the critical region near the transition wave number $k_{tr} \simeq 1/\ell_B$. To obtain more precise predictions in this region, we shall solve our model exactly for the concentration spectrum over the entire range $1/\ell_K \ll k \ll 1/\sigma$. For this purpose, we note that the integral representation

$$C(r) = \frac{\chi}{3\Gamma} \int_r^\infty \frac{\rho^2 \, d\rho}{\rho^3 + \ell_B^2 \rho - \frac{3}{2}\sigma \ell_B^2}, \tag{71}$$

following from (61) can be evaluated exactly by the method of partial fractions, as

$$C(r) = \text{const} - \frac{\chi}{3\Gamma}\left[\frac{\mathcal{A}}{2}\ln[b^2 + (r+a)^2]\right.$$
$$\left. + \frac{\mathcal{B}r_1}{b}\arctan\left(\frac{r+a}{b}\right)\right] + \mathcal{C}\,\ln|r-r_1|, \tag{72}$$

where $\mathcal{A} \equiv \frac{2r_1^2 + \ell_B^2}{3r_1^2 + \ell_B^2}$, $\mathcal{B} \equiv \frac{\ell_B^2}{2(3r_1^2 + \ell_B^2)}$, and $\mathcal{C} \equiv \frac{r_1^2}{3r_1^2 + \ell_B^2}$ are dimensionless constants. Note that the cubic polynomial $r^3 + \ell_B^2 r - \frac{3}{2}\sigma \ell_B^2$ has negative discriminant, so that it has one real root r_1 and a complex pair of roots $-(a \pm ib)$, where $a = \frac{1}{2}r_1$, $b^2 = \frac{3}{4}r_1^2 + \ell_B^2$, and $c^2 = a^2 + b^2$. The real root is given by Vieta's formula as

$$r_1 = w - \frac{\ell_B^2}{3w}, \quad w = \ell_B \sqrt[3]{\frac{3}{4}\left(\frac{\sigma}{\ell_B}\right) + \sqrt{\frac{1}{27} + \frac{9}{16}\left(\frac{\sigma}{\ell_B}\right)^2}}. \tag{73}$$

From this exact solution we can readily verify our previous limiting results. First we observe that for $r \gg \ell_B$ the two logarithmic terms dominate and, using the relation $\mathcal{A} + \mathcal{C} = 1$, one recovers (62) for the viscous-convective range. If instead one sets $\sigma = 0$, then also $r_1 = 0$ and the solution (72) reduces to

$$C(r) = \text{const} - \frac{\chi}{6\Gamma}\ln\left(r^2 + \ell_B^2\right), \tag{74}$$

which is the physical-space analog of the scalar spectrum (2) found by Kraichnan [25]. The correction due to thermal noise in the viscous-diffusive range can be evaluated by a joint expansion of the exact solution (72) in r/ℓ_B and $\epsilon = \sigma/\ell_B$ and, using $r_1/\ell_B = \frac{3}{2}\epsilon + O(\epsilon^2)$, one recovers the result (65). As we show in the next subsection, the concentration spectrum $E_c(k)$ corresponding to (72) by Fourier transform can be found exactly and this result yields the two limiting power laws (64) and (66), thus verifying the giant concentration fluctuations in the viscous-diffusive range but further describing in detail the transition between the two power-law regimes.

C. Concentration spectrum

In this subsection, we discuss the concentration spectrum $E_c(k)$ of our high Schmidt-number model (41), which is obtained from the concentration correlation function $C(r)$ by the isotropic Fourier transform relation (63). As in the previous subsection, we shall here neglect the molecular noise term in Eq. (41), which allows us to obtain an exact result for

$E_c(k)$ in the range $1/\ell_K \ll k \ll 1/\sigma$ by Fourier transform of the formula (72) for $C(r)$. The result is easiest to express in terms of the "one-dimensional spectrum" given by the Fourier cosine transform

$$F(k) \equiv \frac{1}{\pi}\int_0^\infty \cos(kr)C(r)dr \tag{75}$$

in terms of which

$$E_c(k) = -k\frac{\partial}{\partial k}F(k) \tag{76}$$

[see [87], Eq. (3-231]. The result of a somewhat lengthy calculation is that

$$F(k) = F_{\mathcal{A}}(k) + F_{\mathcal{B}}(k) + F_{\mathcal{C}}(k), \tag{77}$$

where the three terms correspond to the three terms in Eq. (72) for $C(r)$ and are given explicitly by

$$F_{\mathcal{A}}(k) = \frac{\chi}{3\pi\Gamma}\mathcal{A}\frac{1}{k}\text{Re}(\text{fi}(k(a+ib))), \tag{78}$$

$$F_{\mathcal{B}}(k) = -\frac{\chi}{3\pi\Gamma}\frac{\mathcal{B}r_1}{b}\frac{1}{k}\text{Im}(\text{fi}(k(a+ib))), \tag{79}$$

and

$$F_{\mathcal{C}}(k) = -\frac{\chi}{3\pi\Gamma}\mathcal{C}\frac{1}{k}(\text{fi}(kr_1) - \pi\cos(kr_1)), \tag{80}$$

where $\text{fi}(z)$ denotes the auxiliary sine integral function

$$\text{fi}(z) = \int_0^\infty \frac{\sin t}{t+z}dt = \int_0^\infty \frac{e^{-zt}}{1+t^2}dt, \quad \text{Re}(z) > 0. \tag{81}$$

See [90] (Sec. 5, formula 5.2.12) and [91] (Sec. 38:13). We consulted many tables of integrals and collections of integral transforms (such as [92]), but we were unable to find the above results in the published literature. We therefore give a complete derivation of (78)–(80) in Sec. III C 1.

However, the reader who is not interested in this derivation can skip to Sec. III C 2 where we discuss the behavior of $E_c(k)$ in the three limiting cases $k\ell_B \ll 1$, $\sigma = 0$, and $1/\ell_B \ll k \ll 1/\sigma$. We then put together our various results to obtain a global picture of the concentration spectrum and we study systematically the effect of varying $\epsilon = \sigma/\ell_B$, exploiting our exact solution (78)–(80) to plot the results for $E_c(k)$ with ϵ varying over realistic values.

1. Evaluation of integrals

The three formulas (78)–(80) are direct consequences of the following two integrals:

$$\lim_{\mu\to 0}\left[\frac{1}{2}\int_0^\infty e^{-\mu r}\log((r+a)^2 + b^2)\cos(kr)dr \right.$$
$$\left. + i\int_0^\infty e^{-\mu r}\arctan\left(\frac{b}{r+a}\right)\cos(kr)dr\right]$$
$$= -\frac{1}{k}\text{fi}(k(a+ib)) \tag{82}$$

and

$$\lim_{\mu\to 0}\int_0^\infty e^{-\mu r}\ln|r-r_1|\cos(kr)\,dr$$
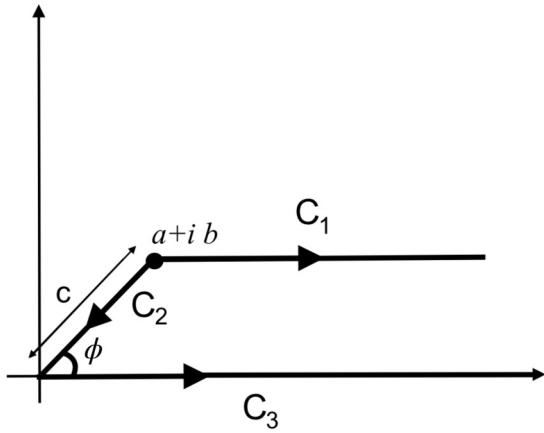$$= \frac{1}{k}[\text{fi}(kr_1) - \pi\cos(kr_1)]. \tag{83}$$

FIG. 2. The contours used in (84) and (85). Here, $a + ib = ce^{i\phi}$ in terms of the constant $c = \sqrt{a^2 + b^2}$ and $\phi = \arctan(b/a)$.

Here μ is an infrared regulation scale whose role in the physical problem is played by $1/L$ and $1/\ell_K$. Since the results for $\mu \ll k$ do not depend upon the particular regularization adopted, however, we chose the above exponential IR cutoff for mathematical convenience. The key idea in the evaluation of the first integral (82) was to realize that the two integrands, $\frac{1}{2} \log[(r + a)^2 + b^2]$ and $\arctan(\frac{b}{r+a}) = \frac{\pi}{2} - \arctan(\frac{r+a}{b})$, are the real and imaginary parts, respectively, of $\ln(r + a + ib)$ and the combined integral may thus be expressed as the contour integral of analytic functions $\ln z \, \cos(kz)$, $\ln z \, \sin(kz)$ along the path C_1 in the complex plane which is illustrated in Fig. 2. A convenient change of the contour allows us to reduce the integral to standard formulas, which we explain in more detail below. The second integral (83) is simpler and will be discussed briefly at the end.

The first integral (82), which we call I_1, can be directly written as the following complex contour integral:

$$I_1 = \lim_{\mu \to 0} \int_{C_1 : \mathbb{R}^+ + a + ib} dz \, e^{-\mu z} \ln z$$
$$\times [\cos(kz) \cos(k_\phi c) + \sin(kz) \sin(k_\phi c)], \quad (84)$$

where $k_\phi := k e^{i\phi}$ and $\phi = \arctan(b/a)$, noting that $a + ib = ce^{i\phi}$. Because the integrand is analytic in the complex plane with a branch cut along the negative real axis, the integration contour can be shifted to $C_2 + C_3$ as illustrated in Fig. 2. This yields directly

$$I_1 = \frac{-1}{c} \int_0^c dr [(a \ln r - b\phi) + i(b \ln r + a\phi)]$$
$$\times [\cos(k_\phi r) \cos(k_\phi c) + \sin(k_\phi r) \sin(k_\phi c)]$$
$$+ \lim_{\mu \to 0} \int_0^\infty dr \, e^{-\mu r} \ln r$$
$$\times [\cos(k_\phi r) \cos(k_\phi c) + \sin(k_\phi r) \sin(k_\phi c)]. \quad (85)$$

The first of these integrals resulting from contour C_2 can now be evaluated using [92], formulas 1.5(1) and 2.5(1), while the second integral resulting from contour C_3 can be evaluated

using [92], formulas 1.5(6) and 2.5(7), giving

$$I_1 = \frac{1}{k} \Big[\Big(\text{Si}[k(a + ib)] - \frac{\pi}{2} \Big) \cos[k(a + ib)]$$
$$+ (\text{Cin}[k(a + ib)] - \gamma - \ln[k(a + ib)]) \sin[k(a + ib)] \Big].$$

Here we use the trigonometric integral functions $\text{Si}(z)$ and $\text{Cin}(z)$ with also $\text{Cin}(x) = \gamma + \ln(x) - \text{Ci}(x)$ where γ is the Euler-Mascheroni constant (see [90], Sec. 5.2; [91], Chap. 38; or [93], Sec. 9.8). Finally, a standard formula

$$\text{fi}(z) = \text{Ci}(z) \sin(z) + \Big(\frac{\pi}{2} - \text{Si}(z) \Big) \cos(z), \quad (86)$$

for the auxiliary sine integral function [see [90] (formula 5.2.6) or [91] (formula 38:13:7)] yields (82).

The second integral (83) can be straightforwardly decomposed into two contributions for $r < r_1$ and $r > r_1$:

$$\lim_{\mu \to 0} \int_0^\infty e^{-\mu r} \ln |r - r_1| \cos(kr) \, dr$$
$$= \int_0^{r_1} \ln r \, \cos[k(r - r_1)] \, dr$$
$$+ \lim_{\mu \to 0} \int_0^\infty e^{-\mu r} \ln r \, \cos[k(r + r_1)] \, dr. \quad (87)$$

The part for $r < r_1$ can be evaluated as

$$\int_0^{r_1} \ln r \, \cos[k(r - r_1)] \, dr$$
$$= \frac{1}{k} \ln r_1 \sin(kr_1)$$
$$- \frac{1}{k} [\text{Si}(kr_1) \cos(kr_1) + \text{Cin}(kr_1) \sin(kr_1)] \quad (88)$$

using $\cos[k(r - r_1)] = \cos(kr) \cos(kr_1) + \sin(kr) \sin(kr_1)$ and [92], formulas 1.5(1) and 2.5(1), while the part for $r > r_1$ can be evaluated as

$$\lim_{\mu \to 0} \int_0^\infty e^{-\mu r} \ln r \, \cos[k(r + r_1)] \, dr$$
$$= \frac{1}{k} (\gamma + \ln k) \sin(kr_1) - \frac{\pi}{2k} \cos(kr_1) \quad (89)$$

using $\cos[k(r + r_1)] = \frac{1}{2} (e^{ik(r+r_1)} + e^{-ik(r+r_1)})$ and[2]

$$\int_0^\infty e^{-zr} \ln r \, dr = -\frac{\gamma + \ln z}{z}, \quad \text{Re } z > 0. \quad (90)$$

---

[2]This result can be obtained, in principle, by combining two results in [92], formulas 1.5(6) and 2.5(7). Note, however, that there is a typographical error in the second of these formulas and, in fact, a surprising number of misprints for these formulas in standard sources. Thus, in [92], formula 2.5(7), the quantity $\tan^{-1}(C/\alpha)$ should instead be $\tan^{-1}(y/\alpha)$. Likewise, in [134], formula 4.441(1), $\ln(p^2 - q^2)$ should instead be $\ln(p^2 + q^2)$. Finally, in [92], formula 4.6(1), $\log(\gamma p)$ should instead be $\gamma + \log p$. The correct result can be easily obtained from the standard integral for Euler's Γ function

$$\int_0^\infty e^{-zt} t^{s-1} dt = \Gamma(s)/z^s, \quad \text{Re } z > 0$$

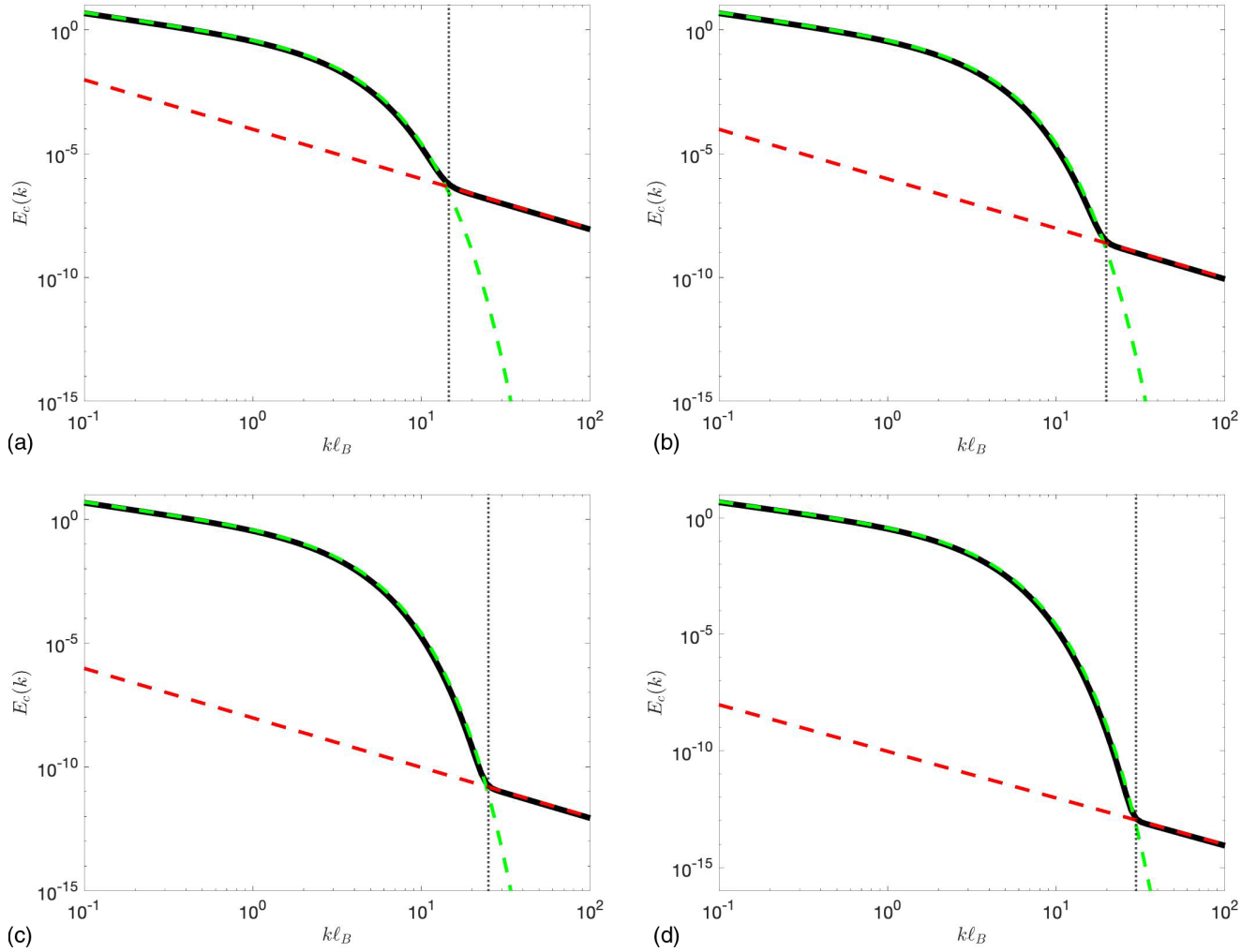by differentiating both sides with respect to s and setting $s = 1$.

FIG. 3. Plots of the exact solution for the concentration spectrum $E_c(k)$ with (a) $\epsilon = 10^{-4}$, (b) $\epsilon = 10^{-6}$, (c) $\epsilon = 10^{-8}$, (d) $\epsilon = 10^{-10}$. The solid black line (—) is the exact result from (78)–(80), the green dashed line (- - -) is Kraichnan's spectrum (92), and the red dashed line (- - -) is the power-law spectrum (93) associated to GCF's. The vertical gray dotted line marks the prediction in (70) for the transition wave number k_{tr}.

Combining the two parts and again using (86) yields the second integral (83).

2. Model spectrum for $1/\ell_K \ll k \ll 1/\sigma$

We now consider the limits of our exact solution (78)–(80) in the viscous-convective and viscous-diffusive ranges. First, however, we verify that our solution recovers the result of Kraichnan [25] when setting $\sigma = 0$. In this case, $a = \frac{1}{2}r_1 = 0$, $b = \ell_B$, $\mathcal{A} = 1$, $\mathcal{B} = \frac{1}{2}$, $\mathcal{C} = 0$, and

$$F(k) = \frac{\chi}{3\pi\Gamma} \frac{\mathrm{Re}(\mathrm{fi}(ik\ell_B))}{k} = \frac{\chi}{6\Gamma} \frac{e^{-k\ell_B}}{k} \qquad (91)$$

using definition (81) of $\mathrm{fi}(z)$ and [92], formula 1.2(11). The standard concentration spectrum obtained from (76) then reproduces exactly the result of Kraichnan

$$E_c(k) = \frac{\chi}{6\Gamma} \left(\frac{1}{k} + \ell_B \right) e^{-k\ell_B} \quad (\sigma = 0). \qquad (92)$$

See Eqs. (2.27) and (5.14) in [25]. Note that in terms of the notations used in Kraichnan's original work, his constants A, $\langle a \rangle$, α, and κ are related to our constants as $\Gamma = A/30 = \langle a \rangle/6$

and $\ell_B^2 = 2\alpha^2 = 30\kappa/A$, with his bare diffusivity κ replaced by our renormalized diffusivity D. We recover also (2) in the Introduction if, following [24], we introduce $C_B = \gamma/6\Gamma$ and if the Batchelor length is redefined in the more conventional way as $\ell_B := (D/\gamma)^{1/2} = (D/6C_B\Gamma)^{1/2}$.

The result of Batchelor for the concentration spectrum in the viscous-convective range can be recovered, however, when $k\ell_B \ll 1$ for all finite σ without taking the limit $\sigma = 0$. This result follows from our exact solution (78)–(80) using $\mathrm{fi}(0) = \pi/2$, which gives

$$F_{\mathcal{A}}(k) \simeq (\chi/6\Gamma)\mathcal{A}k^{-1}, \quad F_{\mathcal{C}}(k) \simeq (\chi/6\Gamma)\mathcal{C}k^{-1}$$

and $F_{\mathcal{B}}(k) \simeq o(1/k)$. Using $\mathcal{A} + \mathcal{C} = 1$ we obtain in general $F(k) = (\chi/6\Gamma)k^{-1}$ so that

$$E_c(k) \simeq (\chi/6\Gamma)k^{-1} = C_B(\chi/\gamma)k^{-1}, \quad k\ell_B \ll 1$$

in agreement with (1) and (64). As already emphasized, the Batchelor spectrum in the viscous-convective range is unaltered by the sub-Kolmogorov scale thermal velocity fluctuations.

The behavior of our model in the viscous-diffusive range for small finite σ, on the other hand, is completely different than that obtained by Kraichnan for $\sigma = 0$. The limit $1/\ell_B \ll k \ll 1/\sigma$ of our exact solution (78)–(80) can be obtained from the standard asymptotic expansion of fi(z) for large arguments z. We are further interested in the limit $\epsilon = \sigma/\ell_B \ll 1$, so that

$$a = \tfrac{1}{2}r_1 = \tfrac{3}{4}\sigma[1 + O(\epsilon)], \quad b = \ell_B[1 + O(\epsilon^2)]$$

and

$$\mathcal{A} = 1 + O(\epsilon^2), \quad \mathcal{B}r_1/b = \tfrac{3}{4}\epsilon + O(\epsilon^3), \quad \mathcal{C} = O(\epsilon^2).$$

In that case, the contributions to $F(k)$ at leading order in ϵ are obtained from

$$\mathrm{Re}(\mathrm{fi}(k(a+ib))) \simeq -ka\,\mathrm{Re}(\mathrm{gi}(ik\ell_B)) + O(\epsilon^2)$$

and

$$\mathrm{Im}(\mathrm{fi}(k(a+ib))) \simeq \mathrm{Im}(\mathrm{fi}(ik\ell_B)) + O(\epsilon),$$

where we have introduced the auxiliary cosine integral function $\mathrm{gi}(z) = -\mathrm{fi}'(z)$. Invoking the asymptotic expansions $\mathrm{fi}(z) \sim 1/z$ and $\mathrm{gi}(z) \sim 1/z^2$ at large arguments z satisfying $|\arg z| < \pi$ [90], 5.2.34 and 5.2.35, and [91], 38:13:10 and 38:13:11, we then obtain

$$F_{\mathcal{A}}(k) \simeq F_{\mathcal{B}}(k) \simeq \frac{\chi\sigma}{4\pi\Gamma}k^{-2}\ell_B^{-2}, \quad F_{\mathcal{C}}(k) \simeq 0$$

and finally

$$E_c(k) \simeq \frac{\chi\sigma}{\pi D}k^{-2}, \quad 1/\ell_B \ll k \ll 1/\sigma. \tag{93}$$

Thus, we confirm the spectrum (66) with k^{-2} power law associated to giant concentration fluctuations.

The effect of varying $\epsilon = \sigma/\ell_B$ can be illustrated by plotting our exact solution over a range of possible values (see Fig. 3). For details of the numerical method used in constructing the plots, see Appendix E. The first observation from the figure is that the spectrum $E_c(k)$ given by (78)–(80) is almost perfectly represented, on the log-log scale of the plots, by the superposition of the Kraichnan spectrum (92) and the power-law spectrum (93), with transition at the wave number k_{tr} predicted by (70). The second conclusion is that the Kraichnan exponential decay spectrum will generally exist for only a very narrow range of wave numbers with $k\ell_B \gtrsim 1$. From a review of the past experiments on turbulent high Schmidt mixing, we find that the ratio $\epsilon = \sigma/\ell_B$ ranges over values between 10^{-4} and 10^{-7}. In the latter extreme case, $k_{tr}\ell_B = 22.3$ and the Kraichnan spectrum exists over just a bit more than a decade of wave numbers. However, even if one considers a very unrealistic value $\epsilon = 10^{-10}$, then $k_{tr}\ell_B = 29.8$ and the extent of the Kraichnan spectrum is barely increased. These considerations suggest that an exponential decay of the concentration spectrum will generally hold in physical fluid mixtures for at most a decade of wave numbers in the viscous-diffusive range.

IV. PHYSICAL PREDICTIONS

We now develop concrete predictions of our theory for two specific binary mixtures: water-glycerol and water-fluorescein. We note that water-glycerol solutions are very commonly employed in fluid turbulence experiments as a means to vary the viscosity by changes in concentration, e.g.

see [57,94]. Giant concentration fluctuations have also been seen experimentally in water-glycerol solutions by a variety of observational techniques [44,95–97]. For prior experiments on the turbulent Batchelor regime, solutions of disodium fluorescein (or, in shorthand, fluorescein) in water have been popular [28,33,34,98] because of the ease of visualization by laser fluorescence. It is worth emphasizing that the Stokes-Einstein relation for the diffusivity is observed to be valid for both mixtures, water-glycerol [99,100] and water-fluorescein [89,101], at sufficiently high temperatures well above the glass transition. The measured hydrodynamic radii in water are $\sigma = 0.35$ nm for glycerol [100] and $\sigma = 0.50$ nm for fluorescein [101], relatively consistent with the molecular volumes. Since the molar masses of water (H_2O), glycerol ($C_3H_8O_3$), and disodium fluorescein ($C_{20}H_{12}Na_2O_5$) are 18.0 g/mol, 92.1 g/mol, and 376.3 g/mol, respectively, the hydrodynamic Stokes-Einstein prediction should be expected to be even more accurate for the water-fluorescein mixture. Our predictions can be easily extended to other binary mixtures.

Before we can discuss our detailed predictions, however, we must first discuss the equilibrium fluctuations of the concentration which we have so far ignored. As is well known, the fluctuations in thermal equilibrium correspond to the structure function (4) given by

$$S_{cc}(k) = \frac{k_B\overline{T}}{\overline{\rho}(\partial\mu/\partial\overline{c})_{\overline{T},\overline{p}}}, \tag{94}$$

which is independent of wave number k, where $\overline{\rho}$, $\overline{c}$, etc., are the mean values in the equilibrium state and $\mu(T, p, c)$ is the chemical potential of the mixture for given temperature T, pressure p, and mass concentration c. See [50], Eq. (5.34), and references therein. At the hydrodynamic level of description, these fluctuations are due to the molecular noise term in Eq. (12) for concentration, whose general form is

$$\partial_t c = -\mathbf{u}\cdot\nabla c + \nabla\cdot\left(D_0\nabla c + \sqrt{\frac{2D_0}{\rho(\partial\mu/\partial c)_{T,p}}}\,\eta_c(\mathbf{x},t)\right) \tag{95}$$

(see [50,69,70,72]). In the prior discussion, following DFV [56] and [102], we have considered for simplicity the special case of an ideal solution of two equal-mass molecules, e.g., the self-diffusion of tagged particles in a single-component fluid. In this setting, we provide in Appendix A a self-contained derivation of (94) from (95), as a convenience for readers. It is important to note, however, that the high Schmidt asymptotics of DFV in Appendix B can be carried out for the general equation (95) and does not require the special assumptions of (12).

The structure function (94) corresponds to a scalar spectrum

$$E_c(k) = \frac{k_B\overline{T}}{4\pi^2\overline{\rho}(\partial\mu/\partial\overline{c})_{\overline{T},\overline{p}}}k^2. \tag{96}$$

This equilibrium spectrum is growing in wave number and it must thus exceed the spectrum (66) of the nonequilibrium fluctuations above some sufficiently high-transition wave number, which we call k'_{tr}. We can estimate the latter by
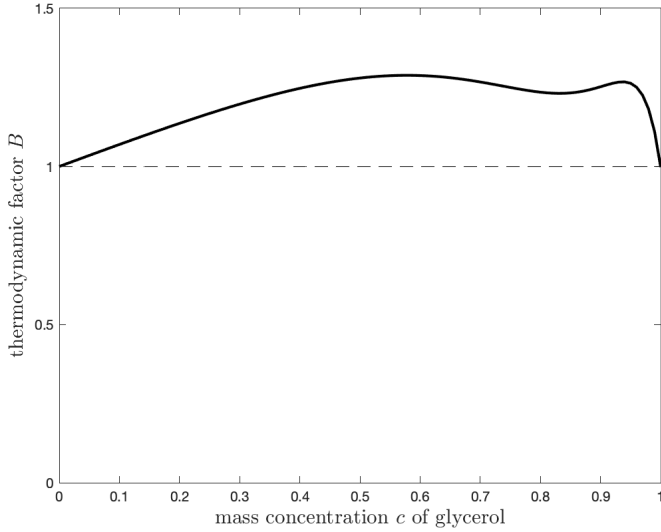
FIG. 4. The nonideality factor B for a water-glycerol solution, from [103] [Eq. (11)], plotted versus mass concentration of glycerol.

equating the two spectra, which yields

$$k'_{tr} = \left[\frac{4\pi \chi \sigma}{D k_B T} \left(\frac{\partial \mu}{\partial c} \right)_{T,p} \right]^{1/4}. \qquad (97)$$

To make a quantitative determination of k'_{tr}, we must evaluate the derivative of the chemical potential. For this purpose, we note the general result

$$\left(\frac{\partial \mu}{\partial c} \right)_{T,p} = \frac{B \cdot k_B T}{c(1-c)[m_0 c + m_1(1-c)]}, \qquad (98)$$

where m_0 is the molecular mass of the solute (water), m_1 is the molecular mass of the solvent (glycerol/fluorescein), and $B = B(T, p, c)$ is a factor which accounts for the nonideality of the mixture, with $B \equiv 1$ in the ideal case. See Appendix F for the derivation of this equilibrium thermodynamic result. In addition, estimation of k'_{tr} requires the diffusion coefficient D.

For water-glycerol solutions at temperature $25\,°C$ and at atmospheric pressure (1 bar) experimental values of both quantities D and B are conveniently provided by the paper [103], in parametrized form as functions of the molar concentration n. We plot in Fig. 4 the factor B versus mass concentration c, where it can be observed that the deviation from ideality is at most about 28.8%. Because of the detailed information provided in [103], we shall present our results for the concentration spectrum of water-glycerol solutions at $T = 25\,°C$ and $p = 1$ bar. For water-fluorescein we shall use the value of diffusivity $D = 5.54 \times 10^{-6}$ cm^2/s at $T = 30\,°C$ and $p = 1$ bar reported in [101]. There has not been much experimental investigation of thermodynamic properties of water-fluorescein solutions and we are unaware of any measurements of the nonideality factor B for that mixture. Here we may remark that the thermodynamics and diffusive transport of an electrolyte such as disodium fluorescein in water may be treated as a binary mixture, at least at not too low concentrations (see [104], Chap. 8). In the lack of precise information, one may simply take $B \equiv 1$. In fact, the deviations from ideality must be much larger for water-fluorescein than for water-glycerol because the differences between water and

fluorescein molecules and their interactions are considerable. However, B is unlikely to be orders of magnitude different from unity and, since it appears in formula (97) to the $\frac{1}{4}$ power, setting $B \equiv 1$ should result in just slight inaccuracy of k'_{tr}.

Before presenting any concrete predictions, we must first note an important consequence of the equipartition spectrum (96). It is easily seen that the concentration gradients become dependent upon the UV cutoff Λ which is necessary for the validity of the fluctuating hydrodynamic equation (95). See Appendix A for a discussion of this point. The concentration gradient develops a large contribution, diverging with Λ, of the form

$$\langle |\nabla c|^2 \rangle = 2 \int_0^\Lambda dk \, k^2 E_c(k) \simeq \frac{2}{5} A \Lambda^5, \qquad (99)$$

where $A = \frac{k_B \overline{T}}{4\pi^2 \overline{\rho}(\partial \mu / \partial c)_{\overline{T},\overline{p}}}$ is the constant prefactor in the equipartition spectrum (96). Note that the estimate of the "effective gradient" $\nabla \bar{c}_\ell$ from Eq. (67) ignored this contribution and is valid only if the filtering scale ℓ is chosen so that $\ell k_\nabla \gtrsim 1$ with $\frac{2}{5} A k_\nabla^5 := (\nabla c)_{\text{eff}}^2 = \chi/D$. It is easy to check from this condition that

$$k_\nabla / k'_{tr} \simeq 1/(k'_{tr}\sigma)^{1/5} \gtrsim 1, \qquad (100)$$

and thus it will suffice to choose $k'_{tr}\ell \gtrsim 1$ (and $\ell \lesssim \ell_B$) to ensure that $\nabla \bar{c}_\ell \simeq (\nabla c)_{\text{eff}}$.

We first present our predictions for possible future experiments on turbulent mixing with water-glycerol. In addition to the thermodynamic parameters of the mixture, discussed above, the two important parameters of the turbulent flow which must be specified are the Kolmogorov turnover rate γ and the rate of injection χ of concentration fluctuations. To identify reasonable ranges for these parameters, we reviewed a set of experimental studies of high Schmidt turbulent mixing [27,28,30,32–34]. Extracting data from these references, we found a range of values within the intervals 0.1 s$^{-1} \leqslant \gamma \leqslant 10^2$ s^{-1} and 10^{-12} s$^{-1} \leqslant \chi \leqslant 10^2$ s^{-1}, on order of magnitude (see Appendix G). None of these experiments studied water-glycerol mixtures, but recent laboratory experiments on fluid turbulence in water-glycerol [57] had $\gamma \doteq 129$ s^{-1}, near the upper range from the experiments on turbulent mixing. We therefore plot our predictions in Fig. 5 for $\gamma = 10$ s^{-1} and in Fig. 6 for $\gamma = 100$ s^{-1}, which are values typical of most of the cited experiments. We also show for both of these choices of γ, three values of χ, the smallest value from the cited experiments $\chi = 10^{-12}$ s^{-1}, the largest value $\chi = 10^2$ s^{-1}, and one intermediate value. We note that in all of our plots the highest wave number considered is well below the value $k_\sigma = 2\pi/\sigma$, which is $\doteq 1.8 \times 10^8$ cm^{-1} for water-glycerol, and thus within the regime of validity of our theory.

The solid curves plotted in Figs. 5 and 6 are our predicted concentration spectra $E_c(k)$, obtained simply as the maximum of the exact solution from (76)–(80) and of the equipartition k^2 spectrum (96). We plot the two curves also individually, the exact solution of our model and the equilibrium spectrum, as black dotted lines, and we indicate the Batchelor wave number $k_B = 2\pi/\ell_B$ by a vertical green dashed line. The most important conclusion from these plots is that, except for very small values of injection rate χ, a few decades of GCF's with spectrum $E_c(k) \sim k^{-2}$ should occur. With decreasing
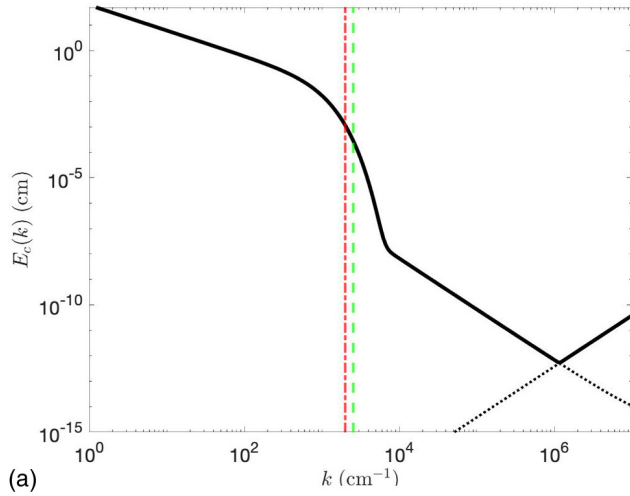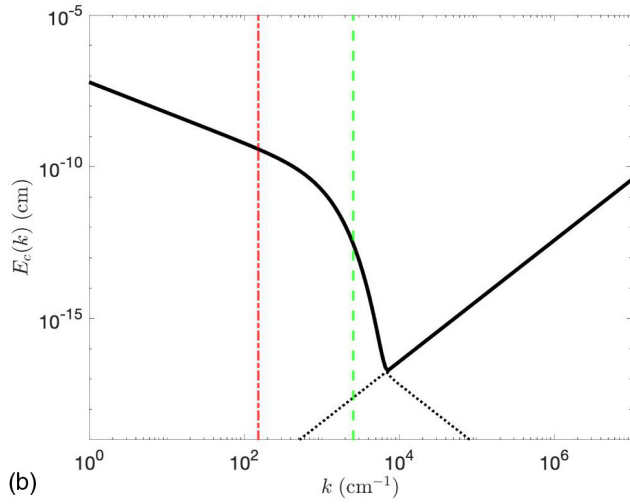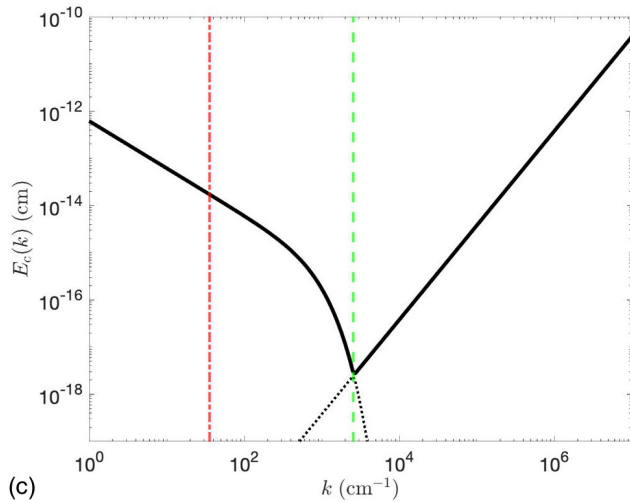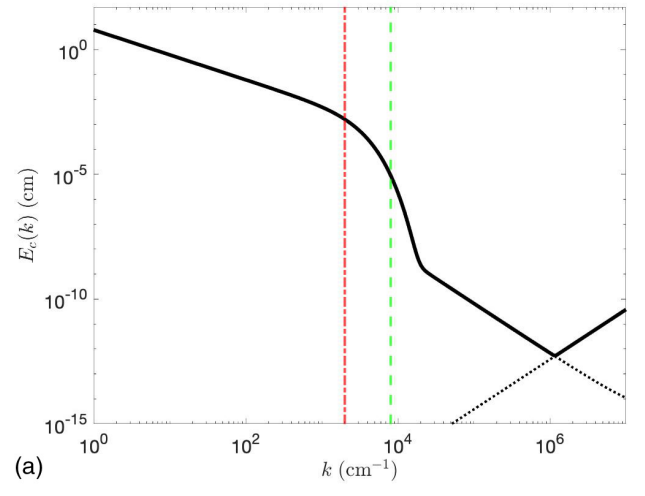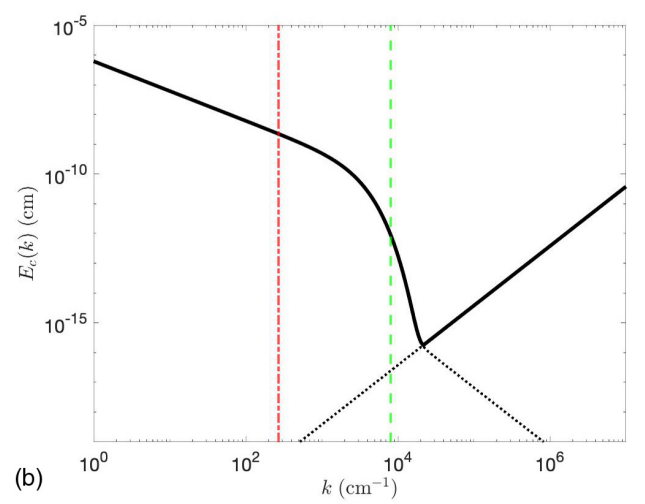
FIG. 5. Plots of the predicted concentration spectrum for water-glycerol mixture ($T = 25\,^\circ$C, $p = 1$ bar, $\bar{c} = 0.5$) with $\gamma = 10$ s^{-1} and (a) $\chi = 10^2$, (b) $\chi = 10^{-7}$, (c) $\chi = 10^{-12}$ s^{-1}. The green dashed line (- - -) marks the Batchelor wave number k_B, and the red dotted-dashed line (- · -) represents buoyancy cutoff wave number k_g.
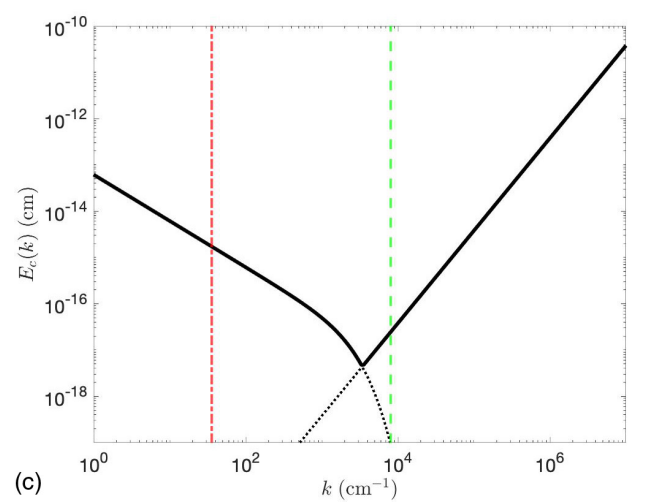

FIG. 6. Similar to Fig. 5 but with $\gamma = 100$ s^{-1} and (a) $\chi = 10^2$ s^{-1}, (b) $\chi = 10^{-5}$ s^{-1}, (c) $\chi = 10^{-12}$ s^{-1}.

χ the statistics of the concentration field become closer to equilibrium and the equipartition k^2 spectrum dominates at increasingly smaller wave numbers. In our plots the interme-

diate value of χ is chosen just small enough so that the range of GCF's entirely disappears, which is $\chi = 10^{-7}$ for $\gamma = 10$ in Fig. 5 and $\chi = 10^{-5}$ for $\gamma = 100$ in Fig. 6. Although these values lie within the range of those sampled in prior studies, most experiments have larger χ and thus correspond to the

upper panels (a) in Figs. 5 and 6. We can thus expect that future laboratory experiments with choices of parameters χ and γ similar to those accessed in prior experiments will exhibit a sizable range of power-law spectra k^{-2} associated to GCF's, appearing just above the Batchelor wave number. With smaller χ the range of GCF's may be very short or disappear entirely, replaced by the equipartition k^2 spectrum, but, in either case, Kraichnan's exponential decay spectrum (2) will exist over only a very narrow range.

In the typical case where a range of CGF's exists below the Batchelor length, these long-range nonequilibrium correlations are quenched in our theory by turbulent shear. This shear quenching is similar to that predicted for weak perturbations of global thermodynamic equilibrium by Wada [58], but, of course, much stronger. Whereas the analysis in [58] could rely on linearized fluctuating hydrodynamics, our solution for turbulent shear requires the asymptotic method of DFV, which treats exactly the nonlinear advection of the concentration field by both turbulent and thermal velocity fluctuations. We note that the effect of increasing γ, with other parameters fixed, is to decrease the Batchelor length scale and to reduce the range of wave numbers where GCF's appear. This effect is seen clearly by comparing the top panels (a) of Fig. 5 for $\gamma = 10$ and of Fig. 6 for $\gamma = 100$, where the sole effect is to increase k_B and push the GCF's to a higher, narrower range of wave numbers.

Since we could not include buoyancy in our exact mathematical analysis, there remains the possibility that gravity (or finite system size) could quench the GCF's rather than shear, as is typical for laminar experiments [59]. Because of the much stronger shear in fluid turbulence compared with laminar flow, one may expect that shear will in fact be dominant. However, it is useful to make some test of this reasonable conjecture, by considering the gravitational wave-number cutoff

$$k_g = (\beta g \nabla c / \nu D)^{1/4}, \tag{101}$$

below which $S_{cc}(k) \sim k^0$ and $E_c(k) \sim k^2$ according to linearized theory. Here $\beta = \frac{1}{\rho} \frac{\partial \rho}{\partial c}$ is the solutal expansion coefficient and g is the acceleration due to gravity. See [23,105,106] for detailed discussion, but note that the result (101) follows intuitively by equating the damping rates from diffusion and buoyancy as $\gamma_{\text{diff}} = Dk^2 \sim \gamma_{\text{grav}} = \beta g \nabla c / \nu k^2$. The theory of DFV makes clear how this estimate for γ_{grav} arises because Eq. (A.27) in [56] shows that buoyancy adds the extra term

$$(\beta / \nu)(\mathbf{G}_\sigma \star c)\mathbf{g} \cdot \nabla c \tag{102}$$

to the right-hand side of the asymptotic high Sc equation (41) for the concentration field. Here $\mathbf{G}_\sigma = \boldsymbol{\sigma} \star \mathbf{G}$ is convolution of smoothing kernel $\boldsymbol{\sigma}$ with the Oseen tensor $\mathbf{G}$ [see (20) and Appendix B]. To make use of expression (101) in a forced steady state with continuous injection of concentration fluctuations, we employ the root-mean-square (rms) gradient from the balance $\chi = D \langle |\nabla c|^2 \rangle$, which yields

$$k_g = (\beta^2 g^2 \chi / \nu^2 D^3)^{1/8}. \tag{103}$$

We shall adopt this estimate below, but note that balancing the buoyancy term (102) against the diffusive term $D_{\text{eff}} \triangle c$ in (41) leads to the much smaller value $k_g' = (\beta^2 g^2 \chi / \nu^2 D_{\text{eff}}^3)^{1/8} \ll$
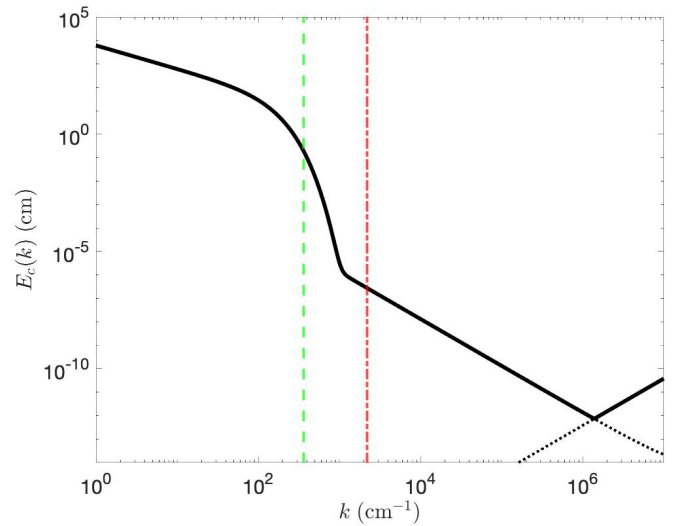

FIG. 7. Predicted concentration spectrum for water-glycerol ($T = 25\,^\circ\text{C}$, $p = 1$ bar, $\bar{c} = 0.5$) for the largest scalar injection rate and smallest strain rate observed in the experiments available to us; $\chi \simeq 2 \times 10^2$ s^{-1} [28], $\gamma \simeq 0.2$ s^{-1} [30]. With these extreme values, buoyancy (red dotted-dashed line) might conceivably cut off the k^{-2} power-law spectrum associated to GCF's. Green dashed line marks the Batchelor wave number k_B.

k_g because the effect of turbulent diffusivity implies $D_{\text{eff}} \simeq D_T \gg D$. Thus, using (103) probably greatly overestimates the effect of gravity.

The wave number k_g is marked in Figs. 5 and 6 by the vertical red, dotted-dashed line. To calculate (103) we used the following convenient parametrizations of the solutal expansion coefficient and kinematic viscosity of water-glycerol solutions as functions of concentration:

$$\beta = 0.2246 + 0.1c - 0.125c^2,$$
$$\nu = 0.01 \exp(2.06c + 2.32c^2) \tag{104}$$

(see [107]). It can be seen immediately that $k_g < k_B$ in all cases shown, which implies that the GCF's for typical values of γ and χ are cut off by turbulent shear rather than by buoyancy. To investigate a possible role for gravity one must consider γ as small as realistic since $k_B \propto \gamma^{1/2}$. Furthermore, one should consider large χ because $k_g \propto \chi^{1/8}$ according to (103). Note that also $k_{tr} \propto \chi^{1/4}$ according to (97), so that increasing χ in addition increases the wave-number range of the GCF's. In Fig. 7 we plot our predicted concentration spectrum for the smallest value $\gamma \simeq 0.2$ s^{-1} [30] and the largest value $\chi \simeq 2 \times 10^2$ s^{-1} [28] that we found in reported experiments on the Batchelor range. With these extreme choices we see that $k_g > k_B$, so that gravitational effects may possibly in this case quench the GCF's rather than turbulent shear. Of course, considering the effects of turbulent diffusivity D_T gives $k_g' \ll k_g$ and thus buoyancy effects even in this extreme parameter range are in fact probably small compared with turbulent shear effects.

Finally, we shall consider the predictions of our theory for water-fluorescein solutions since this fluid mixture has been the choice of most recent experimental studies on high Schmidt turbulent mixing [28,33,34,98]. For specificity, we
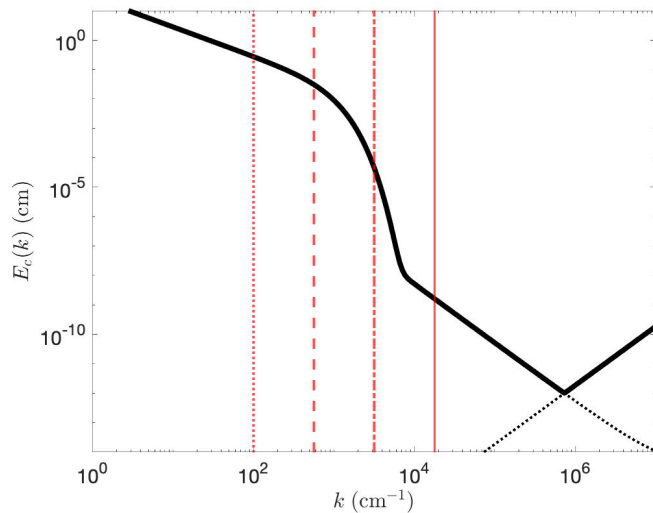
FIG. 8. Predicted concentration spectrum for water-fluorescein ($T = 30\,^\circ$C, $p = 1$ bar). The buoyancy cutoff wave number k_g is marked with vertical lines for $\beta g = 10^3$ G (—), 1 G (- · -); 10^{-3} G (- - -) and 10^{-6} G (· · ·) in units of Earth gravitational acceleration 1 G = 980 cm/s^2. Here, $\gamma \simeq 7.8$ s^{-1} and $\chi \simeq 2 \times 10^2$ s^{-1} corresponding to the experimental parameters in [28].

take $\gamma \simeq 7.8$ s^{-1} and $\chi \simeq 2 \times 10^2$ s^{-1} from the experiment of Jullien *et al.* [28]. One difficulty in making concrete predictions arises from the poor state of knowledge about the thermodynamic properties of water-fluorescein mixtures; in particular, the solutal expansion coefficient β seems not to be available in the literature. Fortunately, the real parameter of interest is the combination βg, in which g may be lowered by performing low-gravity space experiments or increased by centrifugal effect in a rapidly rotating apparatus. Thus, we present results in Fig. 8 on our predicted spectrum for water-fluorescein mixture at $T = 30\,^\circ$C, $p = 1$ bar, for different values of the quantity βg in units of the acceleration due to Earth gravity (1 G $\simeq$ 980 cm/s^2). We expect β to be of order unity (e.g., for water-glycerol $\beta \simeq 0.20$–0.25), so that the values $\beta g = 10^{-6}$, 10^{-3}, 1, 10^3 G considered in Fig. 8 are probably close to the corresponding values of g. Most importantly, we see that there are at least two decades of k^{-2} power law arising from GCF's appearing just above the Batchelor wave number k_B. Furthermore, turbulent shear effects cut off the GCF's for wave numbers lower than k_B, except possibly for $\beta g \geqslant 40$ G, where buoyancy could provide the cutoff, but such large βg would be difficult to achieve experimentally. We want to emphasize that in the actual experiment reported in [28], the concentration fluctuations were strongly damped at wave numbers $k > 7$ cm^{-1} because of additional shear-enhanced diffusion, and the range above that wave number in their setup would not be described by our theory. However, in an ideal experiment with the same values of γ and χ as [28] but avoiding such enhanced diffusion, a k^{-2} spectrum due to GCF's would appear at lengths just below $\ell_B \simeq 22.4\ \mu$m.

V. DISCUSSION AND CONCLUSIONS

Our theoretical predictions clearly demand empirical verification. As already discussed, the prospects for direct

laboratory experiments appear remote because our predictions all involve scales below the Batchelor length. Since $\ell_B \ll \ell_K$ and it is already difficult to get reliable experimentable measurements in the turbulent dissipation range, the difficulties are much more severe for the viscous-diffusive range. Even in the viscous-convective range the Batchelor spectrum $\propto k^{-1}$ has not been observed in some experiments [33,34]. Among experiments which report a Batchelor spectrum [27,28,30–32], only the first [32] reported any measurements in the viscous-diffusive range. That experiment measured fluctuations of both temperature and concentration in salt water and had Batchelor lengths from 14.8–82.5 μm. Nevertheless, the data in [32] (Fig. 9) for the viscous-diffusive range had large scatter and the authors cautioned that "the high wave-number data may have been affected by noise and/or spatial resolution." It is precisely because of these grave experimental difficulties that most modern studies have turned to numerical simulations of deterministic Navier-Stokes equations [35–38], which have verified the Kraichnan-Batchelor predictions in that setting. Likewise, the prospects for verification of our predictions by numerical simulations of Landau-Lifshitz fluctuating hydrodynamics appear excellent since codes have been developed to simulate binary and multicomponent mixtures at low Mach numbers [69,70], especially an overdamped scheme appropriate to high Schmidt numbers [70]. Ultimately, of course, laboratory experiments will be absolutely essential to determine which of the various theoretical predictions are correct in Nature.

In addition to empirical studies, our work suggests many interesting further theoretical investigations within the DFV approach. Here we have studied only the second-order correlation function and the Fourier spectrum of the concentration field in a forced steady state with injection of scalar fluctuations, but many further generalizations are possible. Techniques exist in the Kraichnan model to study higher-order correlations [40,83–85] and even individual realizations of the concentration field [85,108]. Multitime correlations such as $C(\mathbf{x}, t; \mathbf{x}', t') := \langle c(\mathbf{x}, t) c(\mathbf{x}', t') \rangle$ satisfy also closed equations in the Kraichnan model

$$\partial_t C(\mathbf{x}, t; \mathbf{x}', t')$$
$$= \nabla_\mathbf{x} \cdot \left[\left(D_0 + \frac{1}{2} \boldsymbol{\mathcal{V}}(\mathbf{x}, \mathbf{x}) \right) \cdot \nabla_\mathbf{x} C(\mathbf{x}, t; \mathbf{x}', t') \right] \quad (105)$$

for $t > t'$, as a direct consequence of (44). Note that this equation expresses the temporal relaxation of fluctuations by the renormalized diffusivity. In addition to the statistical steady state, free decay can be studied also in the Kraichnan model [86,109]. This is an important problem for further theoretical study because striking experimental observations of giant concentration fluctuations have been made in transient decay [43,96]. The current analytical theory of this problem is based on linearized fluctuating hydrodynamics [106], but systematic deviations are observed between linearized theory and experiment at early times when concentration gradients are very large (see [96], Fig. 8). The DFV approach is not based on linearization and treats nonlinear advection of concentration exactly, even if gradients are large.

Aside from analytical theory, the DFV approach yields also an efficient numerical scheme to solve fluctuating hydrody-

namics of binary mixtures in the asymptotic limit of high Schmidt numbers. As emphasized in their original work [56], numerically solving the high Schmidt limit equations (17) and (21) is more efficient by a factor of Sc than solving the standard equations of fluctuating hydrodynamics (9) and (12). Unlike our analytical approach, the numerical implementation of the DFV limit equations has no difficulty incorporating buoyancy effects of gravity (see [56], Appendix A). A certain puzzle does exist why DFV failed to observe $S_{cc}(k, t) \sim k^{-4}$ in numerical simulation of free diffusive mixing with their high Sc limit equations (17) and (21), but instead reported a scaling closer to $S_{cc}(k, t) \sim k^{-3}$. This is curious because experiments [43,96] and numerical simulations with the full fluctuating hydrodynamics equations [15,69] both yield $S_{cc}(k, t) \sim k^{-4}$ for free decay, as does our exact solution of the DFV correlation equations for the forced steady state. These various results suggest that the DFV theory should yield also such a k^{-4} scaling for free decay. It has been suggested to us by Donev [110] that the k^{-3} scaling reported in [56] might be due to the fact that those numerical simulations were performed for a 2D fluid. However, we have now solved the closed equations of the DFV theory in 2D, for steady-state concentration correlations with random injection of fluctuations and with velocity in thermal equilibrium. Because the calculation in 2D is more difficult than in 3D, we give details in Appendix H. However, we verify the scaling $S_{cc}(k, t) \sim k^{-4}$ also for 2D, in agreement with the prediction of linearized fluctuating hydrodynamics. We cannot advance a definitive explanation why the numerical implementation in [56] failed to observe this power law, but perhaps the computation ran insufficient time or had an insufficient span of wave number. In fact, if one fits a power law to the lower range of wave numbers in [56], inset of Fig. 3, then the result is closer to k^{-4}.

The results that we obtain in this work suggest that, very generally, the effects of thermal noise at scales below the Kolmogorov length in turbulent flows will be quite similar to those that occur in laminar flows. Although the shear quenching of GCF's in the inertial-convective range is stronger than that found by linearized fluctuating hydrodynamics for weak shear [58], they are qualitatively similar. Furthermore, at scales below the diffusive length analogous to ℓ_B [which is the length scale ξ_c defined in [58], Eq. (45)] the predictions for the GCF's in the weakly sheared flow differ from ours only by the constant prefactor in front of the power law. Thus, we imagine that effects of thermal noise existing in laminar flows will generally persist, in perhaps some modified form, in the sub-Kolmogorov scales of turbulent flows. For example, it is known that thermal noise can reduce the efficiency of combustion in laminar flows, via a noise-induced bifurcation which changes the domains of monostability and bistability of the chemically reacting system [111]. Further, thermal noise can accelerate the formation and growth of droplets and bubbles in fluids rapidly cooled or heated in the multiphase regime [112,113]. Finally, it is known that thermal noise is important during collisions of self-propelled microorganisms in laminar flows and strongly affects the postcollision velocity directions of both swimmers [114]. In the sub-Komologorov range, one can expect for all such microscale physical processes some very interesting interplay between effects of turbulence and of thermal noise.

Here we have considered only nonmagnetized molecular fluids, but more generally thermal noise could play an important role in the turbulence of magnetized plasmas at resistive scales, as already suggested by Betchov [6]. In particular, the kinematic magnetic dynamo regime in a turbulent plasma at high magnetic Prandtl numbers is a close analog of the high Schmidt turbulent mixing which we have studied in this work. Much past theoretical work on the high magnetic Prandtl-number dynamo [115–118] is based on the soluble Kazantsev model [119], which is the exact analog for a passively advected magnetic field of the Kraichnan model for a passively advected scalar [24,25]. The kinematic dynamo eigenfunction was found in these studies to be peaked at the resistive scale, where thermal electric-field noise must appear acting on the magnetic field according to the general fluctuation-dissipation relation. Furthermore, thermal random stresses must act on the advecting velocity at the even larger viscous scale. Recently, the theory of thermal fluctuations in a plasma has been developed both for linearized dynamics [120] and as well for the full nonlinear dynamics [121,122]. One can anticipate that there will be significant modifications of the predictions of dynamo theories that neglect such noise. It would be interesting to investigate the effect of thermal noise on the origin and evolution of primordial magnetic fields in cosmology [123,124].

APPENDIX A: FLUCTUATION-DISSIPATION THEOREM FOR THE CONCENTRATION FIELD

We show here as an application of the phenomenological fluctuation-dissipation theorem [50,72,74,75] that the multiplicative noise term in the stochastic equation

$$\partial_t c + \mathbf{u} \cdot \nabla c = \nabla \cdot (D_0 \nabla c + \sqrt{2mD_0\rho^{-1}c(1-c)}\, \boldsymbol{\eta}_c(\mathbf{x}, t))$$

(A1)

is the unique expression which is local in $\mathbf{x}$ so that the equilibrium statistics $P_{eq}[c]$ of the equation are given by the Boltzmann-Einstein formula

$$P_{eq}[c] \propto e^{S/k_B},$$

(A2)

where S is the thermodynamic entropy. Here the appropriate entropy S is the ideal entropy of mixing ([125], Appendix D.6)

$$S[c] = -\frac{\rho k_B}{m} \int d^3x\, (c(\mathbf{x}) \ln c(\mathbf{x}) + [1 - c(\mathbf{x})] \ln[1 - c(\mathbf{x})])$$

(A3)

with particle mass m and fluid density ρ. Note here that we have assumed equal masses for the two species of particles, so that mass concentration c and molar concentration n in this case coincide. A local equilibrium distribution has been assumed in which the statistics in each subvolume is determined

by the specific entropy $s[c(\mathbf{x})]$ of the local concentration field $c(\mathbf{x})$, then integrated against $dM = \rho\, d^3x$ to give the total entropy.

For the purpose of formal calculations, it is useful to rewrite the stochastic equation by inserting a delta function $\delta^3(\mathbf{x} - \mathbf{y})$ and integrating over $\mathbf{y}$, as

$$\partial_t c + \mathbf{u} \cdot \nabla c = D_0 \triangle c + \int d^3y\, g^a[\mathbf{x}, \mathbf{y}; c]\, \eta_{c,a}(\mathbf{y}, t), \quad \text{(A4)}$$

with the definition

$$g^a[\mathbf{x}, \mathbf{y}; c] := \partial_{x_a}\left[\sqrt{\frac{2mD_0}{\rho}c(\mathbf{x})[1 - c(\mathbf{x})]}\,\delta(\mathbf{x} - \mathbf{y})\right]. \quad \text{(A5)}$$

It is important to stress that all "delta functions" in this expression and also in the covariance (13) of the white noise $\boldsymbol{\eta}_c$ should be interpreted as *cutoff delta functions*

$$\delta_\Lambda^3(\mathbf{x}) = \frac{1}{V}\sum_{|\mathbf{k}| < \Lambda} e^{i\mathbf{k}\cdot\mathbf{x}}, \quad \text{(A6)}$$

where V is the domain volume and Λ is some high-wave-number cutoff (see [74]). Here the cutoff Λ should be taken $\lesssim 1/\lambda_{mfp}$, the inverse of the mean-free path length. Physically, fluctuating hydrodynamic equations such as (A4) should not be interpreted as continuum stochastic partial differential equations but instead as low-wave-number effective field theories.

To obtain the Fokker-Planck equation for the probability distribution $P[c]$ corresponding to the Langevin equation (A4), we convert from Stratonovich to Itō calculus. The noise-induced drift term is

$$\frac{1}{2}\iint d^3y\, d^3z\, g^a[\mathbf{z}, \mathbf{y}; c]\frac{\delta g^a[\mathbf{x}, \mathbf{y}; c]}{\delta c(\mathbf{z})}.$$

Because of locality in $\mathbf{x}$ it is easy to check that

$$\frac{\delta g^a[\mathbf{x}, \mathbf{y}; c]}{\delta c(\mathbf{z})} = \delta^3(\mathbf{z} - \mathbf{y})G^a[\mathbf{x}, \mathbf{y}; c]$$

with G^a independent of $\mathbf{z}$. But in that case

$$\int d^3z\, g^a[\mathbf{z}, \mathbf{y}; c]\delta^3(\mathbf{z} - \mathbf{y})$$

$$= \sqrt{\frac{2mD_0}{\rho}c(\mathbf{y})[1 - c(\mathbf{y})]}\,(\partial_{y_a}\delta^3)(\mathbf{0}) = 0. \quad \text{(A7)}$$

Therefore, in this particular problem, the noise-induced drift vanishes and Itō and Stratonovich forms of the equation are identical. We used above the crucial fact that

$$\nabla\delta_\Lambda^3(\mathbf{0}) = \frac{1}{V}\sum_{|\mathbf{k}| < \Lambda} i\mathbf{k} = \mathbf{0},$$

which will be exploited also in the following calculations.

Because of the identity of Itō and Stratonovich here, we obtain easily the Fokker-Planck equation

$$\partial_t P[c] = -\int d^3x\, \frac{\delta}{\delta c(\mathbf{x})}[(-\mathbf{u} \cdot \nabla c + D_0 \triangle c)P[c]]$$

$$+ \frac{1}{2}\iint d^3x\, d^3y\, \frac{\delta^2}{\delta c(\mathbf{x})\delta c(\mathbf{y})}(\mathcal{D}[\mathbf{x}, \mathbf{y}; c]P[c]), \quad \text{(A8)}$$

where

$$\mathcal{D}[\mathbf{x}, \mathbf{y}, c] = \int d^3z\, g^a[\mathbf{x}, \mathbf{z}; c]g^a[\mathbf{y}, \mathbf{z}; c] \quad \text{(A9)}$$

is the probability diffusion coefficient. We must now show that the Einstein-Boltzmann distribution $P_{eq}[c]$ is the stationary distribution of the Fokker-Planck equation when the noise is chosen as in (A4) and (A5).

Note that the contribution from the first probability drift term vanishes because

$$\int d^3x\, \frac{\delta}{\delta c(\mathbf{x})}(\mathbf{u} \cdot \nabla_x c(\mathbf{x})P_{eq}[c])$$

$$= \int d^3x\left(\mathbf{u} \cdot \nabla_x \delta_\Lambda^3(\mathbf{0}) + \frac{\rho}{k_B}[\mathbf{u} \cdot \nabla_x c(\mathbf{x})]s'(c(\mathbf{x}))\right)P_{eq}[c]$$

$$= \frac{\rho}{k_B}\int d^3x\, \mathbf{u} \cdot \nabla_x s(c(\mathbf{x}))P_{eq}[c] = 0,$$

where in the second line we used

$$\frac{\delta}{\delta c(\mathbf{x})}P_{eq}[c] = -\frac{\rho}{m}(\ln c(\mathbf{x}) - \ln[1 - c(\mathbf{x})])P_{eq}[c]$$

$$= \frac{\rho}{k_B}s'(c(\mathbf{x}))P_{eq}[c] \quad \text{(A10)}$$

and in the last line incompressibility $\nabla \cdot \mathbf{u} = 0$ was used.

Next we note using (A5) and (A9) that an explicit expression for the probability diffusion coefficient follows:

$$\mathcal{D}[\mathbf{x}, \mathbf{y}, c] = \int d^3z\, g^a[\mathbf{x}, \mathbf{z}; c]g^a[\mathbf{y}, \mathbf{z}; c]$$

$$= \frac{2mD_0}{\rho}\partial_{x_a}\partial_{y_a}[c(\mathbf{x})[1 - c(\mathbf{x})]\delta^3(\mathbf{x} - \mathbf{y})]$$

$$= -\frac{2mD_0}{\rho}\partial_{x_a}[c(\mathbf{x})[1 - c(\mathbf{x})]\partial_{x_a}\delta^3(\mathbf{x} - \mathbf{y})]. \quad \text{(A11)}$$

A calculation similar to the proof of Itō-Stratonovich identity gives

$$\int d^3y\, \frac{\delta}{\delta c(\mathbf{y})}\mathcal{D}[\mathbf{x}, \mathbf{y}, c] = 0.$$

Finally, using (A10) and (A11)

$$\frac{1}{2}\int d^3y\, \frac{\delta}{\delta c(\mathbf{y})}(\mathcal{D}[\mathbf{x}, \mathbf{y}, c]P_{eq}[c])$$

$$= \frac{1}{2}\int d^3y\, \mathcal{D}[\mathbf{x}, \mathbf{y}, c]\frac{\delta P_{eq}[c]}{\delta c(\mathbf{y})}$$

$$= -\frac{\rho}{2m}\int d^3y\, \mathcal{D}[\mathbf{x} - \mathbf{y}, c]$$

$$\times (\ln c(\mathbf{y}) - \ln[1 - c(\mathbf{y})])P_{eq}[c]$$

$$= D_0\partial_{x_a}\int d^3y\, c(\mathbf{x})[1 - c(\mathbf{x})]\delta^3(\mathbf{x} - \mathbf{y})$$

$$\times \frac{1}{c(\mathbf{y})[1 - c(\mathbf{y})]}\partial_{y_a}c(\mathbf{y})P_{eq}[c]$$

$$= D_0\triangle c\, P_{eq}[c].$$

The second drift contribution in the first line of Eq. (A8) is thus exactly canceled by the diffusion contribution in the second line when $P = P_{eq}$. It is clear from this calculation that the

multiplicative factor $\sqrt{2mD_0\rho^{-1}c(\mathbf{x})[1-c(\mathbf{x})]}$ is the unique local function of the concentration field which can be chosen to multiply the noise term in (A1) so that exact cancellation between drift and diffusion terms is obtained, guaranteeing that P_{eq} is stationary.

Notice, however, that P_{eq} given by (A2) is not the only stationary distribution for the stochastic dynamics described by (A1) because that equation conserves the integral

$$M_1 = \rho \int d^3x \, c(\mathbf{x}, t) \qquad (\text{A12})$$

which represents the total mass of species 1 of the mixture. Conservation of the integral (A12) will hold for any boundary conditions on scalar flux which conserve mass, such as periodic or zero flux. In that case, there is a one-parameter family of invariant distributions of the form

$$P_{\text{eq}}^\lambda[c] \propto e^{S/k_B + \lambda M_1}. \qquad (\text{A13})$$

Comparison with standard equilibrium thermodynamic relations (see Appendix F) reveals that $\lambda = \mu/k_B T$, where μ is the chemical potential per mass which is thermodynamically conjugate to the concentration c. Its value thus determines the mean concentration through the relation $\mu = -Ts'(\bar{c})$ or $\lambda = -s'(\bar{c})/k_B$, with $\bar{c} = \frac{1}{2}$ for $\lambda = 0$.

The small Gaussian fluctuations $c'(\mathbf{x})$ around the mean value $\bar{c}$ can be obtained from the formula (A13) for the distribution $P_{\text{eq}}^\lambda[c]$ by substituting $c(\mathbf{x}) = \bar{c} + c'(\mathbf{x})$ and expanding to quadratic order. Using

$$\frac{\delta^2 S[c]}{\delta c(\mathbf{x})\delta c(\mathbf{x}')} = -\frac{k_B\rho}{m} \frac{\delta^3(\mathbf{x}-\mathbf{x}')}{c(\mathbf{x})[1-c(\mathbf{x})]},$$

the result is

$$P_{\text{eq}}^\lambda[c] \simeq \exp\left(-\frac{1}{2}\frac{\bar{\rho}}{m}\frac{\int d^3x \, [c'(\mathbf{x})]^2}{\bar{c}(1-\bar{c})}\right).$$

It follows that the second-order correlation is given by

$$\langle c'(\mathbf{x})c'(\mathbf{x}')\rangle = \frac{m}{\bar{\rho}}\bar{c}(1-\bar{c})\delta_\Lambda^3(\mathbf{x}-\mathbf{x}').$$

Fourier transforming and using the definition (4) gives the equilibrium structure function

$$S_{cc}(k) = \frac{m}{\bar{\rho}}\bar{c}(1-\bar{c})$$

which is independent of wave number k. Using the result (F1) for $(\partial\mu/\partial c)_{T,p}$ from Appendix F, we see that this special case for an ideal mixture of equal mass particles agrees with the general result (94).

APPENDIX B: HIGH Sc ASYMPTOTICS

We give here the detailed derivation of Eq. (40) for the reader who is interested in the mathematical details. To simplify the notation, in this Appendix we shall use $\mathbf{v}, \mathbf{u}, \mathbf{w}$ instead of $\mathbf{v}_\theta, \mathbf{u}_\theta, \mathbf{w}_\theta$, respectively, and likewise c' and c will be denoted instead as c and c_γ (to remind that the latter depends linearly on $\boldsymbol{\gamma}$). Our analysis follows closely that of DFV in [56], Appendix A, and related works [126–130], so we shall be terse.

The forward Kolmogorov operator $\mathbf{L}$ which corresponds to the Langevin equations (38) and (39) and which evolves an arbitrary functional $F[\mathbf{v}, c]$ is the sum of three terms that are ordered in inverse powers of ϵ as $\mathbf{L} = \mathbf{L}_0 + \mathbf{L}_1\epsilon^{-1} + \mathbf{L}_2\epsilon^{-2}$:

$$\mathbf{L}_0 F = \frac{1}{2}\mathcal{V}_0\int d^3x\,(\mathcal{P}_{ij}\triangle v_j)\frac{\delta F}{\delta v_i(\mathbf{x})} + \frac{1}{2}\iint d^3x\,d^3x'\,\mathcal{P}_{im}\mathcal{P}'_{jn}[\mathcal{V}_{kl}(\mathbf{x},\mathbf{x}')\,\partial_k v_m(\mathbf{x})\partial'_l v_n(\mathbf{x}')]\frac{\delta^2 F}{\delta v_i(\mathbf{x})\delta v_j(\mathbf{x}')}$$

$$+ \frac{1}{2}\iint d^3x\,d^3x'\,\mathcal{P}_{im}\mathcal{P}'_{jn}(v_k(\mathbf{x})v_l(\mathbf{x}')\,\partial_k\partial'_l\mathcal{V}_{mn}(\mathbf{x},\mathbf{x}'))\frac{\delta^2 F}{\delta v_i(\mathbf{x})\delta v_j(\mathbf{x}')} + (D_0+\mathcal{U}_0)\int d^3x\,\triangle c(\mathbf{x})\cdot\frac{\delta}{\delta c(\mathbf{x})}$$

$$+ \frac{mD_0}{\rho}\int d^3x\,c_\gamma(\mathbf{x})[1-c_\gamma(\mathbf{x})]\cdot\triangle\frac{\delta^2 F}{\delta c(\mathbf{x})^2} + \frac{1}{2}\iint d^3x\,d^3x'\,\mathcal{U}_{ij}(\mathbf{x},\mathbf{x}')[\partial_i c(\mathbf{x})+\gamma_i][\partial'_j c(\mathbf{x}')+\gamma_j]\frac{\delta^2 F}{\delta c(\mathbf{x})\delta c(\mathbf{x}')}$$

$$+ \int d^3x\,s(\mathbf{x},t)\frac{\delta F}{\delta c(\mathbf{x})} + \frac{1}{2}\iint d^3x\,d^3x'\,S(|\mathbf{x}-\mathbf{x}'|/L)\frac{\delta^2 F}{\delta c(\mathbf{x})\delta c(\mathbf{x}')}, \qquad (\text{B1})$$

$$\mathbf{L}_1 F = -\int d^3x\,u_i(\partial_i c+\gamma_i)\frac{\delta F}{\delta c(\mathbf{x})}, \qquad (\text{B2})$$

and

$$\mathbf{L}_2 = \nu\int d^3x\,(\mathcal{P}_{ij}\triangle v_j)\frac{\delta F}{\delta v_i(\mathbf{x})}$$

$$+ \frac{\nu k_B T}{\rho}\int d^3x\,\mathcal{P}_{ij}\triangle\frac{\delta^2 F}{\delta v_i(\mathbf{x})\delta v_j(\mathbf{x})}. \qquad (\text{B3})$$

Denote by $(\tilde{\mathbf{v}}(\mathbf{x},t), \tilde{c}(\mathbf{x},t))$ the solution of (38) and (39) with initial conditions $(\tilde{\mathbf{v}}(\mathbf{x},0), \tilde{c}(\mathbf{x},0)) = (\mathbf{v}(\mathbf{x}), c(\mathbf{x}))$ and consider the functional

$$G[\mathbf{v}, c, t] \equiv \langle F[\tilde{\mathbf{v}}(\cdot,t), \tilde{c}(\cdot,t)]\rangle, \qquad (\text{B4})$$

where $\langle\cdot\rangle$ denotes the expectation value over the realization of noise terms $\boldsymbol{\eta}$ and $\boldsymbol{\eta}_c$. The expectation defines a time-dependent functional G of the initial conditions which satisfies the backward Kolmogorov equation:

$$\partial_t G = \mathbf{L}_0 G + \epsilon^{-1}\mathbf{L}_1 G + \epsilon^{-2}\mathbf{L}_2 G, \qquad G|_{t=0} = F. \qquad (\text{B5})$$

One considers this equation in the limit $\epsilon \to 0$. Expanding the solution G as

$$G = G_0 + \epsilon G_1 + \epsilon^2 G_2 + \cdots,$$

and substituting this relation in (B5) and collecting terms of increasing power in ϵ, one finally obtains

$$\mathbf{L}_2 G_0 = 0, \quad \mathbf{L}_2 G_1 = -\mathbf{L}_1 G_0,$$

$$\mathbf{L}_2 G_2 = \partial_t G_0 - \mathbf{L}_0 G_0 - \mathbf{L}_1 G_1, \quad \ldots \qquad (\text{B6})$$

Because $\mathbf{L}_2$ is the Markov generator of the equilibrium fluctuating hydrodynamics equation (9) in the text, which defines an ergodic process, the first equation in Eq. (B6), i.e., $\mathbf{L}_2 G_0 = 0$, indicates that G_0 is a functional of $c(\mathbf{x})$ only and does not depend on both $\mathbf{v}(\mathbf{x})$ and $c(\mathbf{x})$:

$$G_0 = G_0[c].$$

The second equation in (B6) requires a solvability condition as its right-hand side must be in the range of $\mathbf{L}_2$. Because $(\mathrm{Ran}\,\mathbf{L}_2)^{\perp} = \mathrm{Ker}\,\mathbf{L}_2^*$, this is equivalent to the statement that the expectation of $\mathbf{L}_1 G_0$ must vanish when averaged with respect to the invariant Gibbs measure of $\tilde{\mathbf{v}}(\mathbf{x}, t)$ evolving under (9), i.e.,

$$P_{\mathrm{eq}}(\tilde{\mathbf{v}}) = \frac{1}{Z} \exp\left(-\frac{\rho}{2k_B T} \int d^3x \, \tilde{v}^2\right) \delta^3\left(\int d^3x \, \rho\tilde{\mathbf{v}}\right) \delta(\boldsymbol{\nabla} \cdot \tilde{\mathbf{v}}). \tag{B7}$$

Denoting the expectation with respect to this measure by $\langle f \rangle_{\mathbf{v}}$, the solvability condition becomes

$$0 = \langle \hat{\mathbf{L}}_1 G_0 \rangle_{\mathbf{v}} = -\int d^3x \, \langle \mathbf{u}(\mathbf{x}) \rangle_{\mathbf{v}} \cdot [\boldsymbol{\nabla} c(\mathbf{x}) + \boldsymbol{\gamma}] \frac{\delta G_0}{\delta c(\mathbf{x})},$$

which is satisfied because $\langle \mathbf{v}(\mathbf{x}) \rangle_{\mathbf{v}} = 0$. The second equation in (B6) can now be solved for G_1:

$$G_1 = -\mathbf{L}_2^{-1} \mathbf{L}_1 G_0, \tag{B8}$$

where $\mathbf{L}_2^{-1}$ is the pseudoinverse of the operator $\mathbf{L}_2$.

The third equation in (B6) also requires a solvability condition, which using $\langle \mathbf{L}_0 G_0 \rangle_{\mathbf{v}} = \mathbf{L}_0 G_0$ and (B8), can be written

as

$$\partial_t G_0 = \langle \mathbf{L}_0 G_0 \rangle_{\mathbf{v}} + \langle \mathbf{L}_1 G_1 \rangle_{\mathbf{v}} = \mathbf{L}_0 G_0 - \langle \mathbf{L}_1 \mathbf{L}_2^{-1} \mathbf{L}_1 G_0 \rangle_{\mathbf{v}}.$$

Because the operator $\mathbf{L}_1$ defined in (B2) is linear in $\mathbf{u}(\mathbf{x}) = \boldsymbol{\sigma} \star \mathbf{v}(\mathbf{x})$, one can use

$$\mathbf{L}_2^{-1} \mathbf{u}(\mathbf{x}) = \mathbf{L}_2^{-1} \boldsymbol{\sigma} \star \mathbf{v}(\mathbf{x}) = \boldsymbol{\sigma} \star \mathbf{L}_2^{-1} \mathbf{v}(\mathbf{x})$$

$$= -\boldsymbol{\sigma} \star \int_0^{\infty} d\tau \, e^{\tau \mathbf{L}_2} \mathbf{v}(\mathbf{x})$$

$$= -\boldsymbol{\sigma} \star \int_0^{\infty} d\tau \langle \tilde{\mathbf{v}}(\mathbf{x}, \tau) \rangle, \tag{B9}$$

where $\tilde{\mathbf{v}}(\mathbf{x}, \tau)$ denotes the solution of (9) with initial condition $\tilde{\mathbf{v}}(\mathbf{x}, 0) = \mathbf{v}(\mathbf{x})$ and expectation $\langle \cdot \rangle$ is the same as in (B4). This solution, using (9), can be written as

$$\tilde{\mathbf{v}}(\mathbf{x}, \tau) = \exp(-\tau \nu \mathcal{A}) \mathbf{v}(\mathbf{x}) + \int_0^{\tau} d\tau' \exp\left[-(\tau - \tau')\nu \mathcal{A}\right]$$

$$\times \boldsymbol{\nabla} \cdot (\sqrt{2\nu k_B T \rho^{-1}} \boldsymbol{\eta}(\tau')), \tag{B10}$$

in terms of the Stokes operator $\mathcal{A} = -\mathcal{P}\triangle$. The second term has a zero average and does not contribute to the expectation in (B9). Combining relations (B9) and (B10), we find

$$\mathbf{L}_2^{-1} \mathbf{u}(\mathbf{x}) = -\nu^{-1} \mathbf{G}_{\sigma} \star \mathbf{v}(\mathbf{x}),$$

where $\mathbf{G}_{\sigma} = \boldsymbol{\sigma} \star \mathbf{G}$ is the convolution of the smoothing kernel $\boldsymbol{\sigma}$ with the Oseen tensor $\mathbf{G}$ (Green's function for the Stokes flow). It follows that

$$-\langle \mathbf{L}_1 \mathbf{L}_2^{-1} \mathbf{L}_1 G_0 \rangle_{\mathbf{v}} = \iint d^3x \, d^3x' [\boldsymbol{\nabla} c(\mathbf{x}) + \boldsymbol{\gamma}] \frac{\delta}{\delta c(\mathbf{x})} \left(\frac{1}{2} \mathbf{R}(\mathbf{x}, \mathbf{x}') \cdot [\boldsymbol{\nabla}' c(\mathbf{x}') + \boldsymbol{\gamma}] \frac{\delta G_0}{\delta c(\mathbf{x}')}\right)$$

$$= \frac{1}{2} \iint d^3x \, d^3x' \, [\boldsymbol{\nabla} c(\mathbf{x}) + \boldsymbol{\gamma}] \cdot \mathbf{R}(\mathbf{x}, \mathbf{x}') \cdot [\boldsymbol{\nabla}' c(\mathbf{x}') + \boldsymbol{\gamma}] \frac{\delta^2 G_0}{\delta c(\mathbf{x}) \delta c(\mathbf{x}')}$$

$$+ \int d^3x \, \boldsymbol{\nabla} \cdot \left(\frac{1}{2} \mathbf{R}(\mathbf{x}, \mathbf{x}) \cdot [\boldsymbol{\nabla} c(\mathbf{x}) + \boldsymbol{\gamma}]\right) \frac{\delta G_0}{\delta c(\mathbf{x})} := (\delta \mathbf{L}_0) G_0.$$

The operator $\delta \mathbf{L}_0$ which emerges from this last calculation is the generator of the Markov random process corresponding to the following Itô stochastic differential equation for the concentration field

$$\partial_t c = \boldsymbol{\nabla} \cdot \left(\tfrac{1}{2} \mathbf{R}(\mathbf{x}, \mathbf{x}) \cdot (\boldsymbol{\nabla} c + \boldsymbol{\gamma})\right) - \mathbf{w} \cdot (\boldsymbol{\nabla} c + \boldsymbol{\gamma}),$$

where $\mathbf{w}$ is the Gaussian random velocity, white noise in time with spatial covariance $\mathbf{R}(\mathbf{x}, \mathbf{x}')$ which is given by Eq. (18) in the main text.

The solvability condition thus yields the limiting equation for $G_0[c]$ as $\epsilon \to 0$,

$$\partial_t G_0 = (\mathbf{L}_0 + \delta \mathbf{L}_0) G_0,$$

which can be recognized immediately as the backward Kolmogorov equation for the Itô equation

$$\partial_t c = (D_0 + \mathcal{U}_0)\triangle c + \boldsymbol{\nabla} \cdot \left(\tfrac{1}{2} \mathbf{R}(\mathbf{x}, \mathbf{x}) \cdot (\boldsymbol{\nabla} c + \boldsymbol{\gamma})\right)$$

$$- (\mathbf{w} + \mathbf{u}_T) \cdot (\boldsymbol{\nabla} c + \boldsymbol{\gamma}) + s(\mathbf{x}, t) + s_0(\mathbf{x}, t)$$

$$+ \boldsymbol{\nabla} \cdot (\sqrt{2mD_0\rho^{-1}c_{\gamma}(1 - c_{\gamma})} \boldsymbol{\eta}_c(\mathbf{x}, t)),$$

which is exactly Eq. (41).

APPENDIX C: EQUATION FOR THE CORRELATION FUNCTION IN THE ISOTROPIC KRAICHNAN MODEL

Equation (49) in the text can be written explicitly as

$$\mathcal{V}_{ij}(r) = K(r)\delta_{ij} + \partial_{r_i}\partial_{r_j} H(r), \tag{C1}$$

where $-\triangle H(r) = K(r)$. Here $K(r)$ is any positive-definite, radially symmetric, smooth function, which means that it can be written as a Fourier transform $K(r) \equiv \int d^d\mathbf{k} \, e^{i\mathbf{k}\cdot\mathbf{r}} E(k)$ with $E(k)$ a positive, radially symmetric, rapidly decaying spectrum. For any radially symmetric function $H(r)$ it is easy to check that

$$\partial_{r_i}\partial_{r_j} H(r) = J(r)\delta_{ij} + rJ'(r)\hat{r}_i\hat{r}_j \tag{C2}$$

with $J(r) = H'(r)/r$, so that taking a trace gives

$$-K(r) = \triangle H(r) = d \cdot J(r) + rJ'(r) = \frac{1}{r^{d-1}} \frac{d}{dr}[r^d J(r)] \tag{C3}$$

in d dimensions. Integration over r yields the formula (50) in the text.

Using (C2) and (C3) in (C1), we get

$$\mathcal{V}_{ij}(r) = [K(r) + J(r)]\delta_{ij} - [K(r) + d \cdot J(r)]\hat{r}_i\hat{r}_j. \quad \text{(C4)}$$

and substituting this expression into Eq. (48) in the text yields

$$\partial_t C = [\triangle K(r) + \triangle J(r)]\triangle C - [\triangle K(r) + d \cdot \triangle J(r)]\frac{\partial^2 C}{\partial r^2}$$
$$+ 2D_0 \triangle C + S\left(\frac{r}{L}\right),$$

where $\triangle J(r) = J(0) - J(r)$, etc. Using the standard formula for the radial Laplacian

$$\triangle C = \frac{1}{r^{d-1}}\frac{\partial}{\partial r}\left(r^{d-1}\frac{\partial C}{\partial r}\right) = \frac{d-1}{r}\partial_r C + \partial_r^2 C \quad \text{(C5)}$$

then gives further

$$\partial_t C = \frac{d-1}{r}(\triangle K(r) + \triangle J(r))\partial_r C$$
$$+ (1-d)\triangle J(r)\partial_r^2 C + 2D_0 \triangle C + S\left(\frac{r}{L}\right)$$
$$= -\frac{d-1}{r^{d-1}}\frac{\partial}{\partial r}\left(\triangle J(r)r^{d-1}\frac{\partial C}{\partial r}\right) + 2D_0 \triangle C + S\left(\frac{r}{L}\right),$$

where we employed again (C3) to get the second equality. Combining with the radial Laplacian (C5) gives the final result

$$\partial_t C = \frac{1}{r^{d-1}}\frac{\partial}{\partial r}([2D_0 - (d-1)\triangle J(r)]r^{d-1}\frac{\partial C}{\partial r}) + S\left(\frac{r}{L}\right), \quad \text{(C6)}$$

which coincides with (52) in the text.

APPENDIX D: RENORMALIZED DIFFUSIVITY FROM THERMAL VELOCITY FLUCTUATIONS

We here derive the scale-dependent diffusivities (56) and (60) arising from advection by thermal velocity fluctuations. The covariance $\mathbf{R}(\mathbf{x}, \mathbf{x}')$ defined in (19) can be evaluated for $d = 3$ homogeneous, isotropic statistics in the form (49) or (C1), with

$$K_\theta(r) = \frac{1}{(2\pi)^3}\int d^3\mathbf{k}\, e^{i\mathbf{k}\cdot\mathbf{r}}\,|\widehat{\sigma}(k)|^2\frac{2k_BT}{\eta k^2}$$
$$= \frac{k_BT}{\pi^2\eta}\int_0^\infty dk\,\frac{\sin(kr)}{kr}|\widehat{\sigma}(k)|^2. \quad \text{(D1)}$$

The function $J_\theta(r)$ can then be obtained from the integral (50). We now obtain concrete results for the two specific choices of filter kernel considered in the main text.

With the choice of kernel (55) used by DFV, (D1) becomes after the change of variables $x = k\sigma$

$$K_\theta(r) = \frac{k_BT}{\pi^2\eta}\frac{1}{r}\int_0^\infty dx\,\frac{x^4\sin(xr/\sigma)}{x(1+x^2)[(\sigma/L)^4 + x^4]}. \quad \text{(D2)}$$

Although we have worked out the result for finite L, we present here only the limit case $L \to \infty$ which gives

$$K_\theta(r) = \frac{k_BT}{\pi^2\eta}\frac{1}{r}\int_0^\infty dx\,\frac{\sin(xr/\sigma)}{x(1+x^2)}$$
$$= \frac{k_BT}{2\pi\eta}\frac{1 - e^{-r/\sigma}}{r} \quad \text{(D3)}$$

using [92], formula 2.2(20). Substituting this expression into the definition (50) of $J_\theta(r)$ gives by simple integration by parts

$$J_\theta(r) = -\frac{k_BT}{2\pi\eta\sigma}\left(\frac{1}{2}\frac{1}{\frac{r}{\sigma}} + \frac{e^{-r/\sigma}}{\left(\frac{r}{\sigma}\right)^2} - \frac{1 - e^{-r/\sigma}}{\left(\frac{r}{\sigma}\right)^3}\right)$$

and thus the result (56) stated in the text.

We consider next the exponential kernel given by (59) in the text, or $\widehat{\sigma}(k) = e^{-k\sigma/\pi}$. With this choice,

$$K_\theta(r) = \frac{k_BT}{\pi^2\eta}\int_0^\infty dk\,\frac{\sin(kr)}{kr}e^{-2\sigma k/\pi} = \frac{k_BT}{\pi^2\eta r}\arctan\left(\frac{\pi r}{2\sigma}\right), \quad \text{(D4)}$$

using [92], formula 2.4(1). Substituting into (50), after integration by parts and some straightforward algebra, yields

$$J_\theta(r) = -\frac{k_BT}{2\pi^2\eta r^3}\left[\left(\frac{4\sigma^2}{\pi^2} + r^2\right)\arctan\left(\frac{\pi r}{2\sigma}\right) - \frac{2}{\pi}\sigma r\right]$$

and thus the result (60) stated in the text.

APPENDIX E: NUMERICAL METHODS FOR PLOTS

In this Appendix, we describe our numerical method in MATLAB to plot the concentration spectrum for our exact solution (78)–(80). From the formula (76) for $E_c(k)$ in terms of $F(k)$, we need to evaluate fi(z) and its derivative fi$'(z) = -$gi(z). Since the functions cosint and ssinint in MATLAB evaluate the cosine and sine integral functions Ci(z) and si$(z) = Si(z) - \frac{\pi}{2}$, respectively, the most obvious method would be to use (86) for fi(z) and the analogous result

$$\text{gi}(z) = -\text{Ci}(z)\cos z - \text{si}(z)\sin z \quad \text{(E1)}$$

(see [90], formula 5.2.7). Unfortunately, this approach does not work in the asymptotic regime of interest, with z near the imaginary axis and of large magnitude. In this region $\cos z$, $\sin z$ both grow exponentially, but these growing contributions cancel identically in fi(z), gi(z), which instead decay. Numerically, evaluating these functions using formulas (86) and (E1) leads to large loss of significance errors in the region of interest.

We have overcome this problem by alternative expressions for fi(z), gi(z) in terms of Tricomi's confluent hypergeometric function $U(a, b, z)$, as

$$\text{fi}(z) = \frac{i}{2}(U(1, 1, iz) - U(1, 1, -iz)), \quad \text{(E2)}$$

$$\text{gi}(z) = \frac{1}{2}(U(1, 1, iz) + U(1, 1, -iz)). \quad \text{(E3)}$$

The Tricomi function decays for large z near the real axis, so that this representation avoids inaccuracy from large canceling contributions and $U(a, b, z)$ is simply evaluated with the function kummerU in MATLAB.

The formulas (E2) and (E3) can be derived from the standard integral representation for Tricomi's function:

$$U(a, b, z) := \frac{1}{\Gamma(a)}\int_0^\infty e^{-zt}t^{a-1}(1+t)^{b-a-1}dt,$$

for Re$(z) > 0$, Re$(a) > 0$ and with the gamma function $\Gamma(a)$. See [90], formula 13.2.5. Taking $a = b = 1$, and $z \to \pm iz$, we

find

$$U(1, 1, \pm iz) = \int_0^\infty \frac{e^{\mp it}}{z+t} dt = \text{gi}(z) \mp i \,\text{fi}(z), \qquad \text{(E4)}$$

where we used (81) and the corresponding integral formula

$$\text{gi}(z) = \int_0^\infty \frac{\cos t}{t+z} dt = \int_0^\infty \frac{t e^{-zt}}{1+t^2} dt, \quad \text{Re}(z) > 0. \quad \text{(E5)}$$

See [90], Sec. 5, formula 5.2.13, and [91], Sec. 38:13. The formulas (E2) and (E3) follow directly from (E4).

APPENDIX F: THERMODYNAMICS OF BINARY MIXTURES

We briefly review here the results on thermodynamics of binary mixtures required in the main text. We start with the first law of thermodynamics in the form

$$du = T \, ds - p \, dv + \mu_0 d\nu_0 + \mu_1 d\nu_1,$$

where $u = U/M$ is specific energy, s is specific entropy, $v = V/M$ is specific volume, and $\nu_i = N_i/M$, $i = 0, 1$, are the specific particle numbers of the two species (solvent, solute). Mass fractions or mass concentrations of the two species are defined by

$$c := c_1 = m_1 \nu_1 = M_1/M, \quad c_0 = m_0 \nu_0 = M_0/M.$$

From $c_0 + c_1 = 1$ one then easily obtains

$$du = T \, ds - p \, dv + \mu \, dc,$$

where the chemical potential per mass is given by

$$\mu = \frac{\mu_1}{m_1} - \frac{\mu_0}{m_0}$$

(cf. [131], Chap. VI, Sec. 57). One can also introduce the molar fractions or molar concentration $n_i = N_i/N$, $i = 0, 1$, which are easily related to the mass concentrations by

$$n = \frac{m_0 c}{m_0 c + m_1(1-c)}$$

with $n := n_1$.

An *ideal mixture* by definition is one in which the chemical potential of each component in solution satisfies

$$\mu_i = \mu_i^\emptyset(T, p) + k_B T \, \ln(n_i),$$

where $\mu_i^\emptyset$ is the chemical potential of the pure substance. Note then that

$$\mu = \mu^\star(T, p) + \frac{k_B T}{m_1} \ln(n) - \frac{k_B T}{m_0} \ln(1-n).$$

A straightforward calculation gives

$$\left(\frac{\partial \mu}{\partial c}\right)_{T,p} = \frac{k_B T}{c(1-c)[m_0 c + m_1(1-c)]}. \qquad \text{(F1)}$$

Chemical potentials of nonideal mixtures are generally written in the form

$$\mu_i = \mu_i^\emptyset(T, p) + k_B T \, \ln(n_i f_i),$$

where f_i is the *activity coefficient* which takes into account the nonideality of the solution (e.g., see [104]). Note from the Gibbs-Duhem relation $\nu_0 d\mu_0 + \nu_1 d\mu_1 = -s \, dT + v \, dp$ and from the condition $n_0 + n_1 = 1$ that, at constant T, p,

$$n_0 d(\ln f_0) + n_1 d(\ln f_1) = 0.$$

Defining

$$B_i = 1 + \left.\frac{d \ln f_i}{d \ln n_i}\right|_{T,p}, \quad i = 0, 1$$

it then follows that $B_0 = B_1 := B$. Furthermore, from this definition, at constant T, p,

$$\frac{d}{dc} \ln(n_i f_i) = \frac{d}{dc} \ln(n_i) B$$

and thus for a nonideal mixture

$$\left(\frac{\partial \mu}{\partial c}\right)_{T,p} = \frac{B k_B T}{c(1-c)[m_0 c + m_1(1-c)]}. \qquad \text{(F2)}$$

APPENDIX G: SURVEY OF EXPERIMENTS ON TURBULENT HIGH SCHMIDT MIXING

As a convenience for readers, we here briefly survey experiments known to us on high Schmidt-number turbulent advection. These experiments all differ considerably from each other, both in the turbulent flows considered and also in the fluid mixtures employed, which include water-fluorescein [28,33,34], salt water [30,32], and ink in water [27]. We additionally consider here experiments which studied turbulent mixing of temperature fluctuations at high Prandtl numbers, in order to expand our view of the range of parameters which can be practically achieved. We shall briefly describe each experiment and the physical parameters stated in the paper. In addition, some further parameters could be calculated with the reported quantities and with data extracted from the published figures, and we describe our methods for this. We shall discuss the main experiments of which we are aware, in chronological order.

We start with the experiment performed by Gibson and Schwartz [32] who used a single-electrode conductivity probe in a bridge circuit to measure the spectra and decay of homogeneous fields of both concentration and temperature behind a grid in dilute salt water at $\text{Re} \simeq 10^4$ and who reported Batchelor spectrum in the viscous-convective range. Here $\nu \simeq 10^{-2}$ cm²/s and $D \simeq 1.5 \times 10^{-5}$ cm²/s, thus $\text{Sc} \simeq 666.7$. The Batchelor scale can be obtained using $\kappa_B = \kappa_K \sqrt{\text{Sc}}$ in terms of the Kolmogorov wave number κ_K (which is denoted by k_s and given in Table 1 in [32]). For six different runs in this series of experiments, we find $\kappa_B \simeq 761, 2631, 4257, 2505, 1437,$ and 3444 cm⁻¹, respectively, for CM1 through CM17 in Table 1 in [32]. Using $\gamma = D/\ell_B^2 \equiv \kappa_B^2 D$, for six runs CM1 through CM17, we find $\gamma \simeq 8.7, 103.8, 271.8, 94.1, 31,$ and 177.9 s⁻¹, respectively. The injection rate of concentration fluctuations is given by $\chi = \frac{3}{2} \frac{U}{x} \overline{\theta^2}$ with the variance of concentration or temperature fluctuations denoted as $\overline{\theta^2}$, where velocity U and distance from the grid x are given in Table 1 in [32] for different runs. With $0.57 \leqslant \frac{U}{x} \leqslant 4.7$, and $\overline{c^2} \sim 10^{-12}$ from Fig. 1, we estimate $\chi \sim 10^{-12}$–10^{-11} s⁻¹.

In another set of experiments, Nye and Brodkey [27] studied commercial blue ink in water flowing through a pipe with a fiber-optic light probe and reported a full 1.5

decades of $1/k$ spectrum, starting near the velocity spectrum cutoff, which was observed to be at about $0.1\kappa_K$ with Kolmogorov wave number κ_K. The diffusivity of the dye was given as $D = 2.6 \times 10^{-6}$ cm^2/s and viscosity (of water) is $\nu \simeq 10^{-2}$ cm^2/s, hence, the Schmidt number should be around Sc $\simeq 3800$. The Kolmogorov wave number is given as $\kappa_K \simeq 62$ cm^{-1}, thus the Batchelor wave number is given by $\kappa_B \equiv \ell_B^{-1} = \kappa_K\sqrt{Sc} \simeq 3822$ cm^{-1} using which we also find $\gamma \simeq D/\ell_B^2 \simeq 38$ s^{-1}. The energy dissipation rate ε can be estimated using $\varepsilon \simeq \gamma^2\nu \simeq 14.4$ cm^2/s^3 which also agrees with $\varepsilon \simeq \nu^3\kappa_K^4$ as expected. Finally, using [27], Fig. 4, for the scalar spectrum $E_c(k)$, we estimated $\int k^2 E_c(k)dk$ for the three cases presented, by extracting data for $E_c(k)$ and then numerically integrating $k^2 E_c(k)$, and found that the scalar injection rate should be of order $\chi \simeq 10^{-4}$–10^{-2} s^{-1} in this set of experiments.

An experiment of Grant $et\ al.$ [30] measured temperature and velocity fluctuations in the open sea and a tidal channel and they reported observing Batchelor's spectrum over at least one decade in the viscous-convective range. In these experiments, the injection rate for temperature fluctuations varied from $\chi \simeq 7.2 \times 10^{-8}$ degC^2/s to $\chi \simeq 5.2 \times 10^{-4}$ degC^2/s (see Table 1 in [30]). Since these experiments dealt with temperature field, in order to compare the corresponding injection rate (in units of degC^2/s) to those corresponding to a concentration field [in units of (%concent.)^2/s], we converted the reported rates. Extracting data from Figs. 6–11 in [30], we calculated the temperature fluctuations, which is given in terms of the spectrum $\psi(k_1)$ as $\langle \Delta T^2 \rangle \simeq \int \psi(k_1)dk_1$. For Figs. 6–11 in [30],, respectively, we get $\langle \Delta T^2 \rangle \sim 10^{-3}, 10^{-2}, 10^{-3}, 10^{-4}, 10^{-4}, 10^{-4}$ degC^2. Therefore, the quantity $\chi/\langle \Delta T^2 \rangle$ will be in the range $\chi_{\min}/\langle \Delta T^2 \rangle_{\max}$ through $\chi_{\max}/\langle \Delta T^2 \rangle_{\min}$ which turns out to be of order $\sim 10^{-6}$–1 s^{-1}. Also shown in Table 1 of [30] is the energy dissipation rate ε, which varies in the range 4.4×10^{-4}–5.2×10^{-1} (cm^2/s^3). Taking viscosity of order $\nu \sim 10^{-2}$ cm^2/s for water, we can use $\gamma \sim \sqrt{\varepsilon/\nu}$ to estimate γ. Above values for ε translate into values in the range $\gamma \sim 0.2$ s^{-1} through $\gamma \sim 7.2$ s^{-1}.

Miller and Dimotakis [33] used a mixture of water and fluorescein, with diffusivity $D \simeq 5.2 \times 10^{-6}$ cm^2/s, to investigate the temporal, scalar power spectra of high Schmidt-number turbulent jets with Reynolds number of order Re $\simeq 10^4$ and Schmidt number Sc $\simeq 1.9 \times 10^3$. At the smallest scales, the measured spectra were reported not to exhibit Batchelor's $1/k$ power-law behavior, but, rather, seemed to be approximated by a log-normal function, over a range of scales exceeding a factor of 40, in some cases. At $x/d = 305$ (x distance from the injection nozzle and d nozzle diameter), the Kolmogorov scale was reported as $\ell_K \simeq 2.57 \times 10^{-2}$ cm. Using $\ell_K \simeq (\frac{\nu^3}{\varepsilon})^{1/4}$, and taking $\nu \simeq 10^{-2}$ cm^2/s for the viscosity of water, we get kinetic energy dissipation rate $\varepsilon \simeq 2.29$ cm^2/s^3. Using $\ell_B \simeq \ell_K/\sqrt{Sc}$, we find the Batchelor scale $\ell_B \simeq 5.8\ \mu$m. Finally, using $\varepsilon \simeq \gamma^2\nu$, or equivalently using the relation $\gamma = D/\ell_B^2$, we find $\gamma \sim 15$ s^{-1}. In this set of experiments, unfortunately, we were unable to obtain a certain estimate for the scalar injection rate.

Williams $et\ al.$ [34] employed fluorescein dye in a quasi-two-dimensional turbulent flow to investigate the Batchelor

regime at Schmidt number around Sc $\simeq 2000$. They reported that the spectrum falls below k^{-1} at wave numbers lower than expected from theory. In order to estimate κ_B, the authors first considered the competing effects on a dye structure due to the stretching produced by the large-scale flow and also due to the dissipation by diffusion and found $\kappa_B/2\pi \simeq 35$ cm^{-1}. They also estimated κ_B by measuring γ: to determine the rate of strain tensor on a regular grid, the authors obtained the velocity derivatives from their velocity field measurements, then diagonalized this tensor at each location and finally ensemble averaged over space and time. The strain rate determined in this way turns out to be $\gamma \simeq 1.0$ s^{-1}. Using $E_c(k) = \frac{\chi}{\gamma k}\exp(-Dk^2/\gamma)$, with $D = 5 \times 10^{-6}$ cm^2/s, and $\gamma = 0.5(\varepsilon/\nu)^{1/2}$ (and defining κ_B as the wave number for which the exponent is -1) the authors found $\kappa_B \simeq 70$ cm^{-1}. The authors reported a spectral slope steeper than Batchelor's value -1 and more so with increasing wave number, while including a Gaussian tail did not improve the fit. The inclusion of an exponential tail is reported to yield a satisfactory fit but only when unphysical parameters are used. The authors fit the data shown in their Fig. 17(b) to a spectrum of the form $E_c(k) = Ck^{-1}\exp(-k\sqrt{\kappa/\gamma_{\mathrm{eff}}})$ and found $\gamma_{\mathrm{eff}} \simeq 1.1 \times 10^{-3}$ s^{-1}, which is drastically different from their directly measured value of $\gamma \simeq 1.0$ s^{-1}. Putting all this together, the value $\gamma \simeq 10^{-3}$ s^{-1} for the least strain rate seems possible, but quite small and difficult to reconcile with the value $\gamma \sim 1.0$ s^{-1} from direct velocity derivative measurements. As for the scalar injection rate, by extracting data from [34], Fig. 22, for $E_c(k)$, we estimated $\chi \simeq 2D \int k^2 E_c(k)dk \sim 10^{-5}$ s^{-1}.

Jullien $et\ al.$ [28] employed an electromagnetically driven two-dimensional flow of a water-fluorescein mixture, in which Batchelor's $1/k$ spectrum was observed, with exponential tails for the probability distributions of the concentration and concentration increments and logarithmlike structure functions. In this set of experiments, the flow was statistically stationary, whereas the concentration field was in a freely decaying quasiequilibrium regime starting from an initial circular 5-cm blob of fluorescein. The results were also confirmed by a simulation where the scalar advection equation was solved using observed values of the advecting velocity. The trajectories of 6×10^5 particles, located initially in a disk, 5 cm in diameter, were calculated by integrating the experimentally measured velocity field and used to estimate the evolved concentration spectrum at negligible diffusivity. For this experiment, we used Figs. 2(b) and 3 in [28] to extract data for $E_c(k)$, from which we estimated $\chi = 2D \int E_c(k)k^2 dk$ by numerical integration. In this way, χ turns out to be of order 2×10^2 s^{-1}, roughly in agreement with the inset of [28], Fig. 2. Also, with given $\kappa_B = 2800$ cm^{-1}, and the relation $\kappa_B = \sqrt{\gamma/\kappa}$ used in [28] with diffusivity $\kappa \simeq 10^{-6}$ cm^2/s, we find $\gamma \simeq 7.8$ s^{-1}.

Finally, in the most recent experiment of which we are aware, Iwano $et\ al.$ [29] studied concentration fluctuations of the fluorescent dye rhodamine 6G in an axisymmetric turbulent water jet at the Schmidt number Sc $\simeq 2.9 \times 10^3$ and Reynolds number Re $\simeq 2.0 \times 10^4$. The authors observed the $1/k$ Batchelor spectrum in the viscous-convective range although they also report that the spectrum does not perfectly follow this scaling due to "a small bump in the range." The

Batchelor and Kolmogorov length scales in this experiment are given as $\eta_B = 2.6\ \mu$m and $\eta_K = 142\ \mu$m, respectively. For the injection rate, we have $\gamma \simeq \eta_B^{-2}D \simeq 59\ \text{s}^{-1}$, using $D \simeq 4.0 \times 10^{-6}\ \text{cm}^2\,\text{s}^{-1}$ [132]. The latter result can be used to obtain the energy dissipation rate: $\epsilon \simeq \nu\gamma^2 = \text{Sc} \times D \times \gamma^2 \simeq 40.4\ \text{cm}^2\,\text{s}^{-3}$. As for the scalar injection rate χ, by extracting data from [29], Fig. 3, for $E_c(k)/C_0^2$, we numerically estimated the quantity $\int k^2 \frac{E_c(k)}{C_0^2}dk$ cutting off the integral at the Batchelor wave number. For different values of the initial concentration C_0, given as 1, 10, 100, 1000, the value of this integral lies roughly between 10^4 and 10^5. Using $\chi = 2DC_0^2 \int k^2 \frac{E_c(k)}{C_0^2}dk$, we can estimate the range of χ values for different choices of C_0 in this experiment as $10^{-4}\ \text{s}^{-1} \lesssim \chi \lesssim 10\ \text{s}^{-1}$.

APPENDIX H: GCF'S IN A 2D QUIESCENT FLUID

We obtain here the steady-state concentration correlation function $C(r)$ and the corresponding spectrum $E_c(k)$ for a 2D fluid, with velocity field in thermal equilibrium and with concentration fluctuations generated by a stochastic source (34) that is white noise in time. Similar to the 3D case discussed in Sec. III B, we will solve the general expression (52) for the two-point correlation function and then obtain the spectrum by Fourier transformation. However, the analysis is somewhat more difficult in 2D than in 3D. First, the effective diffusivity D_{eff} is well known to be logarithmically divergent in 2D [e.g., see [56] and (H9) below]. Thus, the calculation requires an IR cutoff L in addition to a UV cutoff σ, and we shall be concerned with evaluating $C(r)$ only for $\sigma \ll r \ll L$. Second, Fourier transforms of isotropic correlation functions do not reduce to a Fourier cosine transform as in 3D, but instead require in 2D a more difficult Hankel transform.

The covariance $\mathbf{R}(\mathbf{x}, \mathbf{x}')$ defined in (19) can be evaluated for homogeneous, isotropic statistics in $d = 2$ dimensions using the 2D version of the expression given by the first line of (D1) in terms of $K_\theta(r)$, defined by (49), and $J_\theta(r)$, given by (50). We have

$$
\begin{aligned}
K_\theta(r) &= \frac{1}{(2\pi)^2} \int d^2\mathbf{k}\, e^{i\mathbf{k}\cdot\mathbf{r}} |\widehat{\sigma}(k)|^2 \frac{2k_BT}{\eta k^2} \\
&= \frac{k_BT}{\pi\eta} \int_0^\infty dk\, \frac{J_0(kr)}{k} |\widehat{\sigma}(k)|^2,
\end{aligned}
\tag{H1}
$$

which is a Hankel transform, with the Bessel function of the first kind $J_0(kr)$ [see, e.g., [93], 7.3.1(2)]. We will use an isotropic filter $\boldsymbol{\sigma} = \sigma\mathbf{I}$ whose Fourier transform is given by

$$
\widehat{\sigma}(k) := \frac{k}{\sqrt{k^2 + L^{-2}}} e^{-\frac{\sigma}{2}\sqrt{k^2 + L^{-2}}},
\tag{H2}
$$

with IR cutoff L and UV cutoff $\sigma \ll L$. Aside from required properties for such a smoothing filter, we have made this particular choice due to the fact that it leads to tractable Hankel transforms. It follows that

$$
K_\theta(r) = \frac{k_BT}{\pi\eta} \int_0^\infty dk\, J_0(kr) \frac{k}{k^2 + L^{-2}} e^{-\sigma\sqrt{k^2 + L^{-2}}}.
\tag{H3}
$$

This particular example has not been presented in standard tables of Hankel transforms, as far as we are aware. However, it can be obtained from formula 8.2(24) in [133], which in our notation reads as

$$
\int_0^\infty \frac{ke^{-\alpha\sqrt{k^2+L^{-2}}}}{\sqrt{k^2+L^{-2}}} J_0(kr)dk = \frac{e^{-\sqrt{\alpha^2+r^2}/L}}{\sqrt{r^2+\alpha^2}},
$$

by integrating over the parameter α from σ to infinity. Integrating the left-hand side of the above expression over α, from σ to $+\infty$, is straightforward and gives the integral (H3). On the other hand, the integral of the right-hand side of the above expression over α can be written as

$$
\begin{aligned}
\int_\sigma^\infty \frac{e^{-\sqrt{\alpha^2+r^2}/L}}{\sqrt{r^2+\alpha^2}} d\alpha &= \int_0^\infty \frac{e^{-\sqrt{\alpha^2+r^2}/L}}{\sqrt{r^2+\alpha^2}} d\alpha \\
&\quad - \int_0^\sigma \frac{e^{-\sqrt{\alpha^2+r^2}/L}}{\sqrt{r^2+\alpha^2}} d\alpha,
\end{aligned}
$$

where the integral, from σ to $+\infty$, can be obtained using [92], formula 1.4(27), while the remaining integral in the second line can be estimated by making use of the approximation $\int_0^\sigma d\alpha \frac{e^{-\sqrt{r^2+\alpha^2}/L}}{\sqrt{r^2+\alpha^2}} \simeq \frac{\sigma}{r}e^{-r/L}$ for $\sigma \ll r$. Putting all this together, we find

$$
K_\theta(r) \simeq \frac{k_BT}{\pi\eta}\left[K_0\left(\frac{r}{L}\right) - \frac{\sigma}{r}e^{-r/L}\right],
\tag{H4}
$$

where $K_0(x)$ [not to be confused with $K_\theta(r)$] is the modified Bessel function of the second kind (see, e.g., [93], 7.2.2). The term proportional to σ is much smaller than the first term involving $K_0(r/L)$ for $\sigma \ll r \ll L$, but we retain it here because the analogous small term gave rise in 3D to a nonanalytic contribution to $C(r)$ which was responsible for the GCF's. However, we remark in advance that the contribution from this term will be found in 2D to be negligible compared with that from the Bessel function. The major difference from 3D is that the larger contribution to $C(r)$ from the Bessel function is also nonanalytic in r in 2D.

With $K_\theta(r)$ at hand, we can now proceed to obtain $J_\theta(r)$ [not to be confused with Bessel function $J_0(kr)$] using its definition given by (50) with $d = 2$:

$$
J_\theta(r) = \frac{k_BT}{\pi\eta}\frac{L}{r^2}\left[rK_1\left(\frac{r}{L}\right) - L + \sigma(1 - e^{-r/L})\right].
\tag{H5}
$$

To get this result, we have used the relation $\int zK_0(z)dz = -zK_1(z)$ in terms of the modified Bessel function of the second kind $K_1(z)$ [see [93], 7.14.1(3)]. Note that (H4) is valid only for $r \gg \sigma$ while to calculate $J_\theta(r)$, we need to integrate from 0 to r. Nevertheless, the error in this calculation is of order $(\sigma/r)^2$, which can be easily verified by writing $J_\theta(r) = \frac{-1}{r^2}[\int_0^{N\sigma} \rho K_\theta(\rho)d\rho + \int_{N\sigma}^r \rho K_\theta(\rho)d\rho]$ in terms of a fixed $N \gg 1$ such that our asymptotic relations used to evaluate the second integral remain valid. Even for a large N, we can take σ small enough such that the first integral gives a negligible contribution of order $K_\theta(0)(N\sigma/r)^2$ assuming that for $r \ll N\sigma$, $K_\theta(r) \to K_\theta(0)$. The function $K_\theta(0)$ has only a logarithmic dependence on σ/L, as shown immediately below.

In order to calculate $J_\theta(0)$, we note that in 2D the expression (50) implies $J_\theta(0) = -\frac{1}{2}K_\theta(0)$. We can write

$$K_\theta(0) = \frac{k_BT}{\pi\eta}\int_0^\infty \frac{k\,dk}{k^2+L^{-2}}e^{-\sigma\sqrt{k^2+L^{-2}}} = \frac{k_BT}{\pi\eta}E_1\left(\frac{\sigma}{L}\right). \quad (H6)$$

The first line in the above expression in fact defines the exponential integral function $E_1(x) = -\mathrm{Ei}(-x) = \int_x^\infty \frac{e^{-\kappa}d\kappa}{\kappa}$ as can be seen by a simple change of variable as $\kappa = \sigma\sqrt{k^2+L^{-2}}$ [see [93], 9.7(1)]. Thus, we find $J_\theta(0) = \frac{-K_\theta(0)}{2} = \frac{-k_BT}{2\pi\eta}E_1(\sigma/L)$ and consequently

$$\triangle J_\theta(r) \simeq \frac{k_BT}{\pi\eta}\left[-\frac{1}{2}E_1\left(\frac{\sigma}{L}\right) + \left(\frac{L}{r}\right)^2 - \left(\frac{L}{r}\right)K_1\left(\frac{r}{L}\right) \right.$$
$$\left. - \frac{\sigma L}{r^2}(1 - e^{-r/L})\right].$$

Next, for $r/L \ll 1$, we use the asymptotic relations $K_1(r/L) \simeq L/r + I_1(r/L)\ln(r/2L)$ where $I_1(x)$ is the modified Bessel function of the first kind [see [93], 7.2.5(37)], and also $I_1(r/L) \simeq r/2L$ [see [93], formula 7.2.2(12)]. In addition, we expand the exponential function to the first order in $\sigma/r \ll 1$; $e^{-r/L} \simeq 1 - r/L$, to write the final expression for $\triangle J_\theta(r)$ as

$$\triangle J_\theta(r) \simeq \frac{k_BT}{\pi\eta}\left[-\frac{1}{2}E_1\left(\frac{\sigma}{L}\right) - \frac{1}{2}\ln\left(\frac{r}{2L}\right) - \frac{\sigma}{r}\right],$$
$$\sigma \ll r \ll L. \quad (H7)$$

With $\triangle J_\theta(r)$ at hand, we proceed to calculate the steady-state correlation function $C(r)$ given by the integral (52). Analogous to the 3D calculation presented in Sec. III B, however, it is easier to work with the derivative $\partial_r C(r)$ and, also, since $r \ll L$, to take $S(r/L) \simeq S(0) = 2\chi$. Hence, we proceed by inserting (H7) in $\partial_r C(r)$, obtained by taking the derivative of (52):

$$\partial_r C \simeq \frac{-\chi r}{2}\left[D + \frac{k_BT}{4\pi\eta}\ln\left(\frac{r}{2L}\right) + \frac{k_BT}{2\pi\eta}\frac{\sigma}{r}\right]^{-1}. \quad (H8)$$

Here we have defined the "renormalized diffusivity" D as

$$D := D_0 + \frac{k_BT}{4\pi\eta}E_1\left(\frac{\sigma}{L}\right) \doteq D_0 - \gamma + \frac{k_BT}{4\pi\eta}\ln\left(\frac{L}{\sigma}\right) \quad (H9)$$

with bare diffusivity D_0 and $\gamma = -\Gamma'(1)$. Factoring out a D from the square brackets "[·]" in (H8), note that both the logarithmic term $\propto \ln(r/L)/\ln(\sigma/L)$ and last term containing σ/r in this expression are small and we can expand using $1/(1+x) \simeq 1 - x$ for small x:

$$\partial_r C(r) \simeq -\frac{\chi r}{2D}\left[1 - \frac{k_BT}{4\pi\eta D}\ln\left(\frac{r}{2L}\right) - \frac{k_BT}{2\pi\eta D}\frac{\sigma}{r}\right].$$

Integrating this expression over r, from $N\sigma$ to r, we find

$$C(r) = -\frac{\chi}{2D}\left\{\frac{1}{2}r^2 - \frac{k_BT}{16\pi\eta D}r^2\left[2\ln\left(\frac{r}{2L}\right) - 1\right]\right.$$
$$\left. - \frac{k_BT}{2\pi\eta D}\sigma r\right\} + \text{const.} \quad (H10)$$

The result is very much like (65) obtained in 3D, except that the middle term containing $\ln(r/2L)$ is nonanalytic, whereas the corresponding term in 3D was proportional to r^4

and analytic. We note also that the term proportional to σ has a negative sign, opposite to that in 3D.

We can obtain the spectrum using the general expression $E_c(k) = \frac{k}{2}\int_0^\infty rC(r)J_0(kr)dr$ in 2D. Performing this Hankel transform, the last term in (H10), which is linear in r and σ, yields a negative contribution:

$$\frac{k}{2}\frac{\chi\sigma}{2D}\frac{k_BT}{2\pi\eta D}\int_0^\infty r^2J_0(kr)dr = -\frac{\chi\sigma}{2D}\frac{k_BT}{4\pi\eta D}k^{-2}. \quad (H11)$$

Here, we have evaluated the integral by introducing an IR cutoff μ; $\lim_{\mu\to 0}\int_0^\infty r^2 e^{-\mu r}J_0(kr)dr$, which can be calculated using [133], formula 8.2(20). The quadratic term in (H10), that is $\frac{-\chi}{4D}(1 + \frac{k_BT}{8\pi\eta D})r^2$, will contribute only a rapidly decaying spectrum. This can be easily confirmed by directly taking the integral $\int_0^\infty r^3 J_0(kr)dr$ using, e.g., [133], formula 8.2(20), once again introducing an exponential IR cutoff μ and taking the limit $\mu \to 0$, which gives a vanishing contribution.

Finally, to obtain the contribution to the spectrum of the logarithmic term in (H10), we need to evaluate

$$\int_0^\infty r^3\ln(r/2L)J_0(kr)dr = \int_0^\infty r^3\ln(r)J_0(kr)dr$$
$$- \ln(2L)\int_0^\infty r^3J_0(kr)dr.$$

The integrals on the right-hand side both can be evaluated using a general property of Hankel transforms, which gives the Hankel transform (of arbitrary order ν) of function $x^m f(x)$, $m = 0, 1, 2, \ldots$, in terms of the mth-order derivative of the Hankel transform (of order $\nu + m$) of function $f(x)$ [see [133], 8.1(3)]. This general property allows us to write the two integrals as

$$\int_0^\infty r^3J_0(kr)dr = \left(\frac{d}{k\,dk}\right)^3\left[k^3\int_0^\infty J_3(kr)dr\right]$$

and

$$\int_0^\infty r^3\ln r J_0(kr)dr = \left(\frac{d}{k\,dk}\right)^3\left[k^3\int_0^\infty \ln r J_3(kr)dr\right]$$

in terms of the Bessel function $J_3(z)$ of the first kind. These integrals can then be evaluated using

$$\int_0^\infty J_3(kr)dr = k^{-1}$$

from [133], 8.5(3), and

$$\int_0^\infty \ln(r)J_3(kr)dr = [2\psi(2) - \ln(k^2/4)]/2k,$$

from [133], 8.6(25), for $\mu = -\frac{1}{2}$, $\nu = 3$, where $\psi(z) = \Gamma'(z)/\Gamma(z)$ is the logarithmic derivative of the gamma function $\Gamma(z)$. It is then readily seen that only the logarithmic term yields a nonvanishing contribution to the required integral:

$$\int_0^\infty r^3\ln(r/2L)J_0(kr)dr = -\frac{1}{2}\left(\frac{d}{k\,dk}\right)^3[k^2\ln(k^2/4)]$$
$$= 4k^{-4} \quad (H12)$$

and thus the contribution of the logarithmic term in (H10) to the spectrum is given by

$$\frac{\chi}{2D}\frac{k_B T}{16\pi \eta D}k\int_0^\infty r^3 \ln(r/2L)J_0(kr)dr = \frac{\chi}{2D}\frac{k_B T}{4\pi \eta D}k^{-3}.$$

Combining this result with (H11), therefore, we find the 2D spectrum of the concentration field to be

$$E_c(k) = \frac{\chi}{2D}\frac{k_B T}{4\pi \eta D}(k^{-3} - \sigma k^{-2}), \quad 1/L \ll k \ll 1/\sigma. \quad \text{(H13)}$$

It is interesting that the term proportional to σ has the power-law scaling k^{-2}, just as in 3D. However, the sign of this term is *negative* in 2D and it does not become sizable compared with the first term until $k \simeq 1/\sigma$, when our asymptotic approximations break down. In contrast to 3D where the leading term in $C(r)$ was analytic in r and gave a contribution to the spectrum very rapidly decaying in k, this term is now non-analytic because of the $\ln r$ and produces a power law. Note that the resulting spectrum is again in close correspondence

with the prediction of linearized fluctuating hydrodynamics. Using the relation in 2D between the spectrum and the structure function,

$$E_c(k) = \frac{1}{2}\frac{1}{(2\pi)^2}2\pi k S_{cc}(k) = \frac{1}{4\pi}k S_{cc}(k)$$

and using the relation $\chi = D(\nabla c)_{\text{eff}}^2$ just as in 3D yields

$$S_{cc}(k) \simeq \frac{1}{2}\frac{k_B T}{D\eta}|\nabla c|_{\text{eff}}^2 k^{-4}.$$

This agrees with the prediction of linearized fluctuating hydrodynamics up to a factor of $\frac{1}{2}$. Based on the results in 2D and in 3D we may conjecture that the result of the DFV theory for the case of a random concentration gradient ∇c with homogeneous, isotropic statistics and the prediction of linearized fluctuating hydrodynamics for a fixed mean concentration gradient $\nabla \bar{c}$ will agree in any space dimension d, up to a factor of $(d-1)/d$.

---

[1] D. Bandak, G. Eyink, A. Mailybaev, and N. Goldenfeld, Thermal noise competes with turbulent fluctuations at millimeter scales, arXiv:2107.03184.

[2] G. Eyink, D. Bandak, N. Goldenfeld, and A. A. Mailybaev, Dissipation-range fluid turbulence and thermal noise, arXiv:2107.13954.

[3] J. B. Bell, A. Nonaka, A. L. Garcia, and G. Eyink, Thermal fluctuations in the dissipation range of homogeneous isotropic turbulence, J. Fluid Mech. **939**, A12 (2022).

[4] M. A. Gallis, J. R. Torczynski, M. C. Krygier, N. P. Bitter, and S. J. Plimpton, Turbulence at the edge of continuum, Phys. Rev. Fluids **6**, 013401 (2021).

[5] R. Betchov, On the fine structure of turbulent flows, J. Fluid Mech. **3**, 205 (1957).

[6] R. Betchov, Thermal agitation and turbulence, in *Rarefied Gas Dynamics*, edited by L. Talbot (Academic, New York, 1961), p. 307–321 (Proceedings of the Second International Symposium on Rarefied Gas Dynamics, held at the University of California, Berkeley, CA, 1960).

[7] R. Betchov, Measure of the intricacy of turbulence, Phys. Fluids **7**, 1160 (1964).

[8] A. Kolmogorov, The local structure of turbulence in incompressible viscous fluid for very large reynolds number, Dokl. Akad. Nauk SSSR **30**, 9 (1941) [Proc. R. Soc. Lond. A **434**, 9 (1991)].

[9] R. H. Kraichnan, The structure of isotropic turbulence at very high Reynolds numbers, J. Fluid Mech. **5**, 497 (1959).

[10] U. Frisch and R. Morf, Intermittency in nonlinear dynamics and singularities at complex times, Phys. Rev. A **23**, 2673 (1981).

[11] C. Foias, O. Manley, and L. Sirovich, Empirical and Stokes eigenfunctions and the far-dissipative turbulent spectrum, Phys. Fluids **2**, 464 (1990).

[12] U. Frisch and M. Vergassola, A prediction of the multifractal model: the intermediate dissipation range, Europhys. Lett. **14**, 439 (1991).

[13] L. Sirovich, L. Smith, and V. Yakhot, Energy Spectrum of Homogeneous and Isotropic Turbulence in far Dissipation Range, Phys. Rev. Lett. **72**, 344 (1994).

[14] S. Khurshid, D. A. Donzis, and K. R. Sreenivasan, Energy spectrum in the dissipation range, Phys. Rev. Fluids **3**, 082601(R) (2018).

[15] A. Gorbunova, G. Balarac, M. Bourgoin, L. Canet, N. Mordant, and V. Rossetto, Analysis of the dissipative range of the energy spectrum in grid turbulence and in direct numerical simulations, Phys. Rev. Fluids **5**, 044604 (2020).

[16] D. Buaria, M. P. Clay, K. R. Sreenivasan, and P. K. Yeung, Turbulence is an Ineffective Mixer when Schmidt Numbers Are Large, Phys. Rev. Lett. **126**, 074501 (2021).

[17] G. K. Batchelor, Small-scale variation of convected quantities like temperature in turbulent fluid part 1. General discussion and the case of small conductivity, J. Fluid Mech. **5**, 113 (1959).

[18] D. Bedeaux and P. Mazur, Renormalization of the diffusion coefficient in a fluctuating fluid i, Physica (Amsterdam) **73**, 431 (1974).

[19] P. Mazur and D. Bedeaux, Renormalization of the diffusion coefficient in a fluctuating fluid II, Physica (Amsterdam) **75**, 79 (1974).

[20] J. T. Hynes, R. Kapral, and M. Weinberg, Molecular theory of translational diffusion: Microscopic generalization of the normal velocity boundary condition, J. Chem. Phys. **70**, 1456 (1979).

[21] J. C. Nieuwoudt and B. M. Law, Theory of light scattering by a nonequilibrium binary mixture, Phys. Rev. A **42**, 2003 (1990).

[22] B. M. Law and J. C. Nieuwoudt, Noncritical liquid mixtures far from equilibrium: the rayleigh line, Phys. Rev. A **40**, 3880 (1989).

[23] P. Segrè and J. Sengers, Nonequilibrium fluctuations in liquid mixtures under the influence of gravity, Phys. A (Amsterdam) **198**, 46 (1993).

[24] R. H. Kraichnan, Small-scale structure of a scalar field convected by turbulence, Phys. Fluids **11**, 945 (1968).

[25] R. H. Kraichnan, Convection of a passive scalar by a quasi-uniform random straining field, J. Fluid Mech. **64**, 737 (1974).

[26] K. R. Sreenivasan, Turbulent mixing: A perspective, Proc. Natl. Acad. Sci. USA **116**, 18175 (2019).

[27] J. O. Nye and R. S. Brodkey, The scalar spectrum in the viscous-convective subrange, J. Fluid Mech. **29**, 151 (1967).

[28] M.-C. Jullien, P. Castiglione, and P. Tabeling, Experimental Observation of Batchelor Dispersion of Passive Tracers, Phys. Rev. Lett. **85**, 3636 (2000).

[29] K. Iwano, J. Hosoi, Y. Sakai, and Y. Ito, Power spectrum of high Schmidt number scalar in a turbulent jet at a moderate reynolds number, Exp. Fluids **62**, 129 (2021).

[30] H. Grant, B. Hughes, W. Vogel, and A. Moilliet, The spectrum of temperature fluctuations in turbulent flow, J. Fluid Mech. **34**, 423 (1968).

[31] N. Oakey, Determination of the rate of dissipation of turbulent energy from simultaneous temperature and velocity shear microstructure measurements, J. Phys. Oceanogr. **12**, 256 (1982).

[32] C. Gibson and W. Schwarz, The universal equilibrium spectra of turbulent velocity and scalar fields, J. Fluid Mech. **16**, 365 (1963).

[33] P. L. Miller and P. E. Dimotakis, Measurements of scalar power spectra in high Schmidt number turbulent jets, J. Fluid Mech. **308**, 129 (1996).

[34] B. S. Williams, D. Marteau, and J. P. Gollub, Mixing of a passive scalar in magnetically forced two-dimensional turbulence, Phys. Fluids **9**, 2061 (1997).

[35] P. Yeung, S. Xu, D. Donzis, and K. Sreenivasan, Simulations of three-dimensional turbulent mixing for Schmidt numbers of the order 1000, Flow, Turbul. Combust. **72**, 333 (2004).

[36] D. A. Donzis, K. Sreenivasan, and P. Yeung, The Batchelor spectrum for mixing of passive scalars in isotropic turbulence, Flow, Turbul. Combust. **85**, 549 (2010).

[37] T. Gotoh, T. Watanabe, and H. Miura, Spectrum of passive scalar at very high Schmidt number in turbulence, Plasma Fusion Res. **9**, 3401019 (2014).

[38] M. P. Clay, Strained turbulence and low-diffusivity turbulent mixing using high performance computing, Ph.D. thesis, Georgia Institute of Technology, 2017.

[39] E. Balkovsky and A. Fouxon, Universal long-time properties of lagrangian statistics in the Batchelor regime and their application to the passive scalar problem, Phys. Rev. E **60**, 4164 (1999).

[40] G. Falkovich, K. Gawędzki, and M. Vergassola, Particles and fields in fluid turbulence, Rev. Mod. Phys. **73**, 913 (2001).

[41] J. Bedrossian, A. Blumenthal, and S. Punshon-Smith, The Batchelor spectrum of passive scalar turbulence in stochastic fluid mechanics at fixed Reynolds number, arXiv:1911.11014.

[42] L. Onsager, Theories and problems of liquid diffusion, Ann. N.Y. Acad. Sci. **46**, 241 (1945).

[43] A. Vailati and M. Giglio, Giant fluctuations in a free diffusion process, Nature (London) **390**, 262 (1997).

[44] D. Brogioli, A. Vailati, and M. Giglio, Giant fluctuations in diffusion processes, J. Phys.: Condens. Matter **12**, A39 (2000).

[45] W. B. Li, K. J. Zhang, J. V. Sengers, R. W. Gammon, and J. M. Ortiz de Zarate, Concentration Fluctuations in a Polymer Solution under a Temperature Gradient, Phys. Rev. Lett. **81**, 5580 (1998).

[46] A. Vailati, R. Cerbino, S. Mazzoni, C. J. Takacs, D. S. Cannell, and M. Giglio, Fractal fronts of diffusion in microgravity, Nat. Commun. **2**, 290 (2011).

[47] T. R. Kirkpatrick, E. G. D. Cohen, and J. R. Dorfman, Fluctuations in a nonequilibrium steady state: Basic equations, Phys. Rev. A **26**, 950 (1982).

[48] D. Ronis and I. Procaccia, Nonlinear resonant coupling between shear and heat fluctuations in fluids far from equilibrium, Phys. Rev. A **26**, 1812 (1982).

[49] J. R. Dorfman, T. R. Kirkpatrick, and J. V. Sengers, Generic long-range correlations in molecular fluids, Annu. Rev. Phys. Chem. **45**, 213 (1994).

[50] J. de Zarate and J. Sengers, *Hydrodynamic Fluctuations in Fluids and Fluid Mixtures* (Elsevier, Amsterdam, 2006).

[51] J. M. O. de Zárate and J. V. Sengers, Fluctuations in fluids in thermal nonequilibrium states below the convective rayleigh–bénard instability, Phys. A (Amstedam) **300**, 25 (2001).

[52] J. M. Ortiz de Zárate and J. V. Sengers, Boundary effects on the nonequilibrium structure factor of fluids below the Rayleigh-Bénard instability, Phys. Rev. E **66**, 036305 (2002).

[53] P. Baaske, H. Bataller, M. Braibanti, M. Carpineti, R. Cerbino, F. Croccolo, A. Donev, W. Köhler, J. M. O. de Zárate, and A. Vailati, The NEUF-DIX space project-non-equilibrium fluctuations during diffusion in complex liquids, Eur. Phys. J. E **39**, 119 (2016).

[54] A. Vailati, P. Baaske, H. Bataller, S. Bolis, M. Braibanti, M. Carpineti, R. Cerbino, F. Croccolo, J.-L. Dewandel, A. Donev *et al.*, Giant fluctuations induced by thermal diffusion in complex liquids, Microgravity Sci. Technol. **32**, 873 (2020).

[55] D. Brogioli and A. Vailati, Diffusive mass transfer by nonequilibrium fluctuations: Fick's law revisited, Phys. Rev. E **63**, 012105 (2000).

[56] A. Donev, T. G. Fai, and E. Vanden-Eijnden, A reversible mesoscopic model of diffusion in liquids: from giant fluctuations to Fick's law, J. Stat. Mech.: Theory Exp. (2014) P04004.

[57] P. Debue, D. Kuzzay, E.-W. Saw, F. Daviaud, B. Dubrulle, L. Canet, V. Rossetto, and N. Wschebor, Experimental test of the crossover between the inertial and the dissipative range in a turbulent swirling flow, Phys. Rev. Fluids **3**, 024602 (2018).

[58] H. Wada, Shear-induced quench of long-range correlations in a liquid mixture, Phys. Rev. E **69**, 031202 (2004).

[59] J. M. Ortiz de Zárate and J. V. Sengers, Comment on "Shear-induced quench of long-range correlations in a liquid mixture", Phys. Rev. E **73**, 013201 (2006).

[60] K. Sreenivasan, Possible effects of small-scale intermittency in turbulent reacting flows, Flow, Turbul. Combust. **72**, 115 (2004).

[61] J. F. Driscoll, Turbulent premixed combustion: Flamelet structure and its effect on turbulent burning velocities, Prog. Energy Combust. Sci. **34**, 91 (2008).

[62] T. Echekki and E. Mastorakos, *Turbulent Combustion Modeling: Advances, New Trends and Perspectives*, Fluid Mechanics and Its Applications, Vol. 95 (Springer, Netherlands, 2010).

[63] I. Saito and T. Gotoh, Turbulence and cloud droplets in cumulus clouds, New J. Phys. **20**, 023001 (2018).

[64] S. Elghobashi, Direct numerical simulation of turbulent flows laden with droplets or bubbles, Annu. Rev. Fluid Mech. **51**, 217 (2019).

[65] F. Milan, L. Biferale, M. Sbragaglia, and F. Toschi, Sub-Kolmogorov droplet dynamics in isotropic turbulence using a multiscale lattice Boltzmann scheme, J. Comput. Sci. **45**, 101178 (2020).

[66] W. M. Durham, E. Climent, M. Barry, F. De Lillo, G. Boffetta, M. Cencini, and R. Stocker, Turbulence drives microscale patches of motile phytoplankton, Nat. Commun. **4**, 2148 (2013).

[67] J. D. Wheeler, E. Secchi, R. Rusconi, and R. Stocker, Not just going with the flow: the effects of fluid flow on bacteria and plankton, Annu. Rev. Cell Dev. Biol. **35**, 213 (2019).

[68] F.-G. Michalec, I. Fouxon, S. Souissi, and M. Holzner, Efficient mate finding in planktonic copepods swimming in turbulence, Elife **9**, e62014 (2020).

[69] A. Donev, A. Nonaka, Y. Sun, T. Fai, A. Garcia, and J. Bell, Low Mach number fluctuating hydrodynamics of diffusively mixing fluids, Commun. Appl. Math. Comput. Sci. **9**, 47 (2014).

[70] A. Nonaka, Y. Sun, J. Bell, and A. Donev, Low Mach number fluctuating hydrodynamics of binary liquid mixtures, Commun. Appl. Math. Comput. Sci. **10**, 163 (2015).

[71] A. Donev, J. B. Bell, A. De la Fuente, and A. L. Garcia, Enhancement of diffusive transport by non-equilibrium thermal fluctuations, J. Stat. Mech.: Theory Exp. (2011) P06014.

[72] V. Morozov, On the Langevin formalism for nonlinear and nonequilibrium hydrodynamic fluctuations, Phys. (Amsterdam) A **126**, 443 (1984).

[73] D. N. Zubarev, *Nonequilibrium Statistical Thermodynamics*, Studies in Soviet Science: Physical Sciences (Plenum, New York, 1974).

[74] D. Zubarev and V. Morozov, Statistical mechanics of nonlinear hydrodynamic fluctuations, Phys. A (Amsterdam) **120**, 411 (1983).

[75] P. Español, J. G. Anero, and I. Zúñiga, Microscopic derivation of discrete hydrodynamics, J. Chem. Phys. **131**, 244117 (2009).

[76] D. Forster, D. R. Nelson, and M. J. Stephen, Long-Time Tails and the Large-Eddy Behavior of a Randomly Stirred Fluid, Phys. Rev. Lett. **36**, 867 (1976).

[77] D. Forster, D. R. Nelson, and M. J. Stephen, Large-distance and long-time properties of a randomly stirred fluid, Phys. Rev. A **16**, 732 (1977).

[78] I.-C. Yeh and G. Hummer, System-size dependence of diffusion coefficients and viscosities from molecular dynamics simulations with periodic boundary conditions, J. Phys. Chem. B **108**, 15873 (2004).

[79] A. T. Celebi, S. H. Jamali, A. Bardow, T. J. Vlugt, and O. A. Moultos, Finite-size effects of diffusion coefficients computed from molecular dynamics: a review of what we have learned so far, Mol. Simul. **47**, 831 (2021).

[80] R. H. Kraichnan, Anomalous Scaling of a Randomly Advected Passive Scalar, Phys. Rev. Lett. **72**, 1016 (1994).

[81] B. I. Shraiman and E. D. Siggia, Lagrangian path integrals and fluctuations in random flow, Phys. Rev. E **49**, 2912 (1994).

[82] E. A. Novikov, Functionals and the random-force method in turbulence theory, Zh. Eksp. Teor. Fiz. **47**, 1919 (1965) [Sov. Phys.–JETP **20**, 1290 (1965)].

[83] K. Gawędzki, Turbulence under a magnifying glass, in *Quantum Fields and Quantum Space Time*, Nato Science Series B,

Vol. 364, edited by G. Hooft, A. Jaffe, G. Mack, P. Mitter, and R. Stora (Springer, Berlin, 1997), pp. 123–150.

[84] K. Gawędzki, Easy turbulence, in *Theoretical Physics at the End of the Twentieth Century: Lecture Notes of the CRM Summer School, Banff, Alberta*, CRM Series in Mathematical Physics, edited by Y. Saint-Aubin and L. Vinet (Springer, New York, 2002), pp. 245–275.

[85] K. Gawędzki, Soluble models of turbulent advection, Lectures given at the workshop "Random Media 2000", Mądralin by Warsaw, June 19-26, 2000; arXiv:nlin/0207058.

[86] G. L. Eyink and J. Xin, Self-similar decay in the Kraichnan model of a passive scalar, J. Stat. Phys. **100**, 679 (2000).

[87] J. O. Hinze, *Turbulence*, 2nd ed. (McGraw-Hill, New York, 1975).

[88] R. M. Corless, G. H. Gonnet, D. E. Hare, D. J. Jeffrey, and D. E. Knuth, On the Lambert *W* function, Adv. Comput. Math. **5**, 329 (1996).

[89] Y. Chenyakin, D. A. Ullmann, E. Evoy, L. Renbaum-Wolff, S. Kamal, and A. K. Bertram, Diffusion coefficients of organic molecules in sucrose-water solutions and comparison with Stokes-Einstein predictions, Atmos. Chem. Phys. **17**, 2423 (2017).

[90] M. Abramowitz and I. Stegun, *Handbook of Mathematical Functions: with Formulas, Graphs, and Mathematical Tables* (Dover, New York, 2012).

[91] K. Oldham, J. Myland, and J. Spanier, *An Atlas of Functions: with Equator, the Atlas Function Calculator*, An Atlas of Functions (Springer New York, 2010).

[92] A. Erdelyi, W. Magnus, F. Oberhettinger, and F. Tricomi, *Tables of Integral Transforms*, Vol. 1 (McGraw-Hill, New York, 1954).

[93] B. M. Project, H. Bateman, and A. Erdélyi, *Higher Transcendental Functions*, Vol. 2 (Dover, New York, 2006).

[94] O. Cadot, Y. Couder, A. Daerr, S. Douady, and A. Tsinober, Energy injection in closed turbulent flows: Stirring through boundary layers versus inertial stirring, Phys. Rev. E **56**, 427 (1997).

[95] D. Brogioli, A. Vailati, and M. Giglio, Universal behavior of nonequilibrium fluctuations in free diffusion processes, Phys. Rev. E **61**, R1 (2000).

[96] F. Croccolo, D. Brogioli, A. Vailati, M. Giglio, and D. S. Cannell, Nondiffusive decay of gradient-driven fluctuations in a free-diffusion process, Phys. Rev. E **76**, 041112 (2007).

[97] L. Ortiz, P. Riquelme, and R. Guzmán, Nonequilibrium free diffusion in seed leachate, in *8th Iberoamerican Optics Meeting and 11th Latin American Meeting on Optics, Lasers, and Applications*, Vol. 8785 (International Society for Optics and Photonics, Bellingham, WA, 2013), p. 8785BU.

[98] K. Sreenivasan and R. R. Prasad, New results on the fractal and multifractal structure of the large Schmidt number passive scalars in fully turbulent flows, Phys. D (amsterdam) **38**, 322 (1989).

[99] B. Chen, E. E. Sigmund, and W. P. Halperin, Stokes-Einstein Relation in Supercooled Aqueous Solutions of Glycerol, Phys. Rev. Lett. **96**, 145502 (2006).

[100] K. Elamin and J. Swenson, Brownian motion of single glycerol molecules in an aqueous solution as studied by dynamic light scattering, Phys. Rev. E **91**, 032306 (2015).

[101] M. B. Mustafa, D. L. Tipton, M. D. Barkley, P. S. Russo, and F. D. Blum, Dye diffusion in isotropic and liquid-crystalline aqueous (hydroxypropyl) cellulose, Macromolecules **26**, 370 (1993).

[102] F. B. Usabiaga, J. B. Bell, R. Delgado-Buscalioni, A. Donev, T. G. Fai, B. E. Griffith, and C. S. Peskin, Staggered schemes for fluctuating hydrodynamics, Multiscale Model. Simul. **10**, 1369 (2012).

[103] G. D'Errico, O. Ortona, F. Capuano, and V. Vitagliano, Diffusion coefficients for the binary system glycerol+ water at 25 C. a velocity correlation study, J. Chem. Eng. Data **49**, 1665 (2004).

[104] H. Tyrrell and K. Harris, *Diffusion in Liquids: A Theoretical and Experimental Study* (Butterworth-Heinemann, London, 2013).

[105] P. Segre, R. Schmitz, and J. Sengers, Fluctuations in inhomogeneous and nonequilibrium fluids under the influence of gravity, Phys. A (Amsterdam) **195**, 31 (1993).

[106] A. Vailati and M. Giglio, Nonequilibrium fluctuations in time-dependent diffusion processes, Phys. Rev. E **58**, 4361 (1998).

[107] R. C. Weast, S. M. S. Suby, and C. D. Hodman, *Handbook of Chemistry and Physics*, 69th ed. (CRC Press, Boca Raton, FL, 1988).

[108] S. Lototskii and B. L. Rozovskii, Passive scalar equation in a turbulent incompressible gaussian velocity field, Russ. Math. Surveys **59**, 297 (2004).

[109] M. Chaves, G. Eyink, U. Frisch, and M. Vergassola, Universal Decay of Scalar Turbulence, Phys. Rev. Lett. **86**, 2305 (2001).

[110] A. Donev (private communication).

[111] A. Lemarchand and B. Nowakowski, Fluctuation-induced and nonequilibrium-induced bifurcations in a thermochemical system, Mol. Simul. **30**, 773 (2004).

[112] A. Chaudhri, J. B. Bell, A. L. Garcia, and A. Donev, Modeling multiphase flow using fluctuating hydrodynamics, Phys. Rev. E **90**, 033014 (2014).

[113] M. Gallo, F. Magaletti, D. Cocco, and C. M. Casciola, Nucleation and growth dynamics of vapour bubbles, J. Fluid Mech. **883**, A14 (2020).

[114] I. O. Götze and G. Gompper, Mesoscale simulations of hydrodynamic squirmer interactions, Phys. Rev. E **82**, 041921 (2010).

[115] R. M. Kulsrud and S. W. Anderson, The spectrum of random magnetic fields in the mean field dynamo theory of the galactic magnetic field, Astrophys. J. **396**, 606 (1992).

[116] A. Schekochihin, S. Cowley, J. Maron, and L. Malyshkin, Structure of small-scale magnetic fields in the kinematic dynamo theory, Phys. Rev. E **65**, 016305 (2001).

[117] A. A. Schekochihin, S. A. Boldyrev, and R. M. Kulsrud, Spectra and growth rates of fluctuating magnetic fields in the kinematic dynamo theory with large magnetic Prandtl numbers, Astrophys. J. **567**, 828 (2002).

[118] A. A. Schekochihin, J. L. Maron, S. C. Cowley, and J. C. McWilliams, The small-scale structure of magnetohydrodynamic turbulence with large magnetic Prandtl numbers, Astrophys. J. **576**, 806 (2002).

[119] A. Kazantsev, Enhancement of a magnetic field by a conducting fluid, Zh. Eksp. Teor. Fiz. **53**, 1806 (1967) [Sov. Phys.–JETP **26**, 1031 (1968)].

[120] J. A. Krommes, Projection-operator methods for classical transport in magnetized plasmas. Part 1. linear response, the Braginskii equations and fluctuating hydrodynamics, J. Plasma Phys. **84** (2018).

[121] O. Feliachi and F. Bouchet, Dynamical large deviations for plasmas below the debye length and the landau equation, J. Stat. Phys. **183**, 42 (2021).

[122] O. Feliachi and F. Bouchet, Dynamical large deviations for homogeneous systems with long range interactions and the Balescu–Guernsey–Lenard equation, arXiv:2105.05644.

[123] R. M. Kulsrud and E. G. Zweibel, On the origin of cosmic magnetic fields, Rep. Prog. Phys. **71**, 046901 (2008).

[124] K. Subramanian, The origin, evolution and signatures of primordial magnetic fields, Rep. Prog. Phys. **79**, 076901 (2016).

[125] H. Callen, *Thermodynamics and an Introduction to Thermostatics* (Wiley, New York, 1960).

[126] R. Z. Khas' minskii, Principle of averaging for parabolic and elliptic differential equations and for Markov processes with small diffusion, Theory Probab. Appl. **8**, 1 (1963).

[127] T. G. Kurtz, A limit theorem for perturbed operator semigroups with applications to random evolutions, J. Funct. Anal. **12**, 55 (1973).

[128] G. C. Papanicolaou, Some probabilistic problems and methods in singular perturbations, Rocky Mount. J. Math. **6**, 653 (1976).

[129] C. W. Gardiner and M. L. Steyn-Ross, Adiabatic elimination in stochastic systems. II. application to reaction diffusion and hydrodynamic-like systems, Phys. Rev. A **29**, 2823 (1984).

[130] G. Pavliotis and A. Stuart, *Multiscale Methods: Averaging and Homogenization*, Texts in Applied Mathematics, Vol. 53 (Springer New York, 2008).

[131] L. Landau, *Fluid Mechanics*, Course of Theoretical Physics, Vol. 6 (Pergamon, Oxford, 1959).

[132] P.-O. Gendron, F. Avaltroni, and K. J. Wilkinson, Diffusion coefficients of several rhodamine derivatives as determined by pulsed field gradient–nuclear magnetic resonance and fluorescence correlation spectroscopy, J. Fluoresc. **18**, 1093 (2008).

[133] A. Erdélyi, W. Magnus, F. Oberhettinger, and F. Tricomi, *Tables of Integral Transforms*, Vol. 2 (McGraw-Hill, New York, 1954).

[134] I. S. Gradshteyn and I. M. Ryzhik, in *Table of Integrals, Series, and Products*, 7th ed., edited by D. Zwillinger and A. Jeffrey (Elsevier, Amsterdam, 2007).